

**Modelling of Microstructure Evaluation of Welding by using Finite Element
Method (FEM)**

M.Sc. Thesis

in

Mechanical Engineering

University of Gaziantep

Supervisor

Prof. Dr. Ömer EYERCİOĞLU

By

AHMED SAMIR ANWAR

July 2013

© 2013 [AHMED SAMIR ANWAR]

T.C.
UNIVERSITY OF GAZİANTEP
GRADUATE SCHOOL OF
NATURAL & APPLIED SCIENCES
MECHANICAL ENGINEERING

Name of the thesis: Modelling of Microstructure Evaluation of Welding by using Finite Element Method (FEM).

Name of the student: AHMED SAMIR ANWAR

Exam date: 4/7/2013

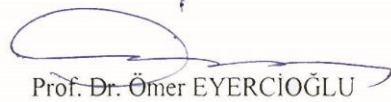
Approval of the Graduate School of Natural and Applied Sciences


Assoc. Prof. Dr. Mevin BEDIR
Director

I certify that this thesis satisfies all the requirements as a thesis for the degree of Master of Science.


Prof. Dr. Sait SÖYLEMEZ
Head of Department

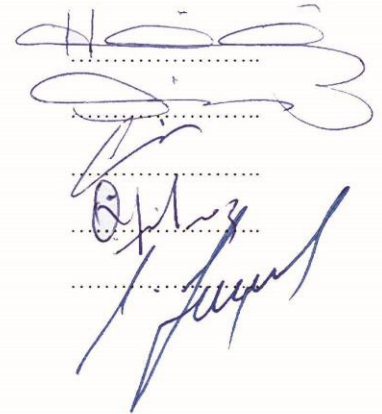
This is to certify that we have read this thesis and that in our opinion it is fully adequate, in scope and quality, as a thesis for the degree of Master of Science.


Prof. Dr. Ömer EYERCİOĞLU
Supervisor

Examining Committee Members

Signature

1. Prof. Dr. İ. Hüseyin FİLİZ
2. Prof. Dr. Ömer EYERCİOĞLU
3. Assoc. Prof. Dr. Abdülkadir ÇEVIK
4. Assoc. Prof. Dr. Oğuzhan YILMAZ
5. Asst. Prof. Dr. Necip Fazıl YILMAZ



I declared that the related thesis is written properly according to academic and ethical rules and using all literature information referenced in the related thesis.

AHMED SAMIR ANWAR

Signature

ABSTRACT

MODELLING OF MICROSTRUCTURE EVALUATION OF WELDING BY USING FINITE ELEMENT METHOD (FEM)

ANWAR, AHMED SAMIR

M. Sc. in Mechanical Engineering

Supervisor: Prof. Dr. Ömer EYERCİOĞLU

July 2013, 85 pages

In the present study, arc welding of the AISI 1045 steel is modelled by using 2D-FEM for three types of welding groove; V, double V and U. The temperature distribution, microstructure, grain growth, and the hardness of the heat affected zone (HAZ) of the welding are simulated. The experimental work is carried out to validate the FE model. The very close value between the simulation and experimental results show that the FE model is very effective for predicting the microstructure, the phase transformation, the grain growth and the hardness. The effect of preheating temperature on the martensite formation is analysed. It is shown that 225°C, 300°C and 350°C pre-heatings eliminate completely the martensite formation for 12 mm thick, V, U and double V-shaped butt welding of AISI 1045 steel. Among the welding grooves, the V-shape is providing the lowest martensite formation and the lowest preheating temperature for martensite elimination.

Key Words: Arc welding, AISI 1045 steel, FEM, Pre-heating, HAZ, Microstructure.

ÖZET

KAYNAK MİKROYAPISININ SONLU ELEMANLAR YÖNTEMİ KULLANILARAK MODELLENMESİ

ANWAR, AHMED SAMIR

Yüksek Lisans Tezi, Makine Mühendisliği Bölümü

Tez Yöneticisi: Prof. Dr. Ömer EYERCİOĞLU

Temmuz 2013, 85 sayfa

Bu çalışmada, AISI 1045 çeliğinin ark kaynağı V, çift V ve U kaynak ağızları için 2B-Sonlu Elemanlar Yöntemi kullanılarak modellenmiştir. Isıdan etkilenen bölgenin sıcaklık dağılımı, mikroyapısı, tane büyüklüğü ve sertliği simule edilmiştir. Sonlu eleman modelini doğrulamak için deneysel çalışma yapılmıştır. Simulasyon ve deneysel çalışma sonuçları arasındaki çok yakın değerler, sonlu eleman modelinin mikroyapı, faz dönüşümü, tane büyüklüğü ve sertlik tahmininde çok etkili olduğunu göstermiştir. Ön ısıtma sıcaklığının, martensit dönüşüm üzerindeki etkisi analiz edilmiş, 225°C, 300°C ve 350°C sıcaklıklardaki ön ısıtmaların, 12 mm kalınlıktaki AISI 1045 çeliğinin sırasıyla V, U ve çift V kaynak ağızlı alın kaynaklarında, martensit dönüşümlerini ortadan kaldırdığı görülmüştür. V kaynak ağzının, diğer kaynak ağızları içerisinde, en düşük martensit oluşumunu sağladığı ve en düşük ön ısıtma değeri ile martensit oluşumunu önlediği görülmüştür.

Anahtar Kelimeler: Ark kaynağı, AISI 1045 çeliği, Sonlu Elemanlar Yöntemi, Ön ısıtma, Isıdan etkilenmiş bölge, Mikroyapı.

This work is dedicated to my beloved Parents, brother & sister for their insatiable love, support & encouragement.

ACKNOWLEDGEMENTS

I would like sincerely to thank my supervisor, Professor Dr. Ömer EYERCİOĞLU for his guidance, valuable advice, encouragement, suggestion, correction and supervision throughout the progress till the completion of this work.

In acknowledging the help of others, I would like to thank Assistant Professor Dr.Necip Fazıl YILMAZ and Mr. Kürşad GÖV for valuable comments and sharing their knowledge. I would also like to thank Technicians in Construction and Manufacturing Department for providing me with their precious time and efforts in preparing samples for shielded metal arc welding.

I wish to express my deepest gratitude to my parents, for their endless support, interest and pray as always, for which my mere expression of thanks likewise does not suffice. I would also like to thank my beloved friend and instructor Dr.Mohammedtahir M. Saeed for his encouragement, criticism, suggestion, valuable advices and sharing knowledge.

Finally, I would like to serve my gratitude to examining committee members spending their valuable time for attending my M.Sc. qualification.

TABLE OF CONTENTS

CONTENT	Page
ABSTRACT.....	v
ÖZET.....	vi
ACKNOWLEDGEMENTS.....	viii
CONTENTS.....	ix
LIST OF FIGURES	xii
LIST OF TABLES.....	xvi
LIST OF SYMBOLS.....	xvii
CHAPTER 1: INTRODUCTION.....	1
CHAPTER 2: LITERATURE REVIEW.....	4
2.1 Introduction.....	4
2.2 Studies on Effect of the Welding Heat on the Residual Stresses and the Cracking	4
2.3 Studies on the Effect of Groove Shape on the Residual Stresses, Microstructure and Distortion	6
CHAPTER 3: WELDING AND FEM MODELLING	9
3.1 Introduction.....	9
3.2 Shielded metal arc welding (SMAW).....	9
3.2.1 The Process	9
3.2.2 Electrode Covering Functions	10
3.2.3 Advantage and Disadvantages	11
3.3 The multi-physics of welding	12
3.4 Welding grooves and types	14
3.5 Recrystallization and grain growth in welding.....	15
3.6 Steel microstructure and TTT diagram	15
3.7 Welding defects	17
3.8 Finite element application method for welding	18

3.9 General processes and steps of the Finite Element Method	
FEM.....	19
3.10 Linear differential equation for FEM formulation.....	20
3.11 Two-dimensional vs. Three-dimensional Modelling.....	21
CHAPTER 4: FE MODELLING AND EXPERIMENTAL STUDY	23
4.1 Introduction.....	23
4.2 Material selection	23
4.3 Experimental work	24
4.3.1 Arc welding and electrode selection	25
4.3.2 Macro and microstructure evaluation of the HAZ.....	26
4.3.3 Hardness Testing	27
4.4 FE Modeling	28
4.4.1 Pre- Processor Mathematical Modeling.....	28
4.4.2 Macro and Microstructure evaluation of the HAZ.....	30
4.4.3 DEFORM™ Hardness Modelling.....	33
CHAPTER 5: RESULTS AND DISCUSSION.....	35
5.1 Introduction.....	35
5.2 Experimental work	35
5.2.1 Visual testing of welded AISI 1045 Steel.....	35
5.2.2 The effect of welding on macro and microstructural features in HAZ of AISI 1045 steel	37
5.2.3 The effect of welding conditions on the Hardness profile of the HAZ	40
5.3 Modelling and experimental results compatibility.....	42
5.4 FE Modeling	45
5.4.1 the effects of welding groove shapes on the temperature distribution and HAZ	45
5.4.2 The effects of welding groove shapes on the heating and cooling curves.....	53
5.4.3 The effect of welding grooves on the grain size and microstructural features in the HAZ.....	57
5.4.4 Preheating effect on AISI 1045 steel welding.....	61

CHAPTER 6: CONCLUSIONS AND RECOMMENDATIONS.....	69
6.1 Conclusions.....	69
6.2 Recommendations.....	70
REFERENCES.....	71
APPENDIX A: 2D-DEFORM™ User's Guide.....	77
APPENDIX B: Input Data.....	85

LIST OF FIGURES

Figure 3.1. Shielded Metal Arc Welding process	10
Figure 3.2. High pressure Arc model for flame where the weld is considered rigid, adapted from Ramirez et al.....	12
Figure 3.3. The fluid flow driving forces in weld pool including models of plasma, adapted from Pavlyk and Dilthey.....	13
Figure 3.4. The common types of groove welds.....	14
Figure 3.5. Base plates and Heat Affected Zone (HAZ).....	15
Figure 3.6. Phase diagram for 0.30% C steel during welding.....	16
Figure 3.7. (TTT) diagram after Isothermal Transformation and Fe-C diagram for 0.30% C steel.....	17
Figure 3.8. Welding Defects with sub-divided heat effected zones	18
Figure 4.1. Single V groove welding dimensions according to ISO 9692.....	25
Figure 4.2. Shielded Metal Arc Welding E 7018 electrodes	26
Figure 4.3. Micro-hardness testing (Vickers Hardness).....	27
Figure 4.4. Modelling welding groove shapes dimensions prepared according to the given specification in ISO 9692 standard	29
Figure 4.5. Flow stress with respect to the strain as a function of temperature for AISI 1045 steel	30
Figure 4.6. Thermal conductivity of the AISI 1045 steel with respect to the temperature for 0.14 and 0.6 C% carbon content	31
Figure 4.7. Time Temperature Transformation (TTT) diagram for AISI 1045 0.41 carbon content	32
Figure 4.8. Volume fractions and transformation per temperature for AISI 1045 steel for 0.14 and 0.6 carbons content	33
Figure 4.9. Jominy Rockwell hardness test, as a function of distance for AISI 1045 steel	34
Figure 5.1. Fabricated single V-shape welding groove, butt joint for AISI 1045 steel, with two successive passes.....	36

Figure 5.2. The effect of the SMAW on the HAZ and hydrogen surface cracking during cooling of AISI 1045 steel.....	36
Figure 5.3. Optical macro and micrographs on a transverse section of HAZ area, through a shielded metal Arc welded (SMAW) AISI 1045 steel 100X.....	38
Figure 5.4. Grain size as a function of the transverse position from the fusion line through the HAZ area of the butt V-shape welded groove AISI 1045 steel 100 X.....	39
Figure 5.5. A demonstrative micro hardness test HV profile across the HAZ area in three points above the weldment root for AISI 1045 steel	41
Figure 5.6. 2D-FEM and experimental grain size distributions HAZ area for the butt welded V-shape groove of the AISI 1045 steel	43
Figure 5.7. 2D-FEM and experimental hardness distribution for a) 3mm, b) 6mm and c) 9mm above the weld root through the HAZ	44
Figure 5.8.a. First pass temperature distribution during welding and cooling time, in the HAZ area, for butt V-shape welding groove AISI 1045 steel in 2D-FEM.	46
Figure 5.8.b. Second pass temperature distribution during welding and cooling time, in the HAZ area, for butt V-shape welding groove AISI 1045 steel in 2D-FEM.	47
Figure 5.9.a. First pass temperature distribution during welding and cooling time, in the HAZ area, for butt U-shape welding groove AISI 1045 steel in 2D-FEM	48
Figure 5.9.b. Second pass temperature distribution during welding and cooling time, in the HAZ area, for butt U-shape welding groove AISI 1045 steel in 2D-FEM	49
Figure 5.10.a. First pass temperature distribution during welding and cooling time, in the HAZ area, for butt double V-shape welding groove AISI 1045 steel in 2D-FEM.....	50
Figure 5.10.b. Second pass temperature distribution during welding and cooling time, in the HAZ area, for butt double V-shape welding groove AISI 1045 steel in 2D-FEM.....	51

Figure 5.11. Generated heat affected area (HAA) after welding for the three groove shapes V, U and double V	52
Figure 5.12. Single V-shape temperature distribution of the HAZ region of the finite element model during a) welding time b) cooling in still air.....	54
Figure 5.13. U-shape temperature distribution of the HAZ region of the finite element model during a) welding time b) cooling in still air.....	55
Figure 5.14. Double V-shape temperature distribution of the HAZ region of the finite element model during a) welding time b) cooling in still air.....	56
Figure 5.15. Cooling curves of the three types of butt welding groove shapes U, V and double V-shape through the HAZ area in 2D-FEM	57
Figure 5.16. Microstructure of martensite phase transformation AISI 1045 steel in the HAZ area of V-Shape weldment in still air cooling process	58
Figure 5.17. Microstructure of martensite phase transformation AISI 1045 steel in the HAZ area of U-Shape weldment in still air cooling process	59
Figure 5.18. Microstructure of martensite phase transformation AISI 1045 steel in the HAZ area of double V-Shape weldment in still air cooling process.....	59
Figure 5.19. Average grain size for the weldment shapes V, U and double V in FEM	60
Figure 5.20. Comparison between the average grain sizes of the three weldment groove shapes through the HAZ area of AISI 1045 steel	61
Figure 5.21. Pre-heating process and martensite microstructure view of HAZ area for the butt V-Shape groove weldment of the AISI 1045 steel	62
Figure 5.22. Pre-heating process and martensite microstructure view of HAZ area for the butt U-Shape groove weldment of the AISI 1045 steel	63
Figure 5.23. Pre-heating process and martensite microstructure view of HAZ area for the butt double V-Shape groove weldment of the AISI 1045 steel.....	64
Figure 5.24. Distribution of average grain size for V-shape welding groove at the mid transverse direction of the welding line through the HAZ for different states of preheating	65
Figure 5.25. Distribution of average grain size for U-shape welding groove at the mid transverse direction of the welding line through the HAZ for different states of preheating.....	66

Figure 5.26. Distribution of average grain size for double V-shape welding groove at the mid transverse direction of the welding line through the HAZ for different states of preheating	66
Figure 5.27. Distribution of hardness of the V-shape welding groove at the mid transverse direction of the welding line through the HAZ for different states of preheating	67
Figure 5.28. Distribution of hardness of the U-shape welding groove at the mid transverse direction of the welding line through the HAZ for different states of preheating	67
Figure 5.29. Distribution of hardness of the double V-shape welding groove at the mid transverse direction of the welding line through the HAZ for different states of preheating	68

LIST OF TABLES

Table 4.1. Chemical composition of AISI 1045.....	24
Table 4.2. Mechanical properties of AISI 1045	24
Table 4.3. Thermal conductivity and temperature as a function of carbon content for AISI 1045steel	31

LIST OF SYMBOLS

SMAW	Shielded Metal Arc Welding
FEM	Finite Element Method
WP	Weld Pool
BS	Base Metal
HAZ	Heat Affected Zone
FZ	Fusion Zone
MPZ	Molten Pool Zone
TTT	Time Temperature Transformation
M_s	Martensite start
M_f	Martensite finish
TIG	Tungsten Inert Gas
CCD	The face-centered central composite design
RSM	Response Surface Methodology
VCCM	Virtual Crack Closure integral Method
JAEA	Japan Atomic Energy Agency
SCC	Stress Corrosion Cracking
C	Carbon
Fe	Iron
Mn	Manganese
P	Phosphor
Si	Silicon
Cu	Copper
Ti	Titanium
S	Sulphur
Cr	Chrome
Mo	Molybdenum
W	Tungsten

V	Vanadium
HAA	Heat Affected Area
AISI	American Iron and Steel Institute
HV	Vickers Hardness
HRC	Rockwell diamond Cone Hardness
ISO	International Standard Organization
ASTM	American Society for Testing and Materials
HD	High Definition
PC	Personal Computer
USB	Universal Serial Bus
T_k	Temperature at k_{th} sampling point (Temp)
ξ	The volume fraction transformed
t	Time, sec
k, n_1	Constants of phase transformation
n	Avrami number
a_2	Strain constant
d_0	Initial grain size, μm
MVF	Martensite Volume Fraction
H_O and K_H	The appropriate constants associated with the hardness measurement
a, a_1 , b_1 , b_2	Grain AISI 1045 steel constants
c_1 , Q_1 , Q_2 ,	Grain AISI 1045 steel constants

CHAPTER 1

INTRODUCTION

Shielded metal arc welding (SMAW) is one of the popular welding methods, which sometimes called manual metal arc welding, that informally known as stick welding. In this process consumable electrode coated in flux is used for joining parts. Until the end of the 19th century there was only forged welding process, which blacksmiths had used to join iron and steel by heating and hammering. In the early 20th century welding technology advanced very quickly because the World War 1 and World War 2 covered the demand for durable and the cheapest joining methods.

Through welding joint, the induced thermal cycles visualized in accordance with the movement of heat source with altered physical state, metallurgical transformation in the phase, and ran over thermal stress and metal motion. When welding is done, the finished product may determine physical interrupt which is the result of the excessively fast solidification, or reverse microstructures that are caused by cooling circumstances, or residual stress and distortion. Which cause to take out of heterogeneous plastic strains [1, 2]. The test methods can be applied to destructive and non-destructive to determine the quality of a large number of welded components. These tests may also use in finite element package simulation to predict the life and preventing from the deformation effect of the remaining pressure in the component that allows evaluation function of simulation; because it would be least expensive test that could be done by computers which undoubtedly reduces the costs. This is very complicated, and therefore it may become more real to simulate the engineering application than the submission of validating results experimentally [3].

Finite element method (FEM) is a method for solving the differential equation or complementary functions. It is presented with a number of natural problems; those could be solved by the ruling of available differential equations.

The way includes the assumption of piecewise continuous function as essential to resolve the problems and get the parameters of functions in a manner of reducing the errors in the solution. Modelling and simulation is becoming appreciated tools in the manufacturing design, with the objectives to reduce exhaustive pre-study experiments and costs. Moreover, the microstructure modelling is designed to be integrated in a thermo-mechanical model of the process [1, 4]. The deformation, heat transfer, phase transformation, and diffusion are coupled with each other in DEFORMTM simulations. Also it is capable of modelling of microstructure evaluation [1, 5]. On the other hand, the average grain size of the fusion zone (FZ) of the heat affected zone (HAZ) is in this consideration to validate and predict the material properties in the mechanical tests, because after welding process, the solidification and the grain structure of the heat affected zone (HAZ) sometimes has a significant effect on the crack formation [6].

There are many studies for FEM welding process in the case of analysing welding residual stresses and deformation due to welding thermal cycle effect. This finite element analysis for solving welding simulation is accepted as a complex thermal Elasto-plastic problem. While some were studying multi pass effects on the residual stress for the simplified fillet welds, meanwhile others studied the effect of the welding groove shape on the residual stress in butt welded pipes. Only few studies discussed welding effect on the microstructure evaluation and transformation on different kind of materials in the HAZ area.

This thesis covers literature survey of evaluating the microstructure of the HAZ area on the butt welded parts of AISI 1045 steel structure. According to its carbon content AISI 1045 steel is a member of the medium carbon steel families. Due to its critical treatment in the welding process and its wide use in the manufacturing processes, this study is carries out the solution of the problems and the defect which occurred during cooling process in the heat affected zone (HAZ) after the welding process in still air cooling process. Medium carbon steel structure AISI 1045 mainly used for automotive parts, building structures, bridges etc... Brief information about shielded metal arc welding (SMAW) process and finite element modelling would be given in Chapter 3. Experimental and modelling procedure definitions for the shielded metal

arc welded part would be explained in the Chapter 4 with related appendices. The experimental study and the modelling results would be discussed in Chapters 5 and 6. Eventually, the modelling results would be verified by the experimental results in comparison with the results of the hardness test and the microstructure evaluation with the average grain size. After the validation of our results have been submitted, it would be proceeded with the other steps of the modelling study in a different manner of pre-heating process and the three types of butt welding groove shapes.

CHAPTER 2

LITERATURE REVIEW

2.1 Introduction

The heat source of the welding process for joining the two parts and the cooling time are important factors that affecting to the significant changes in the microstructure and the grain size of the material. Also according to the cooling rate process, the hardness of the steel which is mainly depend on the carbon and alloy content, effects on the tendency of transformation from austenite to martensite. Therefore, researchers in general concerned with the investigation of studying these parameters by using different type modelling programs. This chapter includes a brief summary of the previous studies. Review of studies is used in investigating the residual stress by the effect of the groove shape, number of passes and different type of welding process. Also studies of the 2D and 3D modelling are presented.

2.2 Studies on Effect of the Welding Heat on the Residual Stresses and the Cracking

Te-Chang Tsai, et al. [7] have presented finite element modelling and analysis of the changes of the physical properties of the magnesium alloy which is joined by the tungsten arc inert gas (TIG) welding, due to the effects of heat treatment. The heat treatment process was for adopting in the tempering processes with different parameters like tempering time and temperature. An experimental work was used to evaluate and explore the mechanical properties and microstructure of the welding joint in the characteristic consideration. The face-centered central composite design (CCD) on the base of the response surface methodology (RSM) is required to take out the experimental work and a plan. The comparisons of experimental data with the (ANOVA) analysis variance results indicated that the mathematical models for elongation and the maximum tensile strength are almost tantamount with the

experimental results, which is about 95% confident. Two main microstructures hcp- α -phase Mg and BCC- β -phase Mg₁₇Al₁₂ are displayed the microstructure of the welding joint in the welding pool during tempering process. As a result, it is indicated that the average grain size and proportion for α -phase Mg decreases with increasing time and temperature of the tempering process. In the same manner, the average size and proportion of β -phase Mg₁₇Al₁₂ grains increase and affect the increase of the maximum tensile strength and elongation.

Guodong Zhang, et al. [8] have investigated to evaluate residual stress and temperature by using finite element models. It was about the creep damage in the welding process by using the finite element code (ABAQUS). The simulation of the creep damage and the welding residual stress of a tube that made of Cr5Mo steel were done. This method had discussed the residual stress effect on the creep damage, which provided as a reference by computing complex residual stress distribution, stress relaxation, and creep damage. As a result, they have noticed that at the initial stage the residual stress of the welding became very large, but at high temperature it relaxed in a short time. Due to the great effect of the welding residual stress which provides life prediction for the design with a high temperature component, the welding residual stress mainly reported to figure out the distribution of the damage and creep.

Masanori Kikuchi, et al. [9] studied on the thermal and residual stresses which cause the formation of the crack growth, by using S-Version FEM (S-FEM). Because the local mesh should be re-meshed they noticed that (S-FEM) technique's crack growth simulation was easier. The crack path modelled easily, because the combination of an auto-meshing with the local meshing technique re-meshed automatically. At the crack tip the energy release rate computed by using Virtual crack closure integral method (VCCM). Combined mode loading condition was used for computing and analysing the rate and the crack growth direction. Through the previous published paper analysis, the similarities and differences were done to the validity confirmation of this analysis and the corresponding which they obtained. The Japan Atomic Energy Agency (JAEA) based data on the numerical simulation of their residual stress provided and a pipe conducted in two dimensional and three dimensional field of stress corrosion cracking (SCC) growth were analysed. The axisymmetric and

non-axisymmetric distributions of the residual stress of the pipe wall in the two cases were noticed then the effects on (SCC) cracking were computed and discussed.

Z. Barsoum, and A. Lundbäck [10] have illustrated the two and three dimensional simulation of finite element welding implements. From the consideration of the welding component of a fillet weld T-type is widely used for the heavy cart machine manufacturing. The plate thickness of 8 mm to 20 mm used consequently. The MSC. Marc and ANSYS software's are used for welding simulation. The main aim of this consideration is to figure out the residual stress formation in the 3D effect in the welding process. Furthermore, by using contact models and solid models, welding simulations in the un-fused roots were carried out as an implement consideration of the effects with respect to the residual stress. By using x-ray diffraction technique on the T welded structure, the measurements of the residual stress were measured. After result comparisons of the case in 2D and 3D welding simulation procedure for residual stress measurement, they have illustrated that the 2D welding simulation showed close and better agreements with the experimental results. It was more suitable for fatigue crack growth analysis and other welding defect action which forms the weld toe and un-fused root.

2.3 Studies on the Effect of Groove Shape on the Residual Stresses, Microstructure and Distortion

I. Sattari-Far, and M.R. Farahani [11] have studied the thermo mechanical behaviour and residual stresses in butt welding of pipe by using the finite element package. According to the hole drilling method, the welding residual stress was measured. The validity and accuracy of the result of the finite element package were taken to the consideration and compared with the experimental work measurements. The accuracy of the finite element modelling is developed. They have studied on the effect of the number of passes and the groove shapes on the welding residual stress for the butt welded pipes. In 6 mm and 10 mm pipe joint, the axial and hoop residual stresses in different groove shapes were considered. This study proves that the amount of residual stresses and the distribution have significant effects on the welded pipes.

D. Akbari, and I. Sattari-Far [12] illustrated the analysis of the residual stresses and thermo-mechanical behaviour of different kind of butt welded pipe by using finite element software. The validity and the accuracy of the results of the residual stresses of welding pipe and the experimental work depended upon the hole drilling method were compared. The measured results of the experiment were close enough to the results which are carried out by the finite element model. According to this consideration, the explored finite element modelling was used on butt welded pipes which were fabricated of ferritic and austenitic steels to analyse the cause of welding heat on the residual stress distribution and its magnitude. In this study the V-shaped groove butt welding of the various kind of pipes with 8 mm thickness, the hoop and axial residual stresses are carried out. In this consideration, it is clarified that the heat of the welding process has a significant effect on the residual stresses as in magnitude and distribution on the stainless steel side welded pipe joint.

V.K. Goyal, P.K. Ghosh, and J.S. Saini [13] have investigated by using two types of heat sources in the different manner to predict the temperature and geometry of the weld pool by using finite element model. The view of pulsed current gas metal arc welding (P-GMAW) has a critical effect on the thermal and metal transfer behaviour. Its effect depends on the pulsed parameters' influences. The finite element model considered for addition to arc heating initiation and the heat impact to the filler metals makes droplets and depositing in the weld pool. Heat transfer modelling was assumed basic arc welding pool primary heating consideration as a constant heat source (Arc heat source) of the double nature of the ellipsoidal followed leaving heated filler metal considered as a point heat source of droplet parts trapped on the first one. Variable analysis techniques were used for two different source of heating to compute the temperature distribution in the HAZ and weld pool. The weld pool shape calculated by the estimated weld isotherms that caused the base metal to melt because of the two heating sources effected on the weld pool. The impinging droplets which collapsed on the weld pool has been analysed to estimate whether the droplets transport its heat into the depth. The experimental work carried out the value of the predicted weld pool shape and temperature effect on the HAZ region with $\pm 10\%$ deviation in comparison with the finite element modelling value. The weld deposition of Al-Mg alloy happened especially when high current of the welding of 180A along with the current transition of the filler rod occurred. Nevertheless, this

consideration analysis for the predicted weld pool shape and temperature was relatively different in lower current condition 150A under the transient current of the filler rod.

Dean Deng [14] preferred both the low and medium carbon steels to study the phase transformation of welding residual stress and the distortion. ABAQUS codes of finite element modelling are applied to the coupled thermal, metallurgical and mechanical 3D. In this study, the above mentioned numerical modelling used to evaluate the fractions of the martensite formation for the fusion zone and the grain size of the HAZ region. The coarse and the fine grained HAZ respectively evaluated by using different continuous cooling transformation diagrams. The volume change on the final residual stress and distortion of the welding are carried out and analysed because of the effect of the transformation of the austenite to the martensite. The modelling results for the two materials are clarified and noticed that the final residual stress and the distortion of the welding are not influenced by phase transformation in the low carbon steel. However, the situation was different in the same manner of medium carbon steel, because it has been significantly affected by the phase transformation to martensite.

CHAPTER 3

WELDING AND FEM MODELLING

3.1 Introduction

In this chapter, shielded metal arc welding (SMAW) and finite element application methods are described briefly. SMAW is considered according to the process of working; electrode covering function and the advantages and disadvantages of the welding process has also been explained. The function of the groove shapes, the microstructure transformation and the grain size of the HAZ and welding defects have been discussed and described.

3.2 Shielded metal arc welding (SMAW)

3.2.1 The Process

The Shielded metal arc welding (SMAW) is the process that melts and connects metals by the heating source with an arc produced between a sticklike covered electrode and workpiece, as shown in Figure 3.1. It generally called as *stick welding*. The gripper of the electrode is connected with a welding cable to one terminal of the power source and the specimen or to the contact place with the workpiece which is connected by another cable to the power source Figure 3.1a. The covered electrode wire passes the electric current to the arc and provides filler metal for the fusion. The top 1.5 cm of the core is free from the cover and is gripped by the holder for the electrical contact. The shielded metal arc welding holder is generally safe and very easy to clamp metals which are insulated of out shelling to prevent electric risks for the welder man. Both the core wire and the flux covering at the electrode tip melt off as droplets continuously because of the arc heat Figure 3.1b.

The molten metal combination which is satisfied by collecting the molten filler in the weld pool solidifies welds metal. While the light molten flux floats up on the pool surface and it would be solidified into an inherent slag slice at the surface of the weld metal [6].

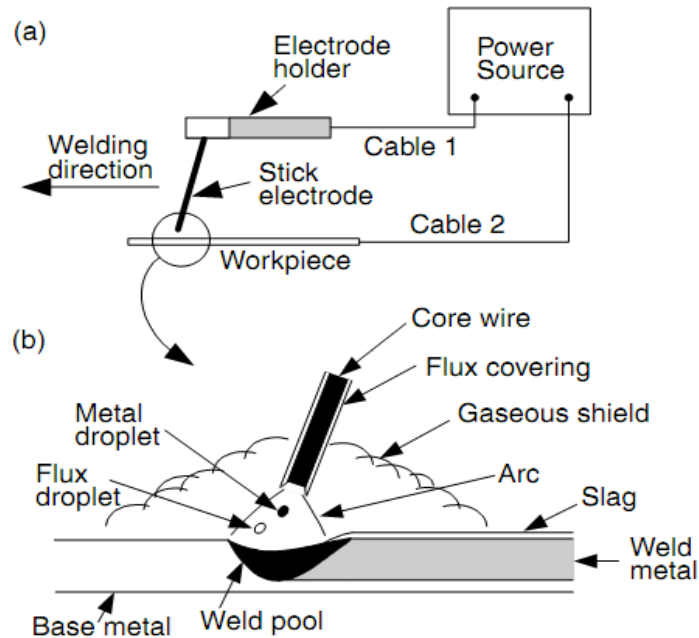


Figure 3.1 Shielded Metal Arc Welding process: (a) overview of the process; (b) the enlarged welding area [6].

3.2.2 Electrode Covering Functions

The electrode covering includes different chemicals within and even metal powder in order to perform one or more than one of the functions mentioned below:

A. Protection It makes adequate preparation for protecting the molten metal from the air by a gaseous shield. For a *cellulose*-type of the electrode, the covering holds cellulose within, $(C_6H_{10}O_5)_x$. The biggest amount of gas mixture of H_2 , CO , H_2O , and CO_2 comes out or produced when cellulose in the covered electrode decays and heated. On the other hand, for $(CaCO_3-SMAW)$ a limestone type electrode, CO_2 gas and CaO slags exist when the limestone is extracted. The limestone electrode types are frequently used for welding of medium carbon steels and high strength steels, because of its hydrogen cracking sensitivity. Generally this type of electrode also

called low hydrogen electrode type, because it produces a gaseous shield in low hydrogen.

B. De-oxidation; It makes adequate preparation during the welding process, like deoxidizes and fluxing agent to cleanse and deoxidize. The produced solid slag over the fusion zone area is also protected, but it has still hot welded metal from oxidation.

C. Arc Stabilization It is available to use during welding the arc stabilizers to stable the arc process. The electrical current conduction is done by the help of the arc which is an ionic plasma gas. The unified arc stabilizers help like potassium oxalate and lithium carbonate readily help to decompose into ions in the arc. They also help to increase the electrical conductivity of the arc and provide the conduction of the current more smoothly during the welding process.

D. Metal Addition: During the welding process it makes adequate preparation for metal powder and alloying elements in the weld pool. Although, it is provided to control the composition of the welding process metallurgy, the latter it provides the increasing rate of the deposition in the welding process [6].

3.2.3 Advantage and Disadvantages

The device of the welding is not complicated. It is a portable and inexpensive device in the comparison with the other arc welding processes. SMAW generally used for maintenance by repair elements, and in the field of the construction. However, the gas shields in SMAW are not clean enough for the reactive metals as aluminium and titanium. The exceeded high welding current cause the falling off and the deposition of the electrode covering which is ranged according to the overheats. The interchangeable electrode's length is around 35 cm, and the overall production rate is reduced far enough in this situation [6].

3.3 The multi-physics of welding

Welding process modelling is a combination of multi-physics problem. Modelling of the welding process is divided into four domains of this problem [15]:

- Flow of the heat and fluid;
- Heat source –metal interactions;
- Microstructures of weld solidification;
- Phase transformations.

Analytic heat input models are categorised as: generation models and the types of heat input models [16]. The biggest generation models are the different type of multiphase models. Every single higher generation includes more physics problems. Examples of different phenomena involved in welding are shown in Figure. 3.2. Modelling should be accounted for high-pressure arc physics, fluid flow, heat transfer and conduction, and deformation. The setup of the modelling for the energy calculations in an arc [17, 18, 19] is shown in Figure 3.2.

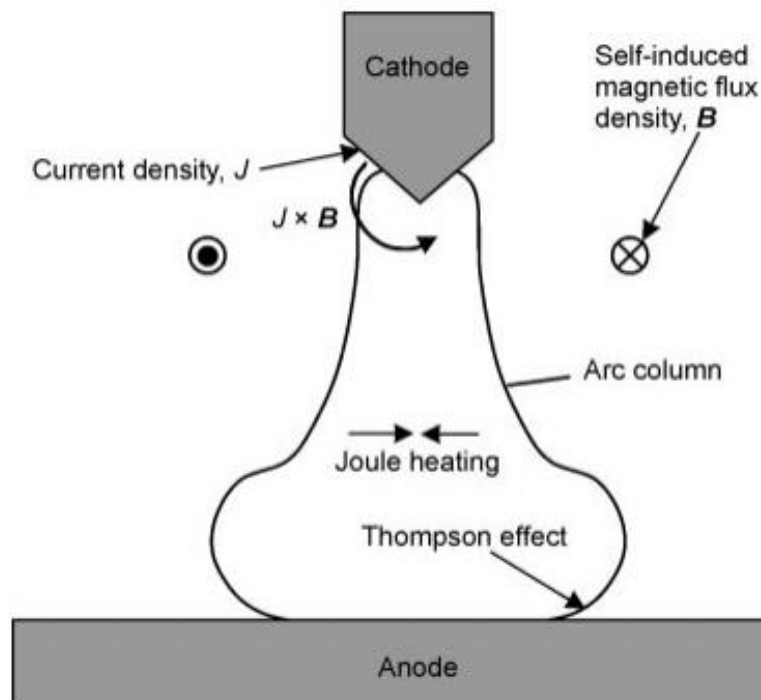


Figure 3.2 High pressure Arc model for flame where the weld is considered rigid, adapted from Ramirez et al [17, 18, 19].

Heat conduction, convection and radiation are found in the modelling together with the contribution to energy generation from different phenomena such as Joule heating and the Thompson effect [20]. Progressed models for predicting energy distribution which is coupled to the fluid flow are available [21, 22]. The fluid flows with driving forces are comprised in this type of model as shown in the Figure 3.3. The prediction of the shape of the weld pool may also include the effect of redistribution of surfactant parts [22, 23].

Welding process models (WPM) for prediction of the heat generation and distribution in the weld pool that comprises the physics problem and combines all welding process parameters together.

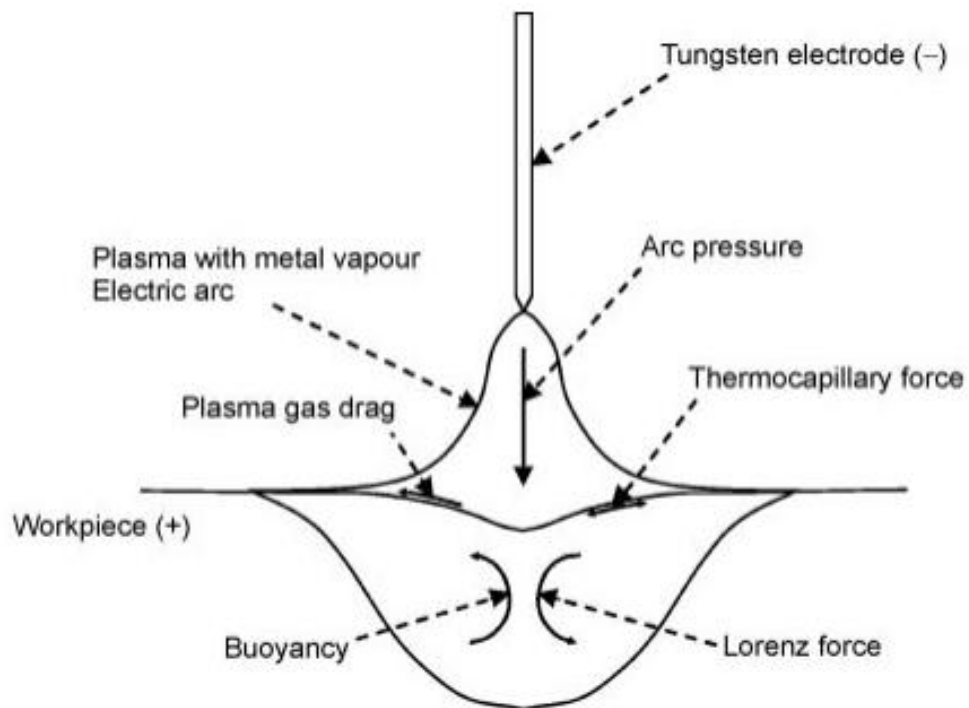


Figure 3.3 The fluid flow driving forces in weld pool including models of plasma, adapted from Pavlyk and Dilthey [24, 25].

During the welding process modelling, the joining between the parts would be done by the grooves and fillings. These groove shapes tend to equalize the metal volume and heat distribution for processing out the results for consideration of the shrinkage and the thermal expansion in FEM [26, 27].

3.4 Welding grooves and types

Arc welding process includes different kinds of groove shapes which are popular in the welding process [28, 29]. It is possible to describe the majority of the contemporary welds. They are known as “groove” or “fillet” weld [30, 31]. A groove weld is produced when the two sides or ends of the pieces are welded together. The shapes of the sample ends that are welded together during the welding process determine the regarded name for a groove weld [32, 33]. The following set of the groove shape is shown in the Figure 3.4.

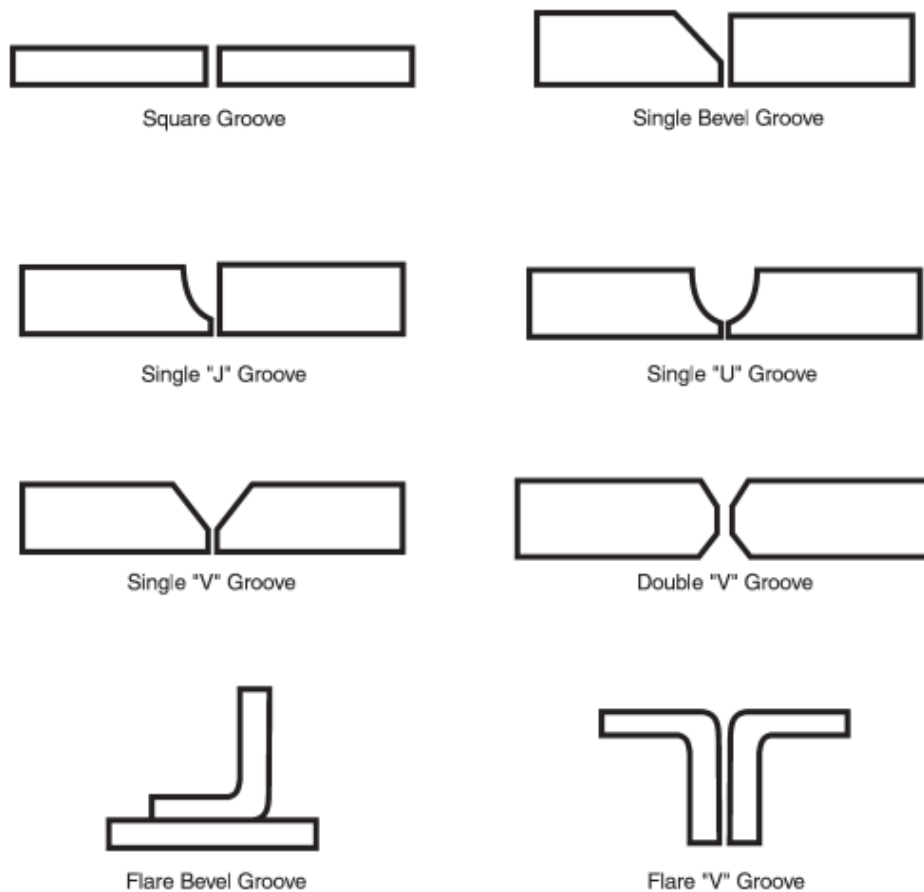


Figure 3.4 The common types of groove welds [33].

3.5 Recrystallization and grain growth in welding

The hardening effect of the work completely disappears in the fusion zone; because of the partial lost in heat affected zone and the melting, the grain growth and the recrystallization. The strength losses of the structural designs involved by welding should be in the consideration [6]. The Heat Affected Zone (HAZ) directly associated with the Fusion Zone (FZ) in the joining and this can be seen on the side of the deposit at the junction with the base plate. The following Figure 3.5 shows the changing in the grain size and microstructure transformation from the unaffected plate to the HAZ [34].



Figure 3.5 Base plates and Heat Affected Zone (HAZ) [34].

3.6 Steel microstructure and TTT diagram

The described welded joint consists of a molten pool zone (MPZ), a fusion zone (FZ) and heat affected zone (HAZ). The (HAZ) is defined as the part of the metal that does not melt, but its material properties or microstructure transformed and changed by the cause of the heat of the welding [35]. (HAZ) zone are subdivided or indicated by the region 4 to 1 in the Figure 3.6 shown below:

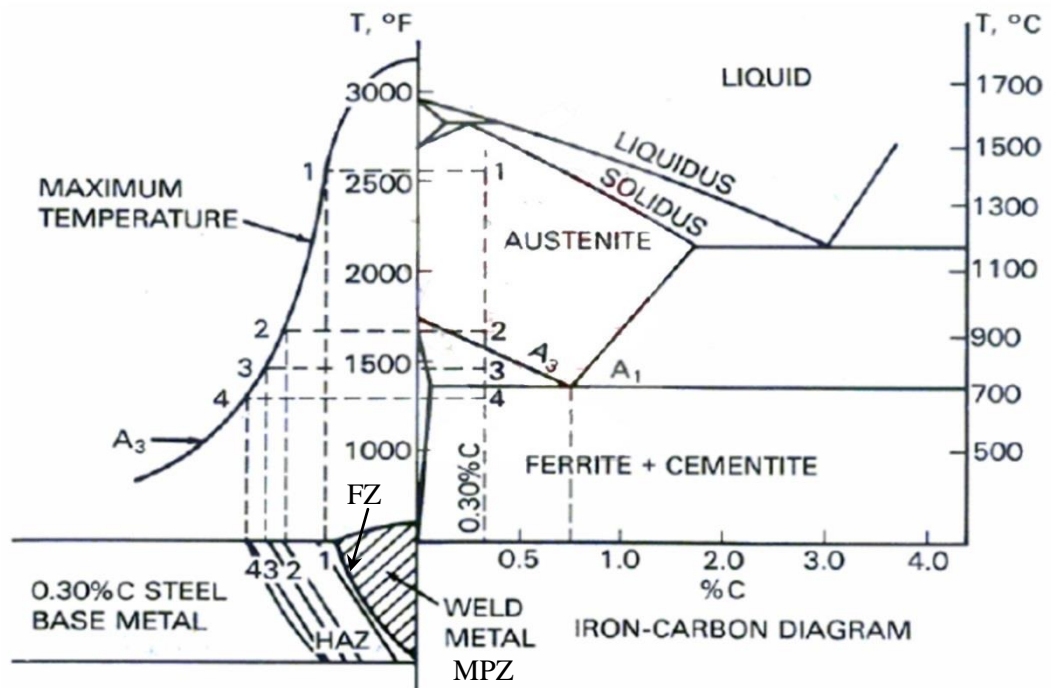


Figure 3.6 Phase diagram for 0.30% C steel during welding [35].

On the other hand, under the certain and different transformation temperatures, bainite is formed during the welding process rather than pearlite. It is clearly shown in the Figure 3.7. Generally, the transformed microstructure is increasingly become fine-grained, when the transformation temperature is decreased. The nucleation rate is increased when the diffusivity and the temperature decreases. The solid curve on the left side indicates nearly 1% completed onset of the transformation. The dashed curve indicates the 50% completion. The solid curve on the right side indicates the effect which occurs when the transformation is nearly 99% completed. This convention is used in subsequent of the Time Temperature Transformation (TTT) diagrams. Furthermore complete (TTT) diagram for eutectoid steel is given in Figure 3.7. The different stages of the time-independent (or less diffusion) martensitic transformation are shown in the horizontal lines. M_S indicates the start, M_{50} indicates the 50% of transformation, and the M_{90} indicates the 90% transformation for the martensite [36]. On the other hand the (TTT) diagrams, affected by the alloying elements (Cr, Mo, W, V, etc.), have considerable influence on the kinetics and mechanism of all three types of transformation of austenite to pearlite, bainite and martensite [37].

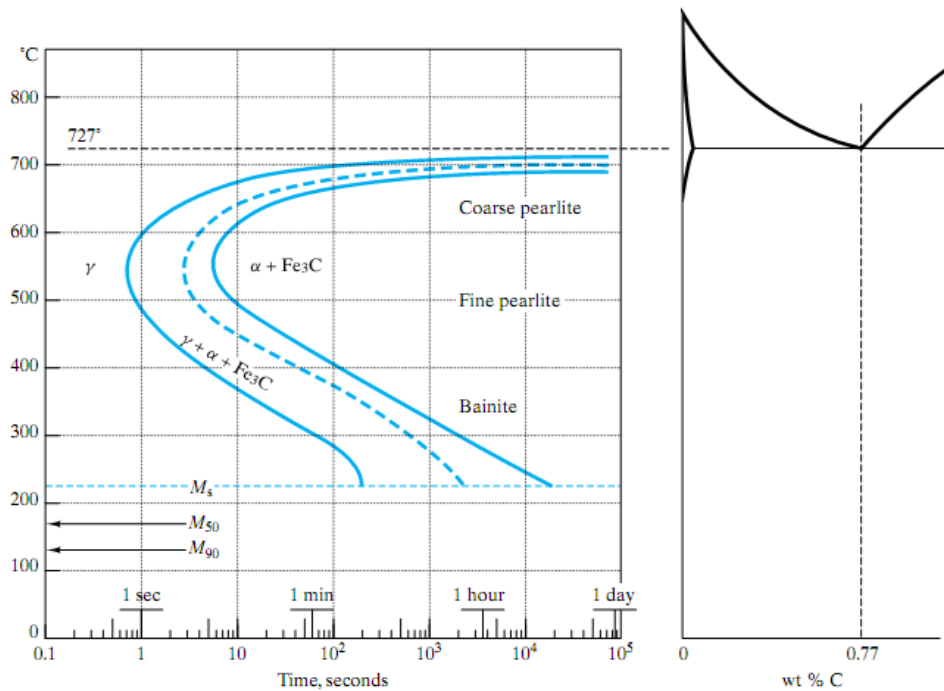


Figure 3.7 (TTT) diagram after Isothermal Transformation and Fe-C diagram for 0.30% C steel [36].

3.7 Welding defects

Cracking induced that occurs in the heat-affected zone (HAZ) is always classified or divided as sub-solidus cracking, because it is the equilibrium solidus temperature that describes the extreme high-temperature of the (HAZ) zone. However, most of such cracking is also generally identified as cold cracking. In such a cracking, the event begins after the solidification is completed and the material has cooled down to room temperature. The liquation cracking that involves tearing along liquated boundaries which is formed below the equilibrium solidus as a consequence of the non-equilibrium heating is an exception. However, other liquation cracking which involves liquid films is really a hot induced cracking, and it can be evaluated by using the hot-cracking weldability tests just described [38]. Sub-solidus and solid-state induced cracking in the heat-affected zone (HAZ) region can be in three general types:

1. Hydrogen-induced cold, or delayed cracking.
2. Postweld heat treatment or reheat or strain-age cracking.
3. Lamellar tearing.

Figure 3.8 illustrates the different types of cracking on the Heat affect zone (HAZ) and Fusion zone (FZ) and clarified subdivided heat affected zone (HAZ) regions.

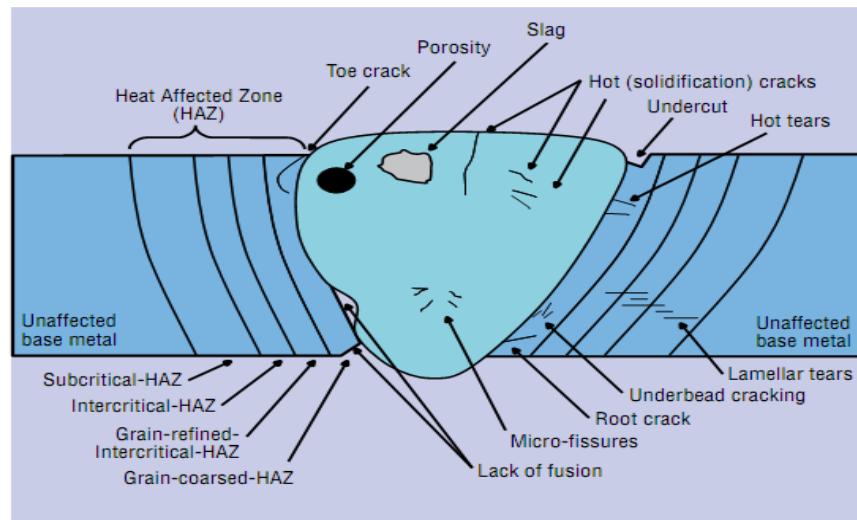


Figure 3.8 Welding Defects with sub-divided heat effected zones [39].

3.8 Finite element application method for welding

Modelling is used as design tool or manufacturing analysis tool for welding processes. FEM computation is useful for the feasibility of design as the phase concept. It is also useful for minimizing the welding distortion and defects by modelling, evaluation of manufacturing analysis tool, fixed designs, different welding processes and sequences [40]. Computational welding mechanics aim to find out useful methods and models for dominating and designing of welding joint processes to figure out the appropriate and feasible mechanical performance of the welded component or structure. It is related to the topics ranging from the generation of the heat and weld pool phenomena and the flow of the heat to the thermal stress and distortion. The physical material and the necessary essential modelling components in welding processes are supplied due to the thermal cycles during welding. The computational welding mechanics model can be coupled with models for microstructure evolution. Other features that are enable the prediction of microstructures like cracking phenomena and other specific phenomena on distortion and the temperature of the material. The heat generation processes are the centrepiece of the welding simulations. Its description related to the domain of thermo mechanics in case of the explosive welding, friction welding and friction stir

welding. Modelling in welding processes focuses on the physics of the heat generation.

Computation welding mechanics models, start with a given heat input that focus on the larger scales and the detail of the heat generation process. On the other hand the heat input model is calibrated with respect to experiments or obtained welding process modelling. Therefore, the classical computation welding mechanics models have some limitations on their predictive power when they used to solve different engineering problems. For example, they cannot prescribe what penetration a given welding procedure will give. The appropriate procedure to determine the heat input model is therefore important in computation welding mechanics [4]. It can evaluate different design concepts when the power of computer models is applied. Furthermore, the more established simulations exist in a given field, the less validation testing is needed. However, more demands are placed on determination of material properties and boundary conditions needed for the computational model[1,4].

3.9 General processes and steps of the Finite Element Method FEM

In general, the finite element method and the finite element formulation of the microstructure evaluation are similar procedure with the other problem of finite element methods [1]. Finite element analysis steps are as follows:

1. Pre-processor; which includes number of steps and mesh generation.
2. Security for gathering system of equations, to evaluate different matrix elements and vectors.
3. Implementing the boundary conditions.
4. Finding a solution of the linear system of equations.
5. Post-processor; which is the final part of the simulation start.

3.10 Linear differential equation for FEM formulation

Usually there are two types of differential equations which are subjected to the boundary conditions; the essential boundary conditions and the natural boundary conditions, where the linear differential equation has the following form:

$$Lu + q = 0 \quad (3.1)$$

Where:

u: Vector of primary variables of the problem, in the functions of the coordinates.

L: Differential operator.

q: Vector of the known function.

Essential boundary conditions are the arrangement of the boundary conditions in orders to adequate the differential equations completely. The natural boundary conditions are caused to be concerned with higher order derivative terms and are not suitable for finding a solution of differential equation completely. It needs the smallest degree of the essential boundary condition.

Meshing is very significant task of the pre-processor part. It can require a big period of time for the one who analyses. Generally an experienced examiner will harvest more confident mesh for a complex problem. The domain should be meshed correctly into elements of a suitable purpose shapes like triangles and quadrilaterals. It exists only in the mind to have a fully automated meshing generation, but at present this is unluckily not ready to use in the market. Fortunately, there is a semi-automatic pre-processor which is valid in the greatest extend for the commercial application software package, such as DEFORMTM. In addition, there are packages designed principally for meshing. A similar kind of package can be generated from the files of a mesh that can be read by other simulation and modelling packages. Triangular elements are the main flexible and well-recognized way of creating meshes, and it's available in fully automated for two dimensional and three dimensional planes. The modelling of complex geometry shapes and its boundaries are suitable to use triangular elements. [41].

Specifically, in the post-processor section, advanced and modern graphics permit a wide different scale of output for visualization of the analysis results, and it gives the user a finite element package to select the best and suitable output analyses according to their demands. Particularly, in many computer aided design packages the finite element methods are found at the heart of the package. The characteristic pictures of the output can be found in the reference. This process unit has been advanced very quickly. Because at the present ,finite element packages are suitable to simulate the vibration of the structure ranging from the bridges and musical instruments and of fluid flow around aircraft and racing bicycles [42].

3.11 Two-dimensional vs. Three-dimensional Modelling

Sufficiently fine meshed 3D-FEM permits to model the heat flow as precisely as the material properties and prepared model with the most reduced errors for temperature input, convection and radiation of heat transfer parameters [43]. Existed thermal analyses those came out from the use of three-dimensional finite element methods (3D-FEM) are not taken into the consideration as a standard modelling guide in the welding process. But it is loss of time and intensive resource. The selection of suitable models for weld analysis, the analyst must level the accuracy against the cost. In two dimensional finite element methods (2D-FEM) of cross sectional models, the temperature flow is restricted in the plane of the plate. The 2D-FEM models can get precise results for plates. Excepting the cross sectional plane, assuming of the temperature distribution can provide a functional and economical approximation for many welding situations. The results of a low- cost cross sectional analysis can be used in designing an effective mesh for more complex models [40]. 2D-FEM provided precise results for predicting residual stresses. Sometimes the large structures may buckle due to the parallel residual stresses formations of the welding direction. The 2D-FEM models generally cannot analyses buckling caused by longitudinal residual stresses, while the 3D-FEM thermo mechanics modelling of a large structure can represent this distortion mode [44]. Earlier studies on weld response were limited with 2D-FEM cross sectional modelling. Most of the researchers had shown that very good correlations were found between numerical predictions and experimental results for different type of modelling software. Residual stress predictions in 2D-FEM modelling provided very precise evaluations

in comparison with the 3D-FEM modelling, since the stress field exhibits a uniform distribution through the length of the work piece [45]. These models have been especially useful for its high efficiency and accuracy in computing the solution in the analysis plane and decreased computational demands. The 2D-FEM does create inaccurate results where the tack welding or fixturing can permit the plane movement. Longitudinal direction of welding temperature distribution, instability of the sides and end executes cannot be realized in the cross-sectional 2D-FEM formulations. A numerical analysis technique can be used for the prediction of welding distortion by combining the in-plane 2D-FEM welding simulation with the 3D-FEM structural analysis in a decoupled analysis approach [40]. At the beginning, a 2D-FEM welding simulation of the portion had to be performed to evaluate the residual stress; meanwhile a 3D-FEM structural analysis can be performed on all of the structures, by using the residual distribution of the welding simulation as loading. The shell element can be used to model the thermal welding process when the temperature distribution gradients through the thickness of the plates are lowest in the 3D-FEM analysis. The simplicity and efficiency of the determination become from the advantages of the decoupled approach, because this approach is very beneficial for the estimation of the initial design and modifications without any demand for extra welding simulations. While some others assumed complete penetration welds at every joint by using 2D-FEM shell element [46], another one supposed that, the temperature distribution gradient through the thickness in the Z direction of the plate was zero. The error in the model becomes higher when the temperature flow in the Z direction is high. On the other hand, the 2D-FEM analysis does provide useful data away from the weld in the plate. It allows variations in modelling geometry and temperature source to be analysed precisely and more economically [43]. Using a simple 2D-FEM model is useful to identify and solve problems that would have been occurred in the 3D-FEM models with a minimum time requirement.

CHAPTER 4

FE MODELLING AND EXPERIMENTAL STUDY

4.1 Introduction

This chapter includes the detail descriptions of the experimental works and the finite element methods of the DEFORMTM 2D-FEM, of the mathematical modelling. The experimental work was done in the Department of Mechanical Engineering at Gaziantep University, except the test of the SPECTROMAX 3 x material analyser machines for the chemical composition of the material was done in the Mechanical Engineering Department of Salahaddin University in IRAQ. Properties of the technical work of preparation of the specimen for the shielded metal arc welding process and testing are explained in this chapter. On the other hand the detail mathematical modelling and the definition requirements for the selected metal data in the DEFORMTM 2D-FEM are described.

4.2 Material selection

AISI 1045 steel, is a medium carbon steel which is widely used as in engineering applications such as; structural works, machine parts, gears studs, axels, cold extrude, etc... Thus; in the most cases parts are welded together to form permanent joints, but unfortunately, due to its amount of carbon content, martensite phase transformation occur and sometimes is liable to form hydrogen cracks in the heat affected zone HAZ and may cause brittle failure of the joint. For this reason, AISI 1045 steel provided for experimental work to prepare a specimen 12 mm in thickness to validate modelling results and proceeding this modelling with three different types of butt welding groove shapes: V-shape, double V-shape, and U-shape for butt welding.

The chemical composition has been carried out by using SPECTROMAX 3 x spectrometer metal analyser. The results of the measured chemical composition and taken mechanical properties of the material are given in Table 4.1 and Table 4.2 respectively.

Table 4.1 Chemical composition of AISI 1045

C %	Fe %	Mn %	P %	Si %	Cu %	Cr %	Ti %	S %
0.41	98.31	0.849	0.0005	0.161	0.0119	0.0323	0.0005	0.008

Table 4.2 Mechanical properties of AISI 1045 [47]

Vickers Hardness test HV	252
Ultimate Tensile Strength	565 MPa
Yield Tensile Strength	310 MPa
Elongation at Break (in 50 mm)	16 %
Reduction of Area	40 %
Modulus of Elasticity (Typical for steel)	200 GPa
Bulk Modulus (Typical for steel)	140 GPa
Poisson Ratio (Typical for steel)	0.29
Shear Modulus (Typical for steel)	80 GPa

4.3 Experimental work

The main purpose of doing the experimental work and test is to validate the results of the finite element modelled part as a sample of the work to proceed in a different case of simulation. For this reason one sample has been taken into account which is single V-shaped butt weld groove for the AISI 1045 steel. According to the specification which is given in the ISO 9692 standard [48], as it is shown in the Figure 4.1 the groove has been prepared. In Shielded metal arc welding SMAW process, there are many specifications depending on like; the kind of the material that is in use for joining, electrode type and welding circumstance that have been considered in this work, where the experimental work was covered by the following;

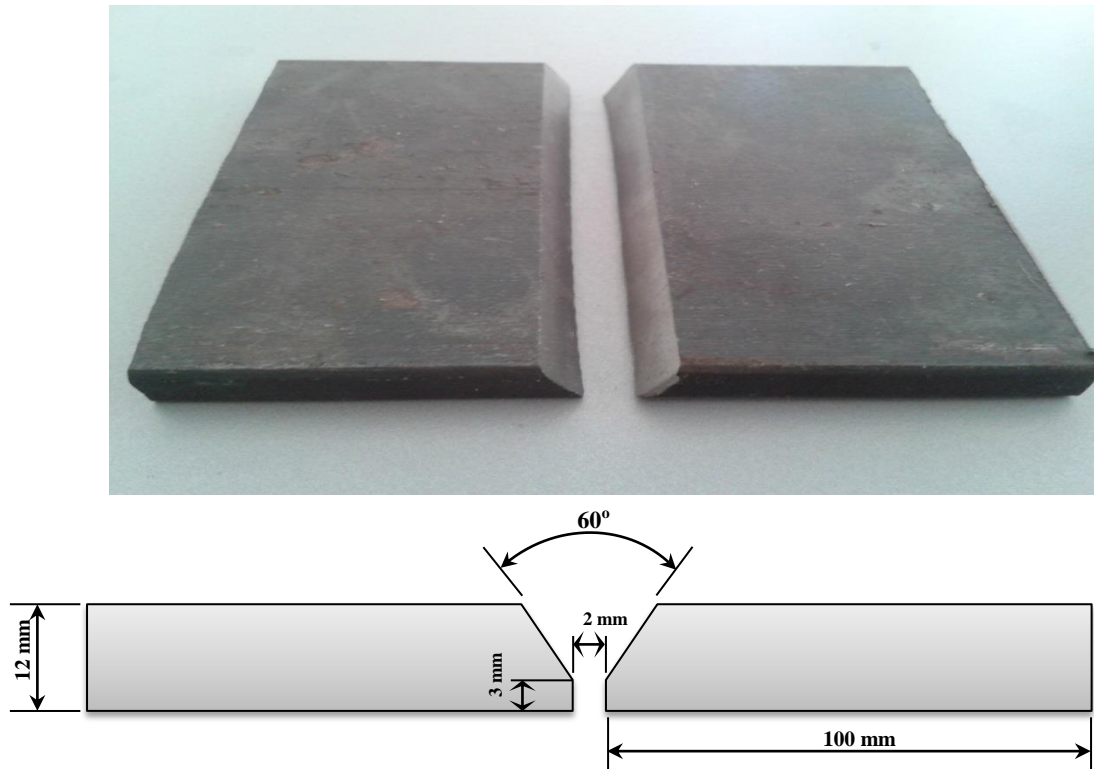


Figure 4.1 Single V groove welding dimensions according to ISO 9692 [48].

4.3.1 Arc welding and electrode selection

AISI 1045 is one of the critical steels which is unfortunately has welding problems in normal aging conditions during joining by shielded metal arc welding. Nevertheless, it's possible to weld and joint the parts together by respecting the electrode selection. According to the specification given in the ISO 2560 standard for electrode selection [49], the low hydrogen electrodes are preferred for welding AISI 1045 steel. E7018 electrode was used for this welding process, as it is shown in the Figure 4.2. In the shielded metal arc welding process, depending on the kind and the thickness of the material there are some specifications in terms of number of passes, electrode size and type, current and welding speed. The welding process was carried out for 1 mm/sec welding speed; 5 mm diameter E7018 electrode and 200 A current.



Figure 4.2 Shielded Metal Arc Welding E 7018 electrodes [49].

4.3.2 Macro and microstructure evaluation of the HAZ

The HAZ area of the specimen was sliced to the required sizes. The specimen is then prepared according to ASTM E3 through a sequence of thriving steps starting from grinding by using different grades of emery papers (220, 320, 400, 600, and 1000 grit) [50], polished to a mirror finish. After polishing finally has been done on the disc polishing machine using two successive grades of diamond compound suspension, were 1 μ m particle size a coarse compound followed by 0.25 μ m particle size finer compound. The polished section is then well washed in warm water and dried by air blower. The etching of the prepared section was done by using Nital etch kit solution to reveal microstructural features of the different zones of shielded metal arc welded joint. Then macro and microstructural features of the shielded metal arc welding (SMAW) of the HAZ region were investigated by using 8 HD mega-pixel digital cameras and a compound optical metallurgical microscope equipped with 5 mega-pixel eyepiece digital cameras which is connected to the PC via a USB port driven by the software of image capture. Grain size measurement of the HAZ area and the base metal for welding joint was done by using the linear intercept method as it is specified in ASTM E112 [51].

4.3.3 Hardness Testing

After welding operation, the welded parts were sliced into suitable parts by using a hacksaw and then the pieces were machined to the required size to prepare the sample for the micro hardness testing. Before the testing, the machining marks and to provide a suitable flat surface for hardness testing requirements has been done by using different grades of emery papers. The micro hardness tester (Vickers Hardness HV) method of the HAZ area was conducted according to ASTM E92-03 [52]. It is shown in Figure 4.3. The Micro Hardness (HV) measurement was taken 3mm above the weld root of the specimen perpendicular to the welding direction using a diamond pyramid indenter with the applied load of 200 g and loading weight in 10sec required where the red indicator turns to green. Vickers Hardness profile is recorded at the prepared finished surface in the transverse direction to the weld centreline with the interval 2mm between two points. The microstructural changes with the data's taken from the micro hardness tester (HV) profile are valuable for prediction, this change made due to the thermal cycle of the shielded metal arc welding operation.



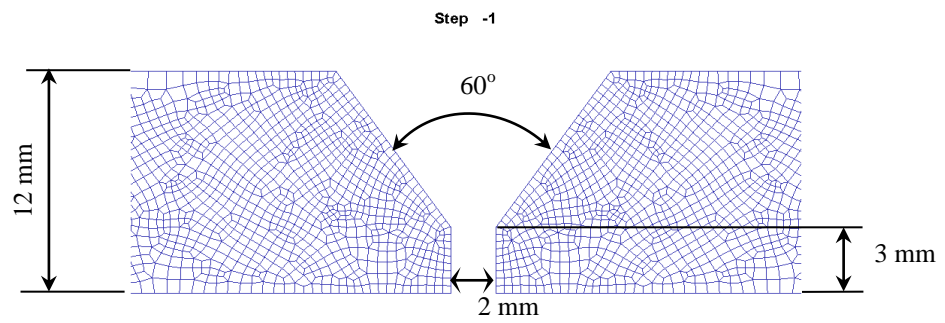
Figure 4.3 Micro-hardness testing (Vickers Hardness HV).

4.4 FE Modelling

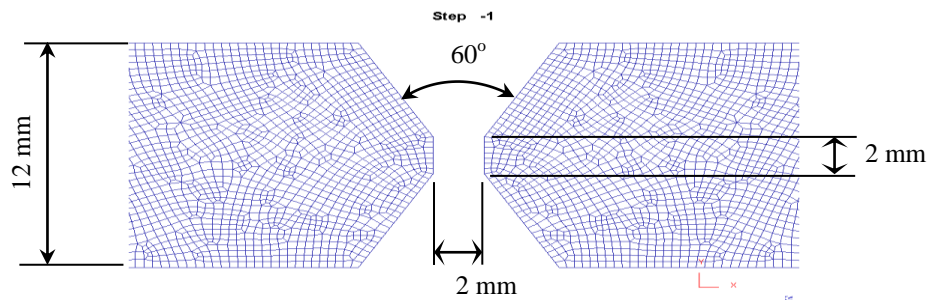
The preparation of the modelling has been done by using the DEFORMTM 2D-FEM finite element package [18]. The process of simulation systems is designed to analyse different construction processes such as forming and heat treatment. FEM modelling generally has been sub-divided into three main parts for analysing the mathematical modelling as it is mentioned in the previous chapter three; also, these three parts almost divided and found similar to each other in other FEM packages. The welding simulation is carried out in two successive passes and welding pool is taken as a heat source. The heat transfer through parent metal is analysed by time for heating (welding) and cooling stages. The deformation, heat transfer, phase transformation, and diffusion are coupled with each other in DEFORMTM 2D-FEM simulations. For example, for carbon steel, the material properties are functions of the carbon content. As the concentration of carbon may be changed by diffusion, the mechanical and thermal properties of the steel will change accordingly. Also it needs to many requirements for definition data inside the program especially for preparation welding model, which is described as in the following:

4.4.1 Pre- processor mathematical modelling

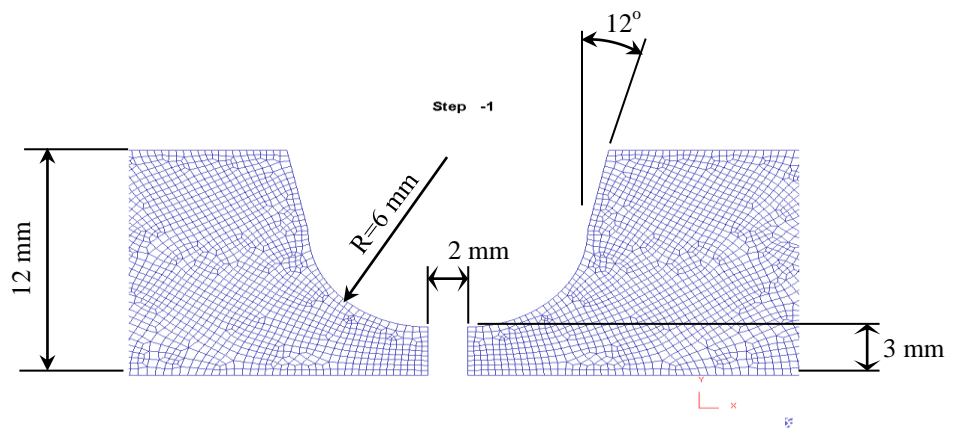
Elasto-Plastic mechanical analysis and the Newton-Raphson iteration solution method have been selected. The flow stress data and the material are defined with regard the material properties of the AISI 1045 steel; Young's modulus (YOUNG=206754 Pa); Poisson's ratio (POISON=0.3). Also; the thermal expansion coefficient (thermal expansion= 1.2×10^{-5}) at elastic section has been defined [53, 54]. The thermal conductivity has been defined as a function of temperature. The heat capacity and emissivity has been automatically defined. After checking the geometry of the sample, meshing is applied according to the weighting factor and the concentration examination zone. Due to the symmetry of the geometry, one half of the shape is modelled and meshed to 3000 elements. For the three geometries V-Shape, double V-Shape and U-Shape samples respectively, as it is clearly shown in the Figure 4.4. All the dimensions of welding groove shapes geometry have been defined to the modelling design preparation accordingly to the specification given in the ISO 9692 standard [48].



a. Single V-Shape welding groove



b. Double V-Shape welding groove



c. U-Shape welding groove

Figure 4.4 Modelling welding groove shapes dimensions prepared according to the given specification in ISO 9692 standard [48].

4.4.2 Macro and microstructure evaluation of the HAZ

For the phase transformation and the microstructure evaluation in the DEFORMTM 2D-FEM, it is necessary to define all of the phases (austenite, bainite, pearlite and martensite). The phases for the AISI 1045 steel has been defined and the phase transformation of the material determined by the volumetric weighting of each phase. This phase has been performed on the three types of the welding groove shapes respectively. The flow stress of the material is defined as a function of strain, strain rate and temperature as shown in the following Figure 4.5 [54]. The flow stress data not necessary for this work, but due to the DEFORMTM 2D-FEM pre-processor requirement has been defined as one of the gradual routine step.

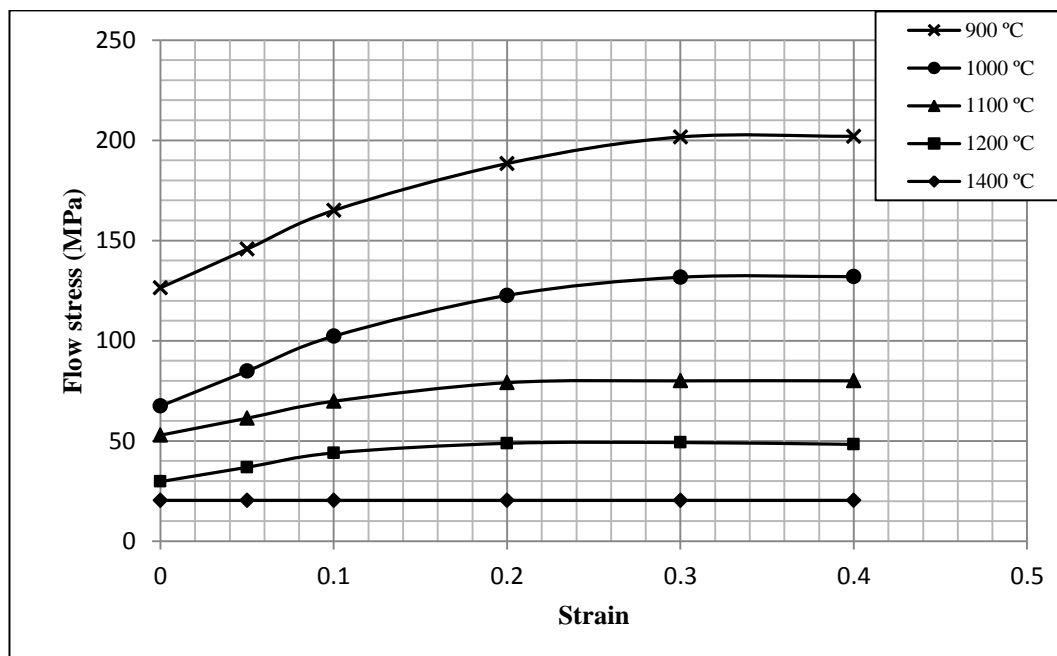


Figure 4.5 Flow stresses with respect to the strain as a function of temperature for AISI 1045 steel [54].

At the thermal section in the material properties window, it is necessary to input the thermal properties of the AISI 1045 steel. The given thermal conductivity data in the Table 4.3 for AISI 1045 steel has been defined successfully [54]. The curves of the thermal conductivity with respect to the temperature have been defined for two carbon contents as a limit (upper and lower). The thermal conductivity of AISI 1045 steel carried out automatically by interpolation according to the carbon content during simulation [54]. It is shown in the Figure 4.6.

Table 4.3 Thermal conductivity and temperature as a function of carbon content for AISI 1045 steel.

Thermal conductivity		Carbon content (C %)	
		0.14	0.6
Temperature °C	0	22.32	21.48
	200	24.01	23.04
	400	25.7	24.59
	600	27.39	26.15
	800	29.08	27.71
	900	29.93	28.49

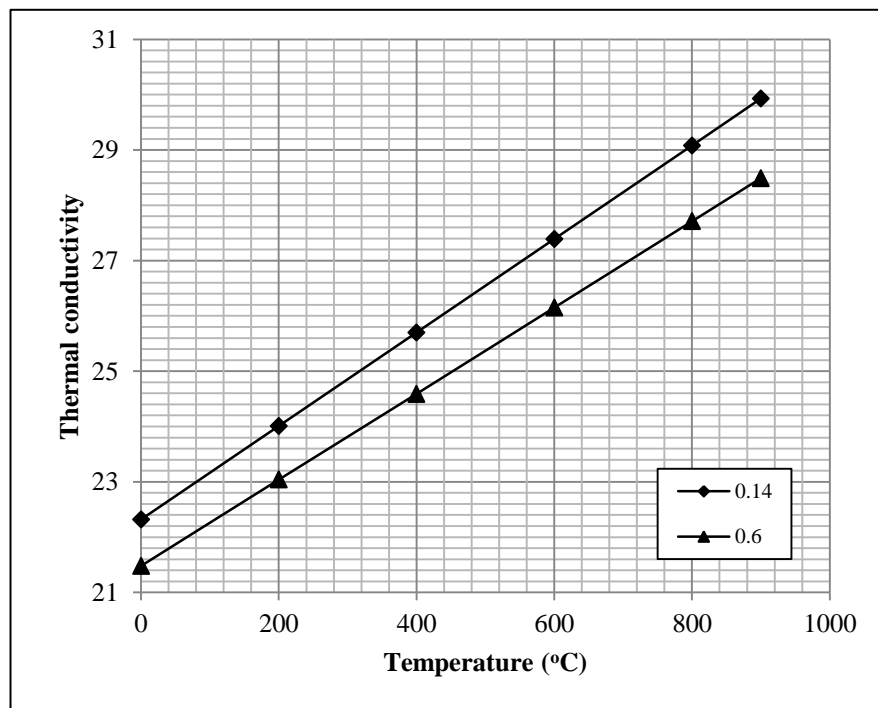


Figure 4.6 Thermal conductivity of the AISI 1045 steel with respect to the temperature for 0.14 and 0.6 C% carbon content [54].

After thermal conductivity, the most important section coming up with the next step in DEFORMTM is the phase transformation definition in the material library of AISI 1045 steel. Phase transformation section of the material in DEFORMTM demands for the definition of the Time Temperature Transformation (TTT) Diagram. The transformation has been done by the volumetric weighting for each phase. In the material properties section the transformation has been defined in relation to each

other (from one phase to another phase transformation) as like a mother to child relationship [54]. Then TTT diagram defined for the AISI 1045 steel [53, 55]. TTT diagrams have been defined according to the carbon content for steel of starting transformation to end of the transformation line; it is shown in the Figure 4.7 below;

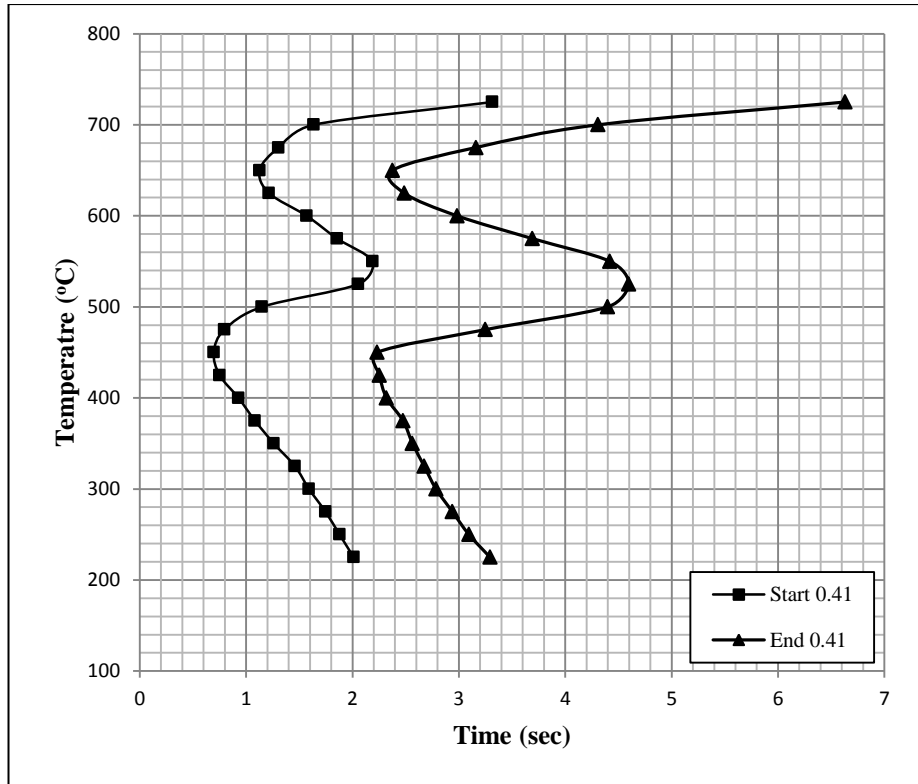


Figure 4.7 Time Temperature Transformation (TTT) diagram for AISI 1045 steel 0.41 carbon content [53, 54, 55].

In DEFORMTM the Avrami equation is used for solving volume fraction and transformation as it is shown in the Figure 4.8, which is playing an important role in the transformation process and grain size, where it is defined in the following form:

$$\xi = 1 - \exp(-kt^n) \quad (4.1)$$

Where:

ξ : is the volume fraction transformed,

t: is the time, and

k and n: are constants (n being the Avrami number).

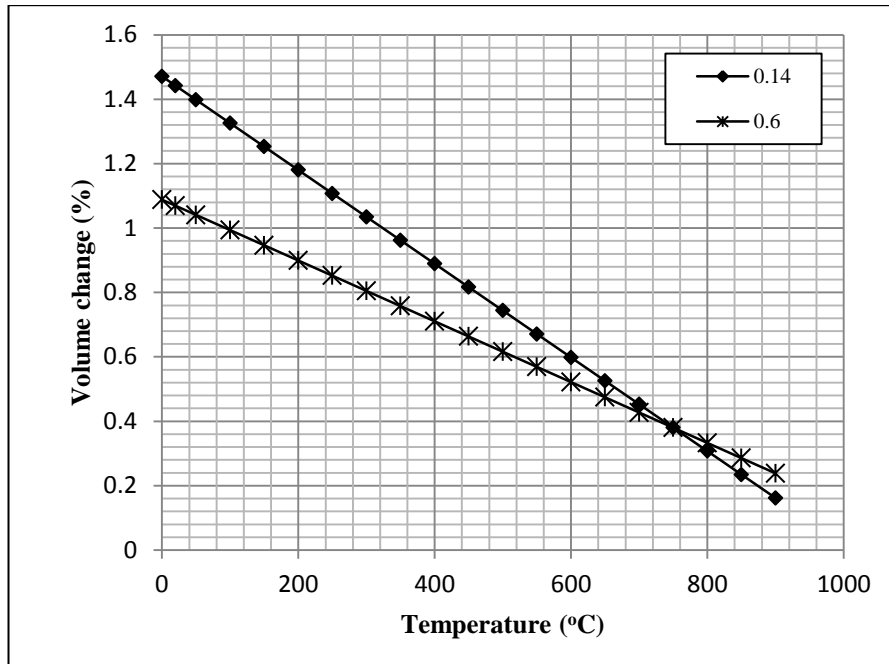


Figure 4.8 Volume fractions and transformation per temperature for AISI 1045 steel for 0.14 and 0.6 carbon content [54, 55].

In terms of TTT data, two curves are required in order to solve for k and n. For the grain modelling, the grain size, the peak strain and the strain rate boundary are defined as a function of the temperature in the 2D-DEFORMTM heat treatment section. The initial grain size has been defined to the 2D-DEFORMTM by the measured value of the experimental work. All other data have been loaded automatically in the FEM software according to the carbon content and initial grain size of AISI 1045 steel. The constant values have been defined as well; the procedure of the 2D-FEM has been illustrated in the related section of appendices [54].

4.4.3 DEFORMTM Hardness Modelling

The hardness value is based on the Rockwell C hardness test (HRC), where DEFORMTM allows users computing hardness by using Jominy curve data. DEFORMTM 2D-FEM computed the cooling rate for each element and make a hardness estimate based on the Jominy curve [55]. The Jominy curve (hardness as a function of distance). This will fully specify the required information for the hardness estimation as it is shown in the Figure 4.9.

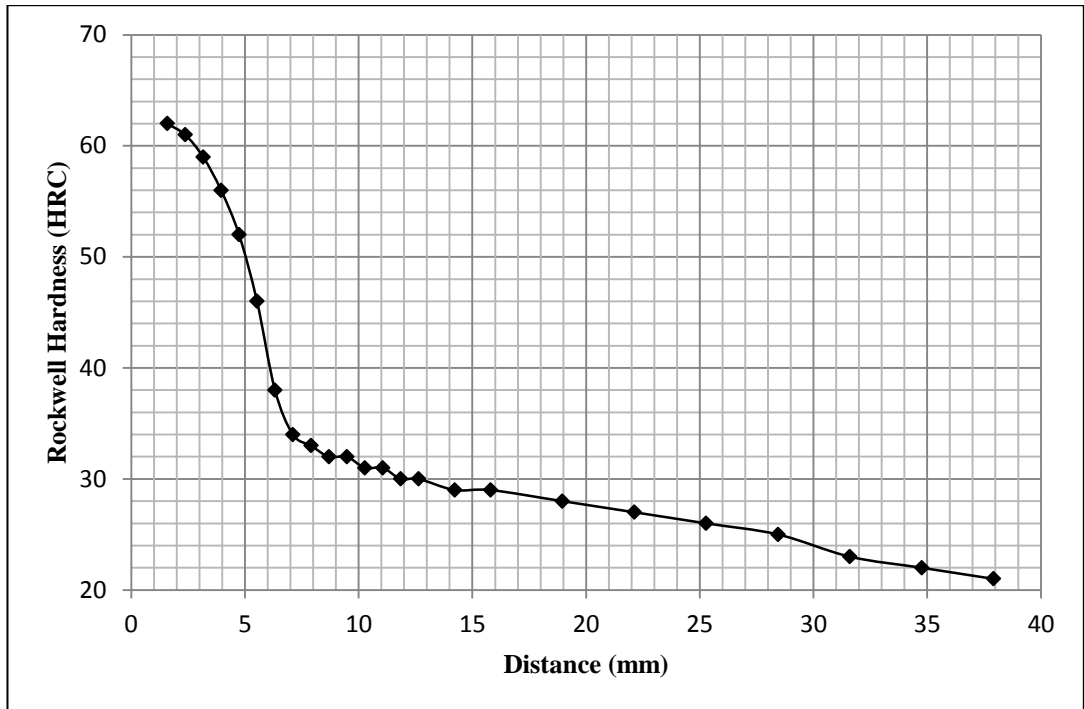


Figure 4.9 Jominy Rockwell hardness test, as a function of distance for AISI 1045 steel.

In the material properties of DEFORMTM there is a giving facility also for the phase transformation by hardness value of each transformed phase accordingly. The hardness has been defined for each phase which is for %100 martensite is 55 (in Rockwell C), the hardness for bainite is 30 and the hardness for austenite is 20. The composite hardness of the final product is estimated by using a volume fraction weighted calculation. Therefore, if a partial transformation of an element transforms to Pearlite and the other partial transformation transforms to martensite, the estimated hardness value is the volume fraction weighted average of the two phases. In the DEFORMTM 2D-FEM simulation the hardness in each phase does not become variable as a function of carbon content. In any event, by changing the hardness data to a function of an atom, the hardness for each phase can vary with carbon. In the present simulation, the TTT diagram has been preferred on thus the phase transformation and micro structure evaluation has been done.

CHAPTER 5

RESULTS AND DISCUSSION

5.1 Introduction

This chapter presents 2D finite element model of three types of welding groove shapes which have been used to fabricate welding butt joints of AISI 1045 steel. The temperature distribution, microstructure, grain growth, and the hardness of the heat affected zone (HAZ) were simulated. The results of the simulation were compared with the experimental ones. By applying different pre-heating processes for eliminating the martensite phase transformation in the heat affected zone HAZ during the normal air cooling process.

5.2 Experimental work

5.2.1 Visual examination of welded AISI 1045 Steel

The shielded metal arc welding process is done by the two successive numbers of passes by depending on the kind and the thickness of the material. The number of passes and the dimensional specifications of the specimen are illustrated in the Figure 5.1. After welding the weldment surface was cleaned and grinded thus Nital etch kit used for visual examination to visualize defects has been noticed in the heat affect zone HAZ. The effect of the welding pool heat source in the heat affected zone HAZ and aging process during cooling are mainly responsible for the martensite phase formation which is sometimes causing the hydrogen surface cracking as shown in Figure 5.2. The amount of carbon content and alloying elements may also have a significant effect.

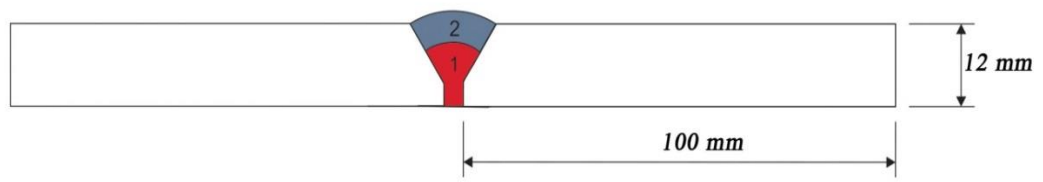


Figure 5.1 Fabricated single V-shape welding groove butt joint for AISI 1045 steel, with two successive passes.

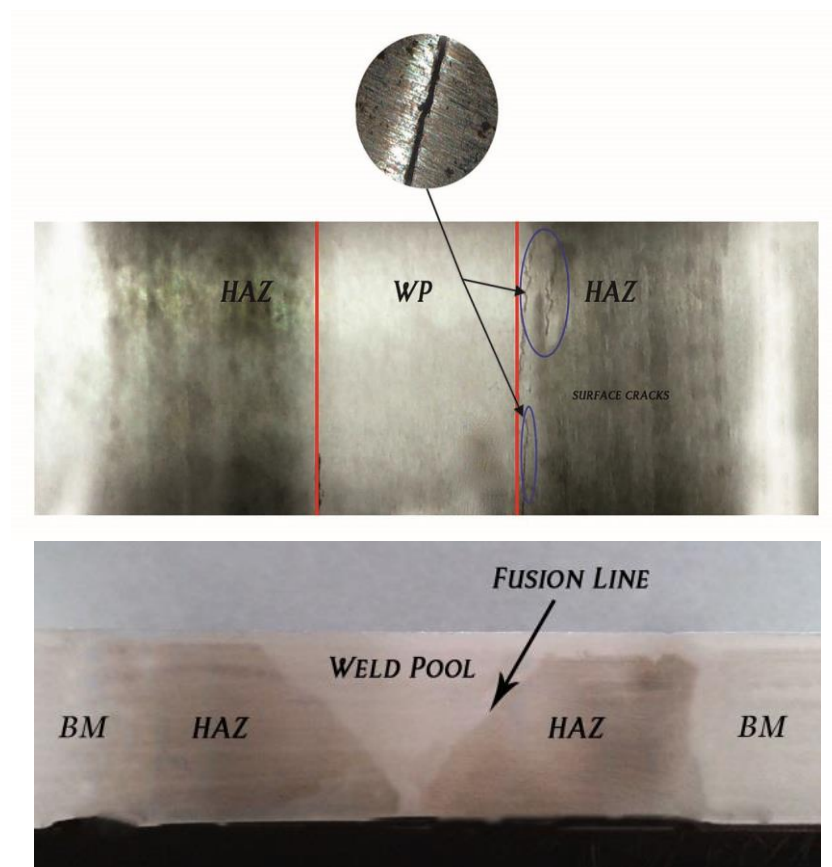


Figure 5.2 The effect of the SMAW on the HAZ and hydrogen surface cracking during cooling of AISI 1045 steel.

5.2.2 The effect of welding on macro and microstructural features in HAZ of AISI 1045 steel

Where the molten pool moves through the material, the growth rate and temperature gradient vary considerably across the weld pool, therefore V-shape groove profile change during welding has been less affected by the SMAW thus it is out of the case study. Welding pool heating source for fabricating joints has a significant effect on the phase transformation changes and the average grain size growth in the HAZ area. Transverse macro-section through the HAZ of AISI 1045 steel in the microstructure examination has showed; the average grain sizes adjacent to the fusion line are large. Due to the welding effect of the temperature rises in the HAZ meanwhile causing to the martensite phase formation during cooling. The chemical composition of the medium carbon steel (AISI 1045 steel) makes significant changes in the curve shape of the Time Temperature Transformation (TTT) diagram and the phase transformation time of the steel. In this state, the phase transformation time from austenite to the pearlite or bainite phase transformation required longer time. For this reason in the present specimen (AISI 1045 steel) martensite phase transformation has been seen at the different points in the HAZ area during the normal air cooling process. Where the measured grain size near the fusion line was 1200 μm with compared to the 1mm away from the fusion line and in unaffected base metal are 475 μm and 25 μm respectively, as shown in Figure 5.3 and Figure 5.4. In the state of formation of the martensite phase and the grain growth has significant effects of inducing the hydrogen cracking, which was clearly shown in Figure 5.2, where the darken area on the specimen representing the HAZ and the rest of the parts are illustrated clearly in the figure as well.

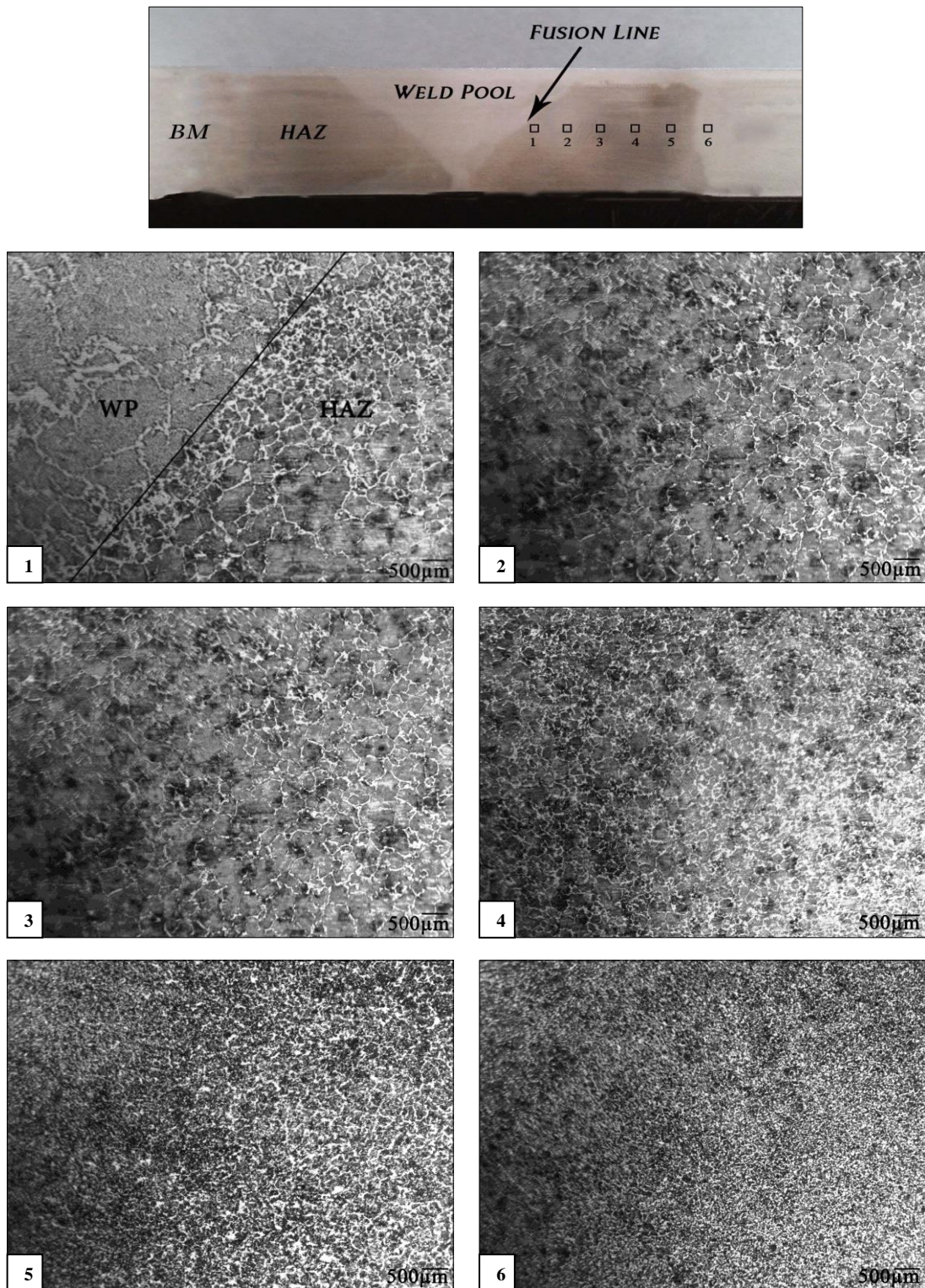
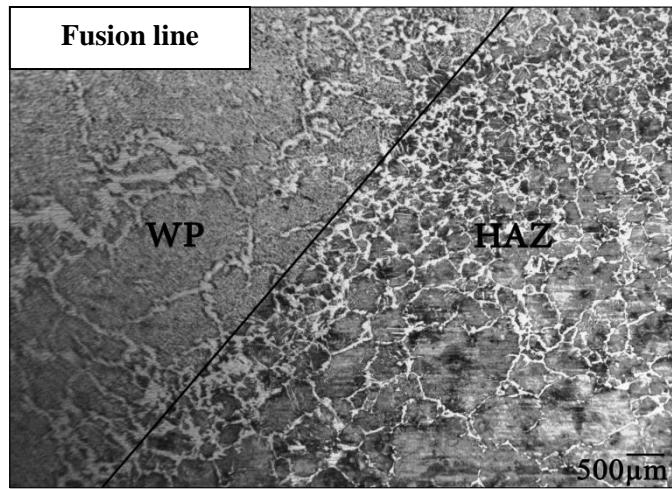
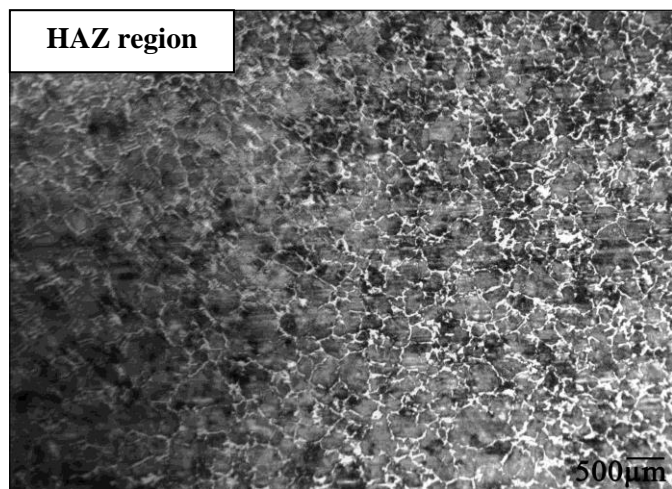


Figure 5.3 Optical macro and micrographs on a transverse section of HAZ area, through a shielded metal Arc welded (SMAW) AISI 1045 steel 100 X.

Grain size $\approx 1200 \mu\text{m}$



Grain size $\approx 475 \mu\text{m}$



Grain size $\approx 25 \mu\text{m}$

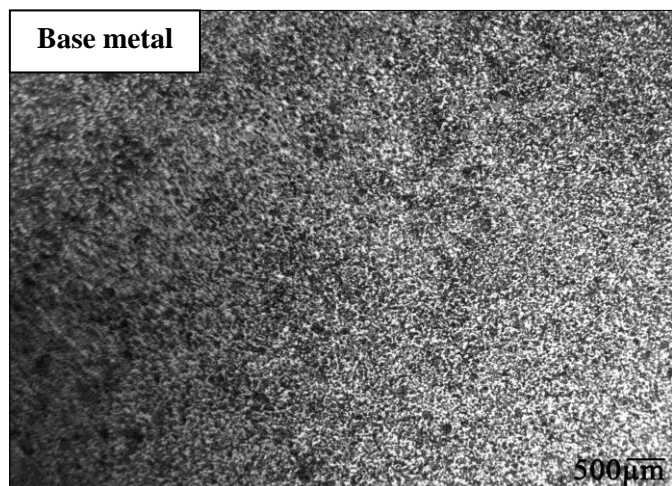


Figure 5.4 Grain size as a function of the transverse position from the fusion line through the HAZ area of the butt V-shape welded groove AISI 1045 steel 100 X.

In the Figures 5.4 showing that, the average grain size adjacent to the fusion line for the HAZ was found to be bigger due to the existing temperature gradient through the HAZ. The grain growth phenomena in the entire HAZ have been increased when become close to the fusion line zone. At the same time, the area near the fusion line undergoes a higher temperature and longer cooling time therefore there is more opportunity for the grain growth.

5.2.3 The effect of welding conditions on the Hardness profile of the HAZ

In the most of the time the hardness test is a common method to find the width of the heat affected zone in weldments, which is done by measuring the hardness value through the transverse section of the weld joint. On the other hand, hardness profile through the transverse section HAZ area can be useful tool for predicting the microstructure changes that might occur due to the heat of the welding joint [57]. Figure 5.5 shows for demonstration the measured micro hardness tester (Vickers hardness HV) profile across the SMAW joint through the HAZ of AISI 1045 steel.

It is obvious that for heat treatment process as the grain size become larger the hardness and the strength to become lower, but what is surprising here is that after welding joint the grain size of the HAZ area become larger while the hardness and the strength becomes higher. This is attributed to the fact that the hardness and strength are related to the grain size d , through the Hall-Petch formula which is written as follow [58]:

$$\sigma_y = \sigma_o + k_y d^{-\frac{1}{2}} \quad (5.1)$$

Where:

σ_y : is the yield strength,

σ_o : is the frictional stress,

k_y : is a positive yielding constant.

A positive yielding constant associated with the stress required to extend dislocation activity into adjacent not yielded grains. In the absence of appreciable work

hardening, equation 5.1 was reformed in the terms of hardness, Hv through the following equation:

$$Hv = H_o + K_H d^{-\frac{1}{2}} \quad (5.2)$$

Where H_o and K_H are the appropriate constants associated with the hardness measurements. This relationship shows that hardness and the strength of the material are related to the grain size, i.e. when the grain size become smaller, the hardness and the strength becomes higher.

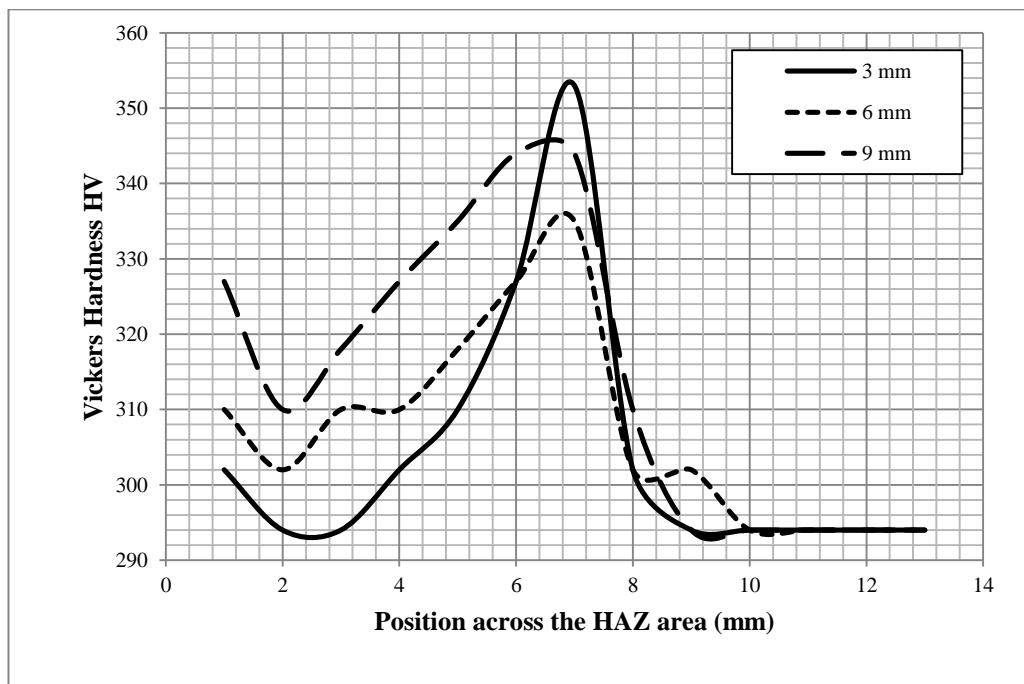


Figure 5.5 A demonstrative micro hardness test HV profile across the HAZ area in three points above the weldment root for AISI 1045 steel.

This means that during shielded metal arc welding, grain refinement of the heat affected zone HAZ has a little effect on the steel hardness. It is dominated by the value of the heat remaining in the heat affected zone HAZ for providing natural ageing during the cooling cycle. These results indicate that mechanical properties of the heat affected zone HAZ are not taken into the consideration only as a function of the grain size, because existing a complex competition between the effect of grain refining and HAZ cooling cycle strengthening. This means the martensite formation

has a significant effect on the hardness. In the case of the taken measurements from the 3mm in between of the three transverse lines above the weld root for measuring the micro hardness testing HV in the heat affected zone HAZ, seen that there is a difference between the three points in line for the hardness values, due to the effect of the cooling cycle of the heat affected zone HAZ and different volume fraction of martensite formation.

5.3 Modelling and experimental results compatibility

Broadly, Finite element FE Modelling demands sometimes for something to prove the validity of the results. Also many researchers have been compared practical experimental data with the FEM in different simulation programs. For the purpose of development and work on the different experiences of scientific theory and to find solutions in the shortest possible time with the lowest cost of labour whereas this is the main aim of the finite element method FEM. Where the modelling becomes more realistic if a practical experimental sample taken into the consideration as a backing for the development, meanwhile, testing the rest part of the experimental study will done by the prepared model with the help of the finite element software FEM.

In the present study, a V-shaped weldment specimen has been taken into the consideration for proving the validity of the results by comparing with the prepared modelling results in the DEFORMTM 2D-FEM. Investigation of the results has been done through two testing techniques; the grain size and hardness measurement test. The average grain size distribution found in the finite element model and practical experimental work is shown in the Figure 5.6. From the results of the grain size investigation of the AISI 1045 steel, it is found that the grain size of the FE model at the adjacent point to the fusion line of the welding was 1258 μm whereas in the practical experimental result was 1200 μm . Similar results were obtained from different regions of HAZ of the welding as shown in the Figure 5.6. Therefore, there is a good agreement between the practical experimental work and simulation results.

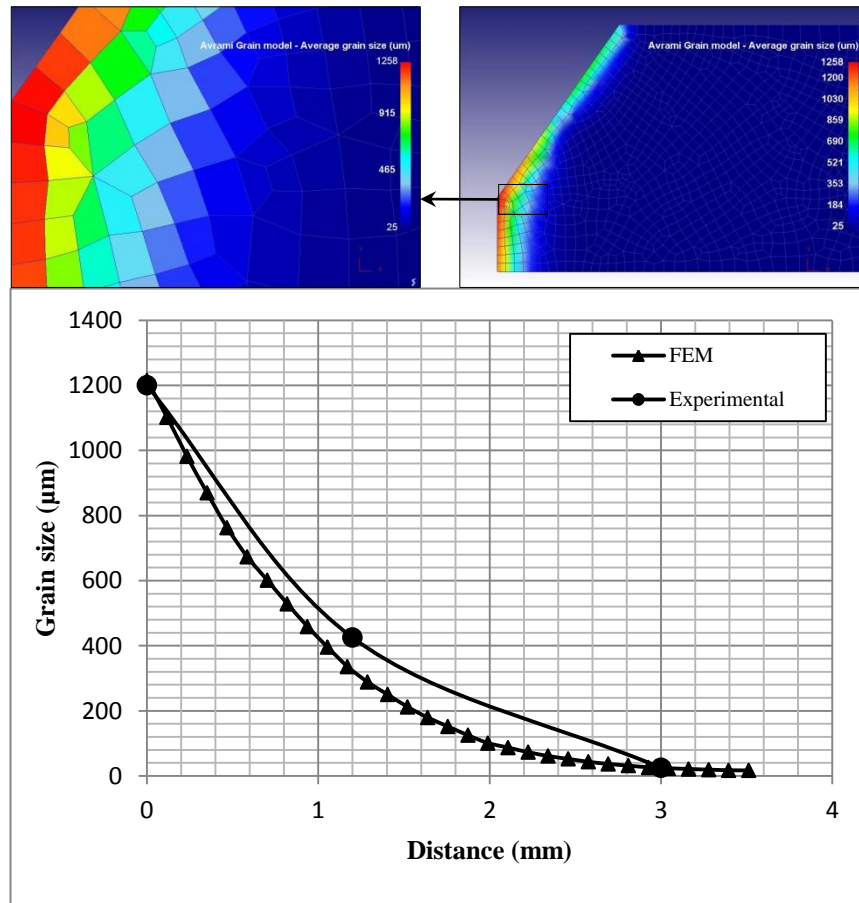
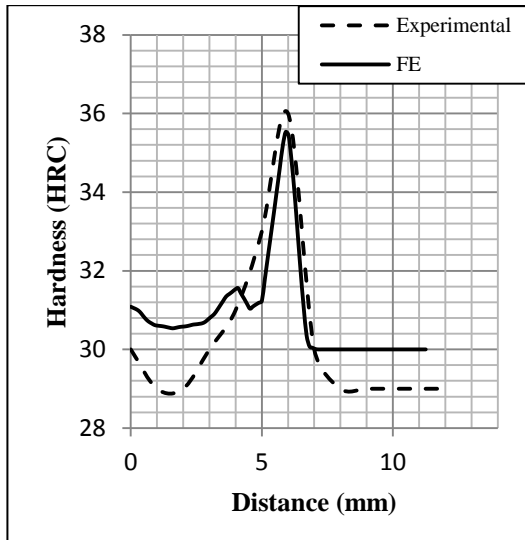
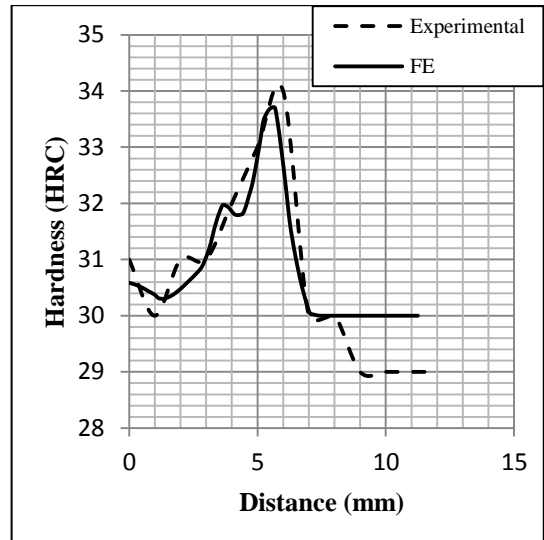


Figure 5.6 2D-FEM and experimental grain size distributions HAZ area for the butt welded V-shape groove of the AISI 1045 steel.

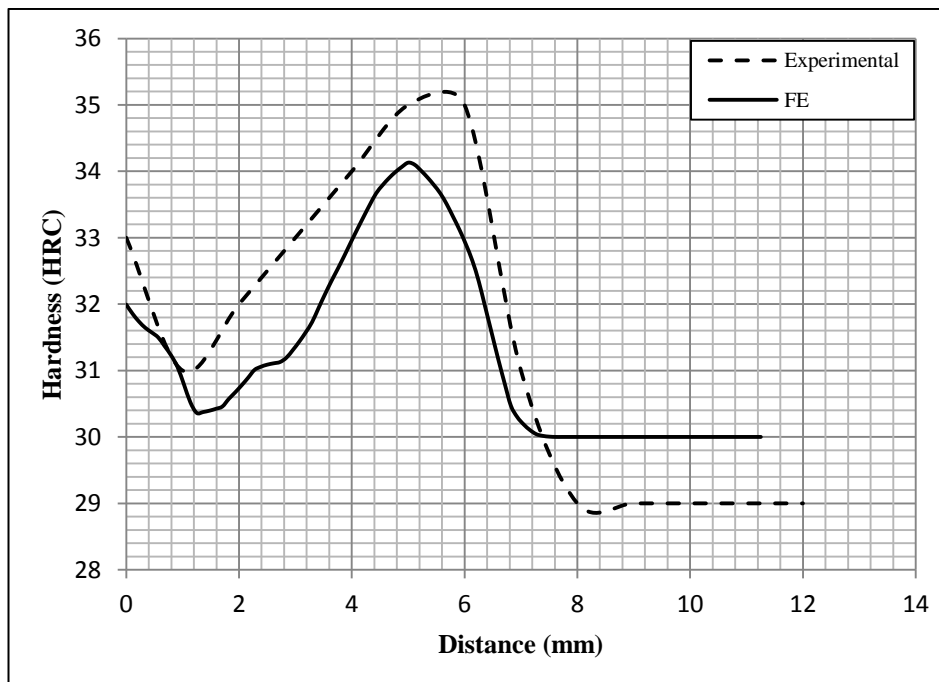
On the other hand, through hardness test comparison where in the DEFORMTM finite element software giving the hardness number results as Rockwell C hardness basement whereas, the measured experimental values have been converted from the micro hardness testing (Vickers hardness HV) number to the Rockwell C hardness number HRC according to ASTM E140–97 [56]. The hardness values of the practical experimental work and 2D-FEM is shown in the Figure 5.7. The results show that the FE model and the experimental measurements are in good agreement. The maximum difference between the experimental and FE model is lower than 2 HRC. Meanwhile now the prepared modelling is ready for exploring the rest part of the experimental simulation by 2D-FEM.



a. HRC 3 mm above the weld root



b. HRC 6 mm above the weld root



c. HRC 9 mm above the weld root.

Figure 5.7 2D-FEM and Experimental hardness distribution for a) 3mm, b) 6mm and c) 9mm above the weld root through the HAZ.

5.4 FE Modelling

5.4.1 The effects of welding groove shapes on the temperature distribution and HAZ

It is obvious that the welding process done only by thermal generation. It is the main effect on the HAZ and alters the microstructure properties of welded metal. Sometimes this thermal generation and cooling process leads to the appearance of defects in the metal foundation in the heat affected zone and that causes the failure of welded piece, and these defects whether internal or external defects. Over three models have been prepared to the welding processes (single V-shape, double V-shape and U-shape) within 2D-FEM, has been analysed the heat generation and cooling times of welding process on the three pieces. The simulated spread temperature distribution inside the metal foundation in the heat affected zone has been noticed. In the Figure 5.8 (a) and (b) showing the two successive interpass of single V-shape respectively, where Figure 5.9 (a) and (b) showing two welding interpass of U-shape and Figure 5.10 (a) and (b) showing two welding interpasses of double V-shape groove weldments. In the three mentioned shapes, the temperature distribution carried out during the welding process and cooling time in the exposed normal air cooling process.

It is possible through the 2D-FEM to examine the area affecting by the heat of the welded pieces, by measuring the width of the heat affected area (HAA) and compare it with each other between three welding groove shapes at the same welding boundary condition. Through the Figure 5.11 different widths of the heat affected area (HAA) for each of the welding groove shapes have been found. The measured width of the HAA of the two successive interpasses found; 26.5mm of V-shape, 24mm of U-shape and 21mm of double V-shape welding grooves. In double V-shape welding groove the smallest zone width of heat affected area (HAA) has been found in comparison the U-shape and V-shape welding grooves.

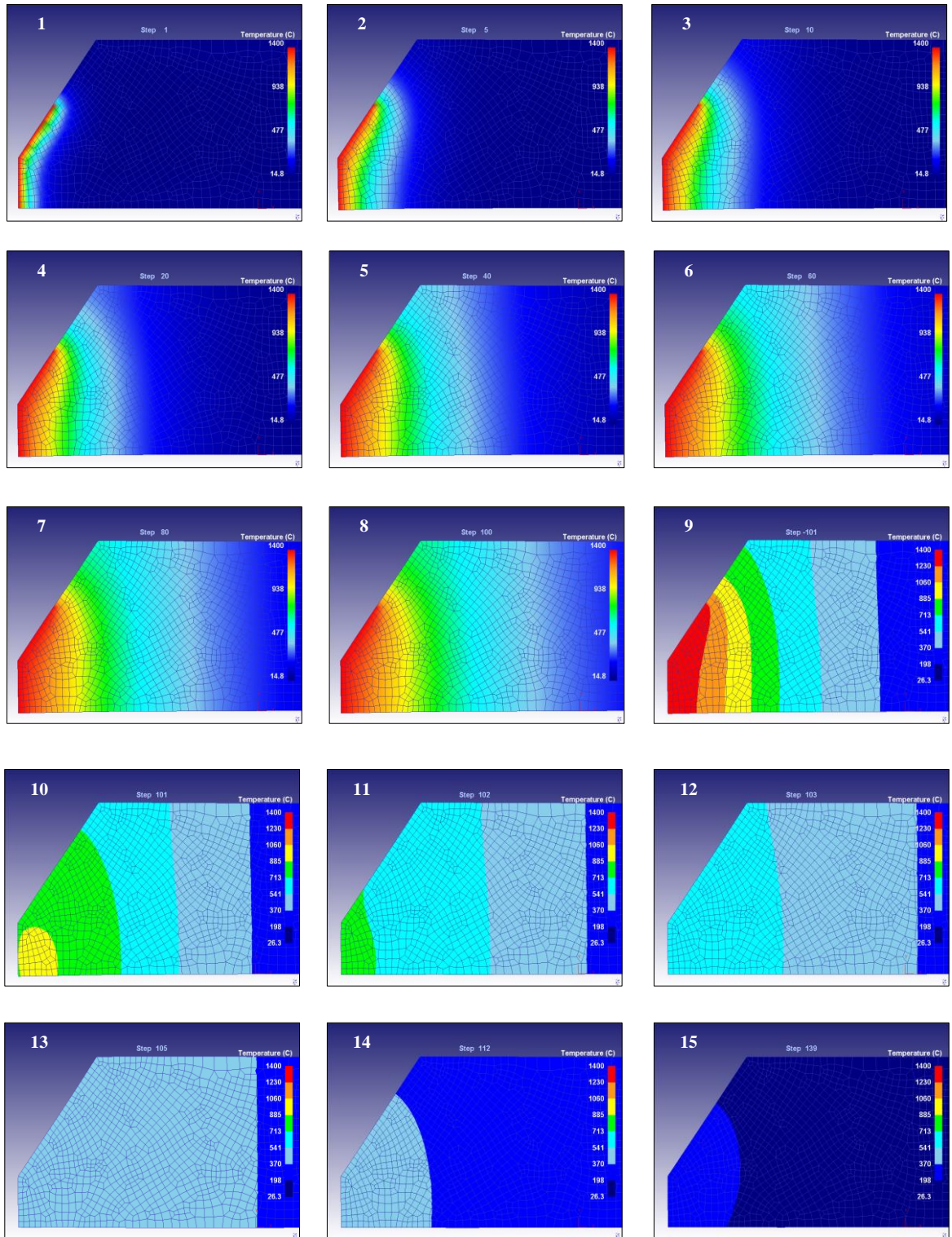


Figure 5.8 a. First pass temperature distribution during welding and cooling time, in the HAZ area, for butt V-shape welding groove AISI 1045 steel in 2D-FEM.

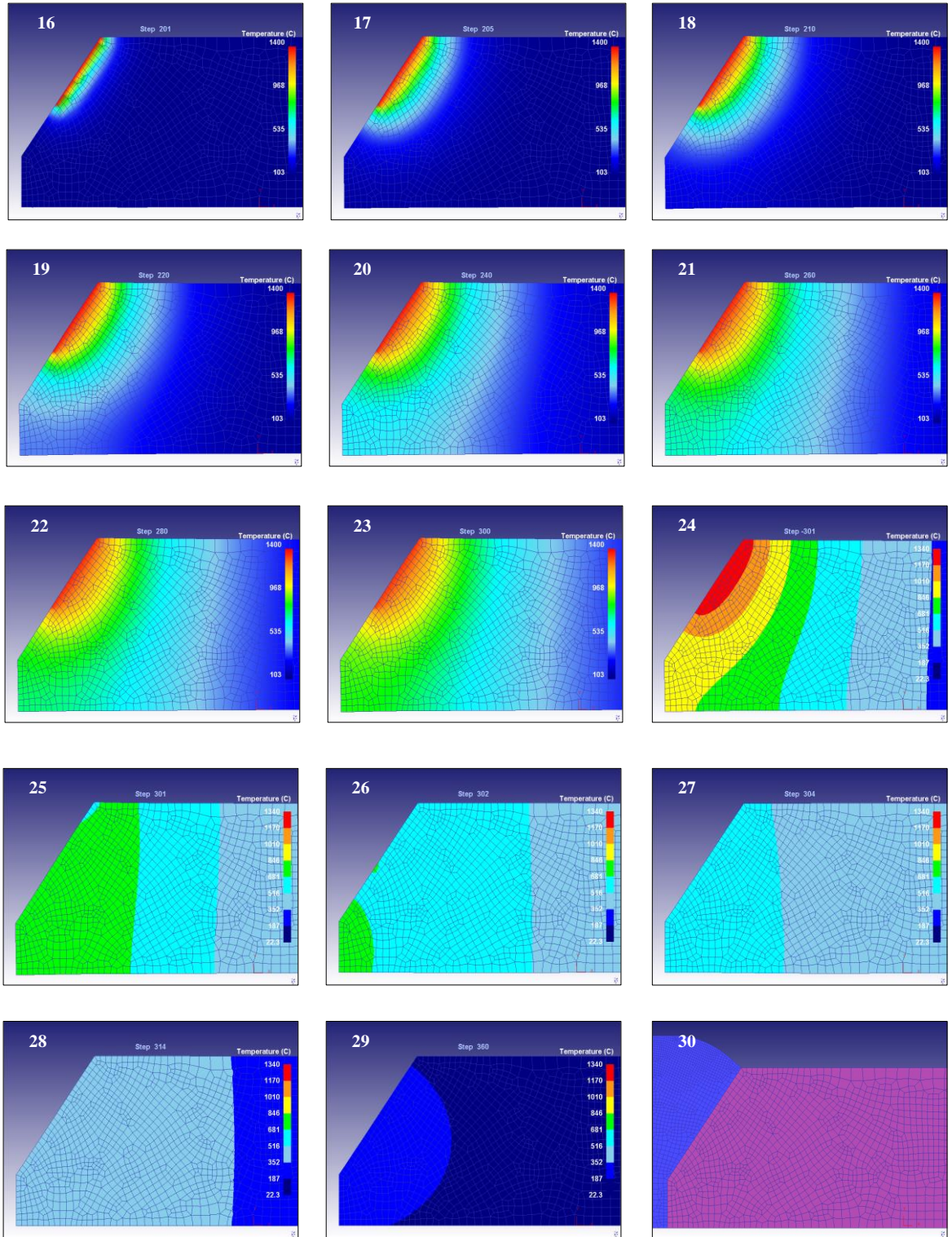


Figure 5.8 b. Second pass temperature distribution during welding and cooling time, in the HAZ area, for butt V-shape welding groove AISI 1045 steel in 2D-FEM.

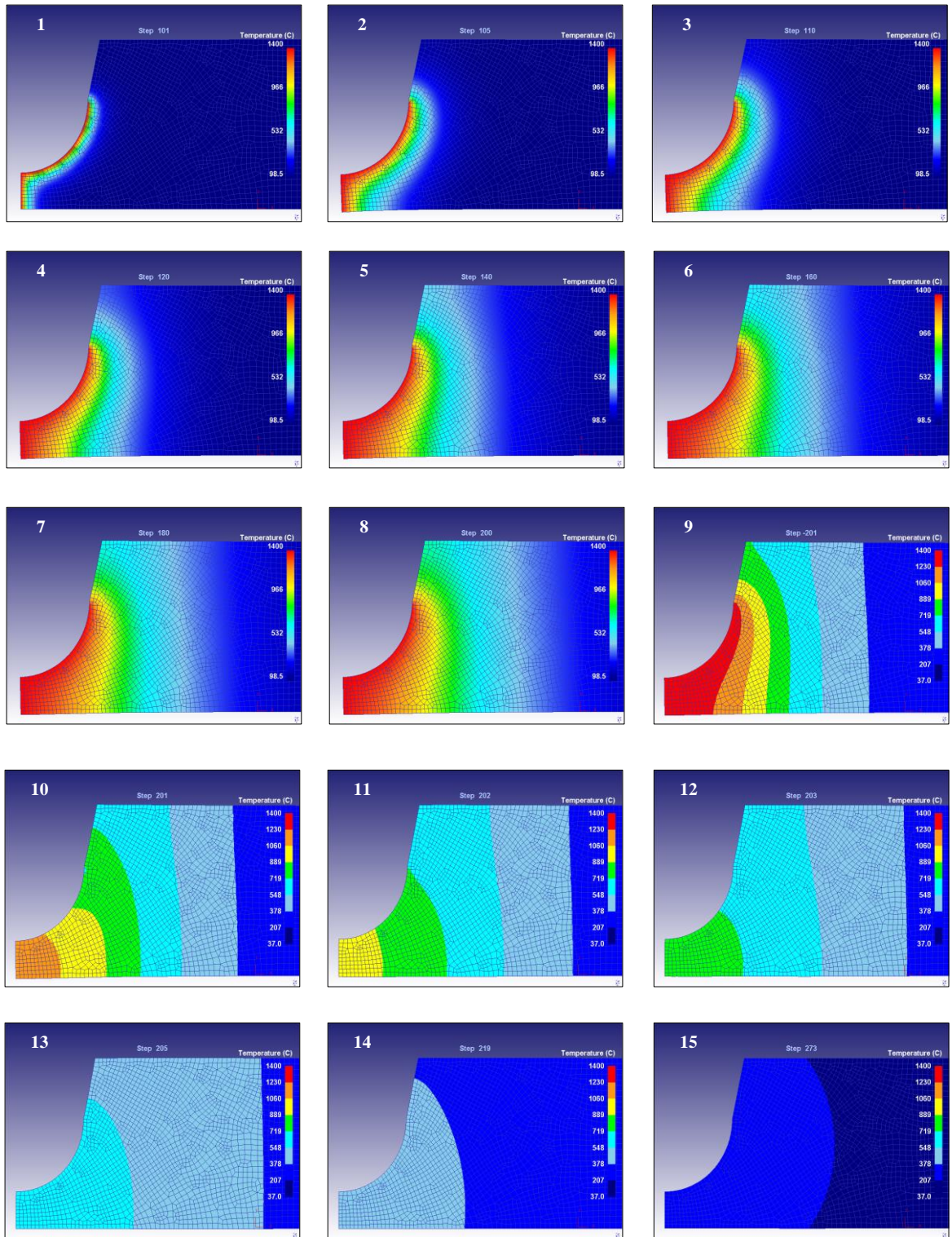


Figure 5.9 a. First pass temperature distribution during welding and cooling time, in the HAZ area, for butt U-shape welding groove AISI 1045 steel in 2D-FEM.

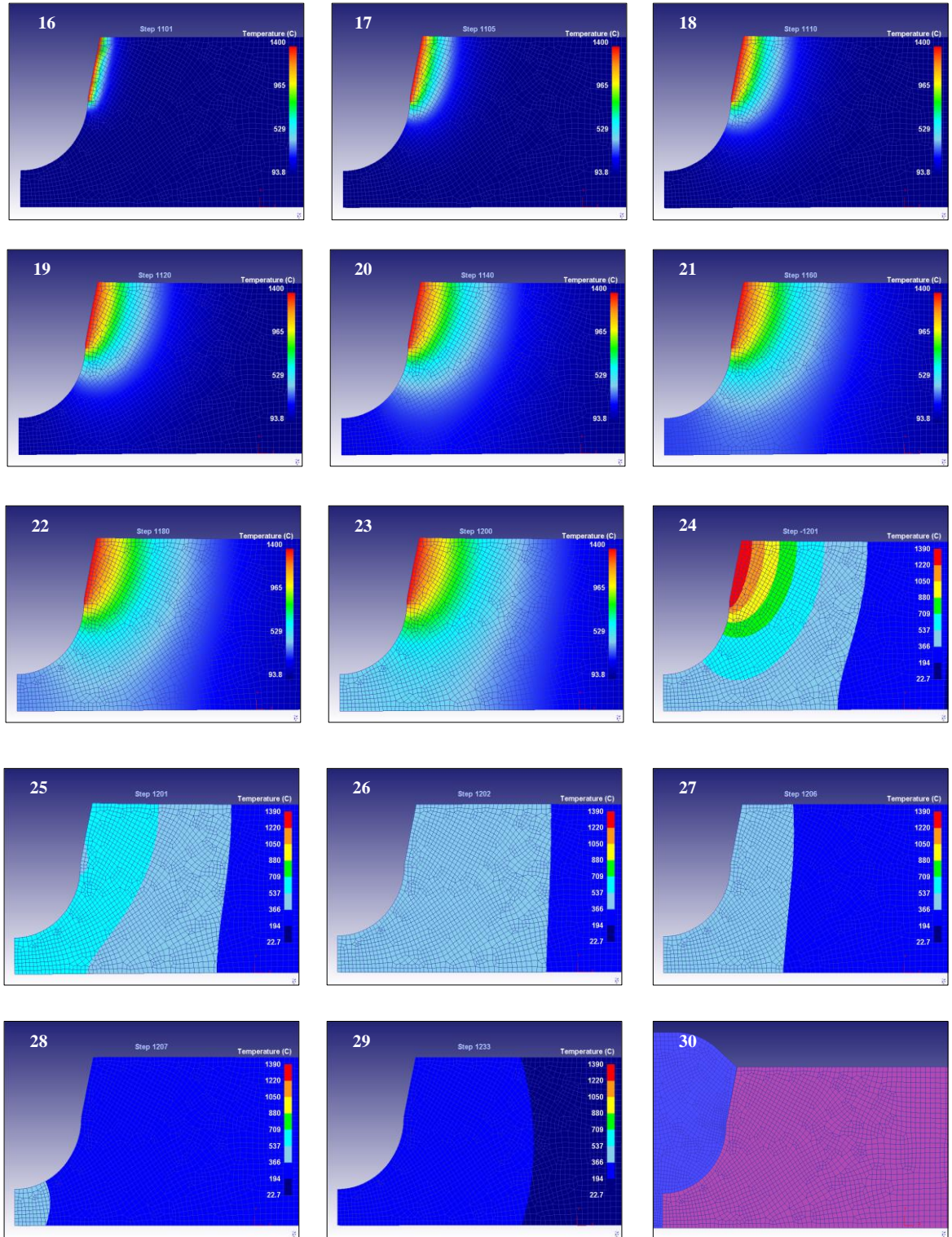


Figure 5.9 b. Second pass temperature distribution during welding and cooling time in the HAZ area, for butt U-shape welding groove AISI 1045 steel in 2D-FEM

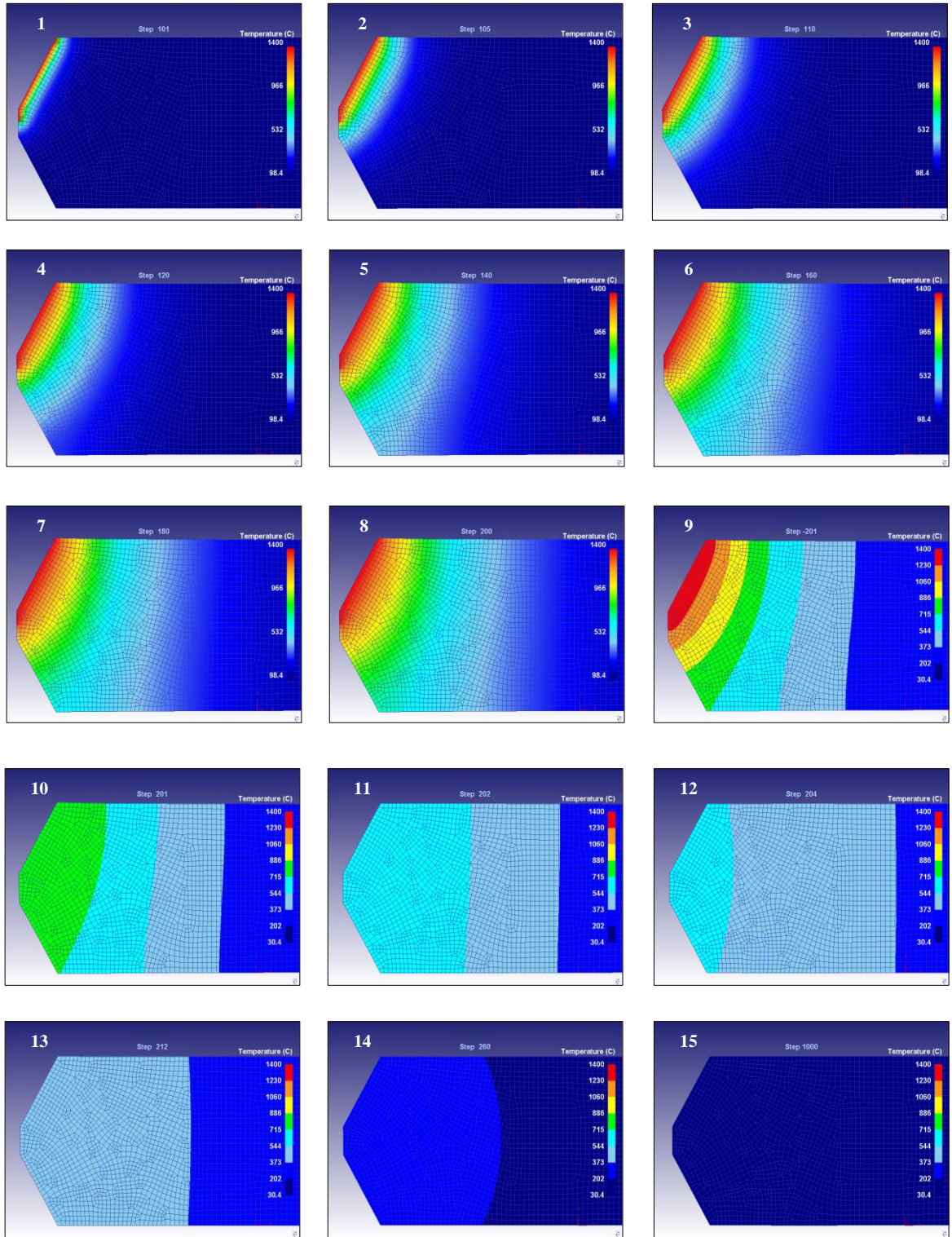


Figure 5.10 a. First pass temperature distribution during welding and cooling time, in the HAZ area, for butt double V-shape welding groove AISI 1045 steel in 2D-FEM.

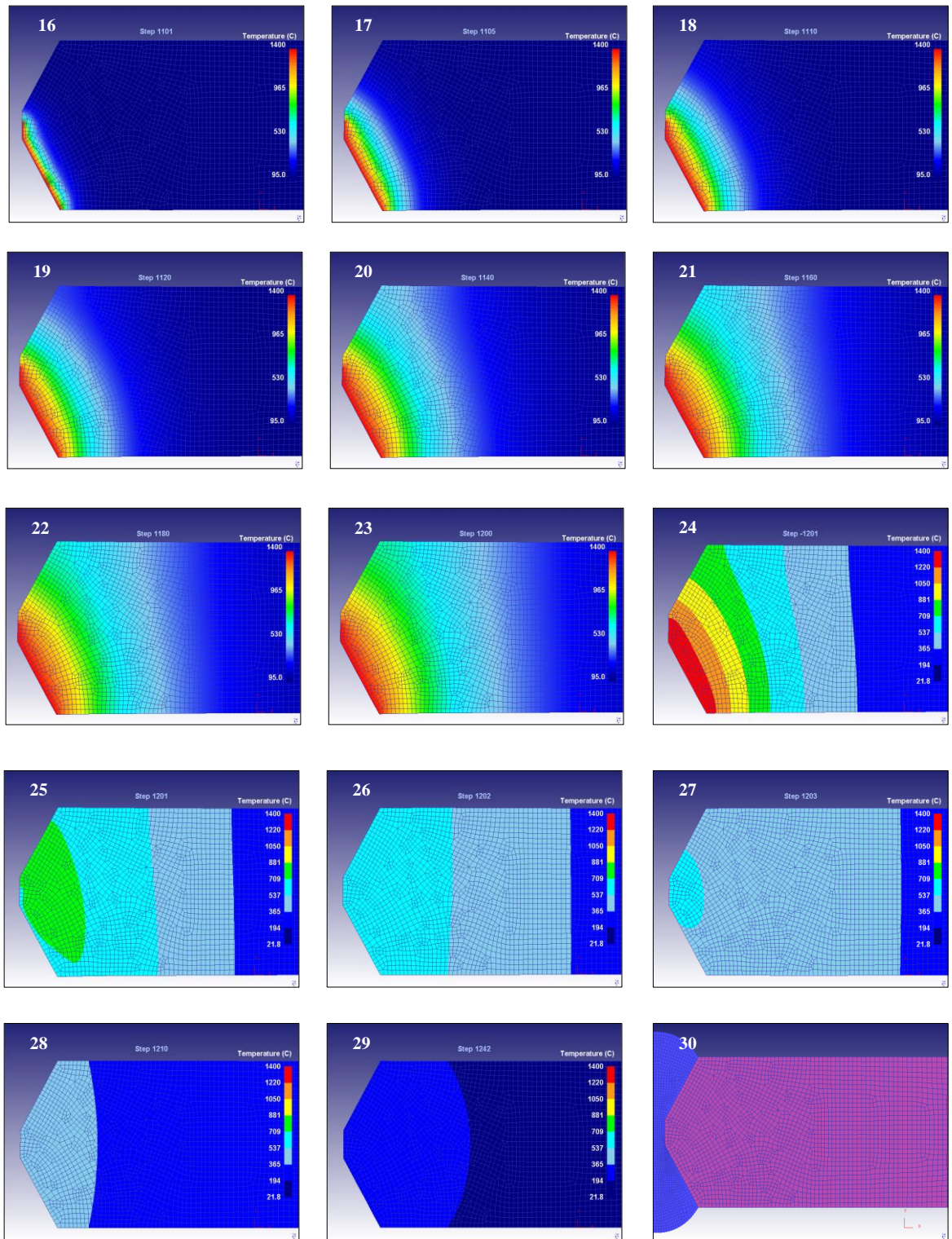
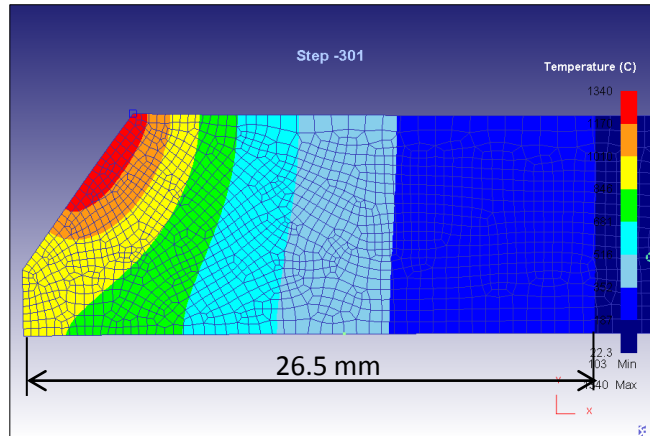


Figure 5.10 b. Second pass temperature distribution during welding and cooling time, in the HAZ area, for butt double V-shape welding groove AISI 1045 steel in 2D-FEM.

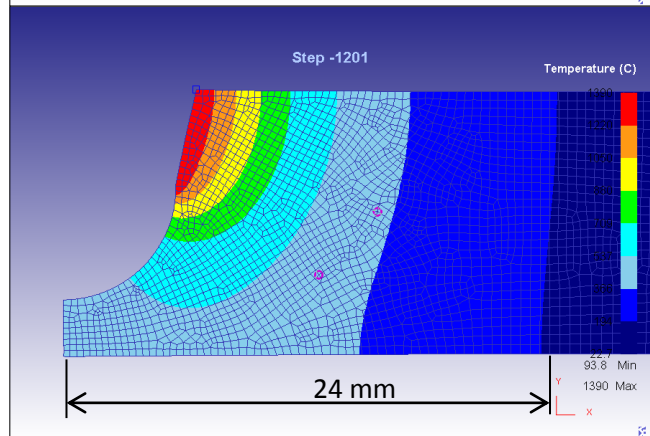
(HAA) width \approx 26.5 mm

(Double pass)



(HAA) width \approx 24 mm

(Double pass)



(HAA) width \approx 21 mm

Double pass (reverse side)

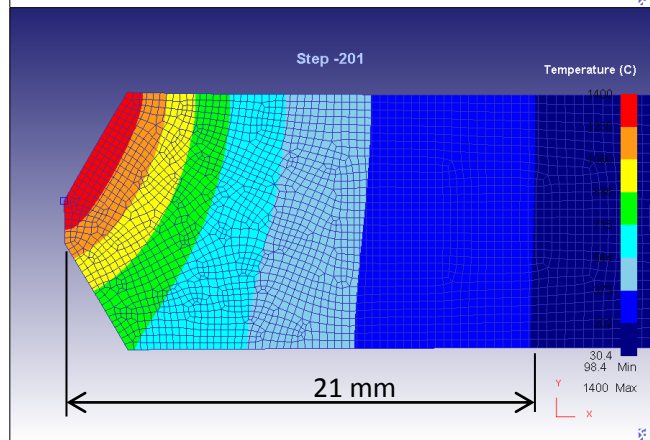


Figure 5.11 Generated heats affected area (HAA) after welding for the three grooves shapes V, U and double V.

5.4.2 The effects of welding groove shapes on the heating and cooling curves

It is possible through the DEFORMTM 2D-FEM program to measure the temperature distribution curves during the welding process and in the cooling time for the three welding groove shapes and compares with each other. The temperature distribution results of second interpass for the SMAW process during welding time and cooling in still air has been found, where Figure 5.12 is for V-shape weldment, Figure 5.13 is for U-shape weldment and Figure 5.14 is for double V-shape. The measurement has been taken through the middle tracking points of HAZ section from seven positions according to the measured width of the HAZ region of each welding groove shape, starting from the point adjacent to the fusion line. The measured maximum temperature reaction from the welding process was found 1400°C for the three shapes. The generated temperature distribution during welding for the three shapes has been noticed that they are nearly close to each other, but some differences found in the still air cooling process time. In the Figure 5.15 comparisons between the cooling curves for the three weldment shapes after second passes has been carried out. The cooling curves playing an important role because cooling time difference between the three shapes stating to predict the microstructure difference according to the Time Temperature Transformation (TTT) diagram. Where the double V-shape weld grooves has been cooled down in the exposed normal air cooling process faster than the U and V-shape welding grooves, while comparing the V-shape weldment groove with the U-shape welding groove seen that from the cooling curves of the V-shape weldment groove has been cooled down slower than the U-shape. Therefore, the prediction of the phase transformation of martensite phase formation in heat affected zone (HAZ) is more in the U-shape and double V-shape welding grooves by comparing with the V-shape welding groove.

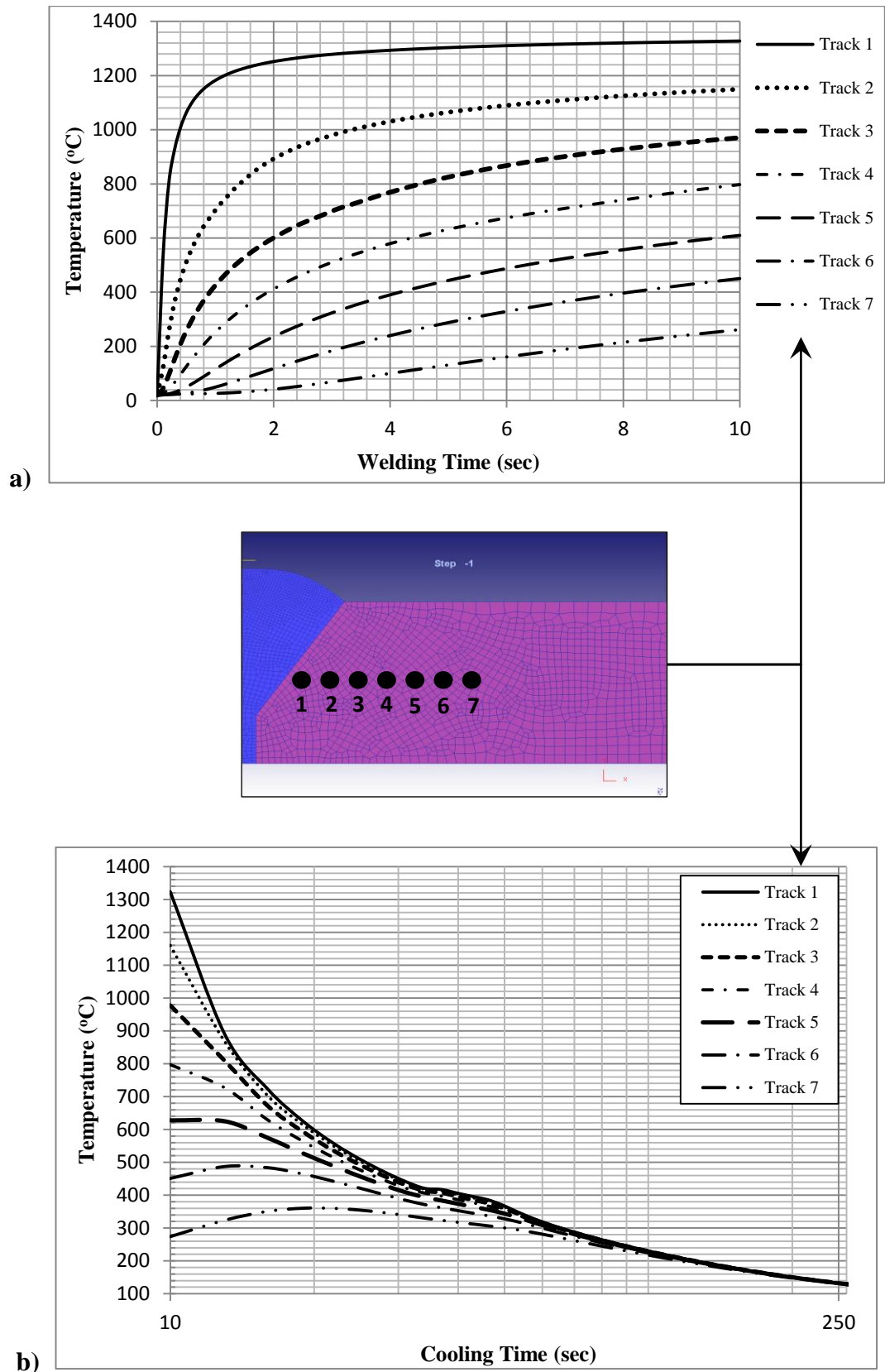


Figure 5.12 Single V-shape temperature distribution of the HAZ region of the finite element model during a) welding time b) cooling in still air.

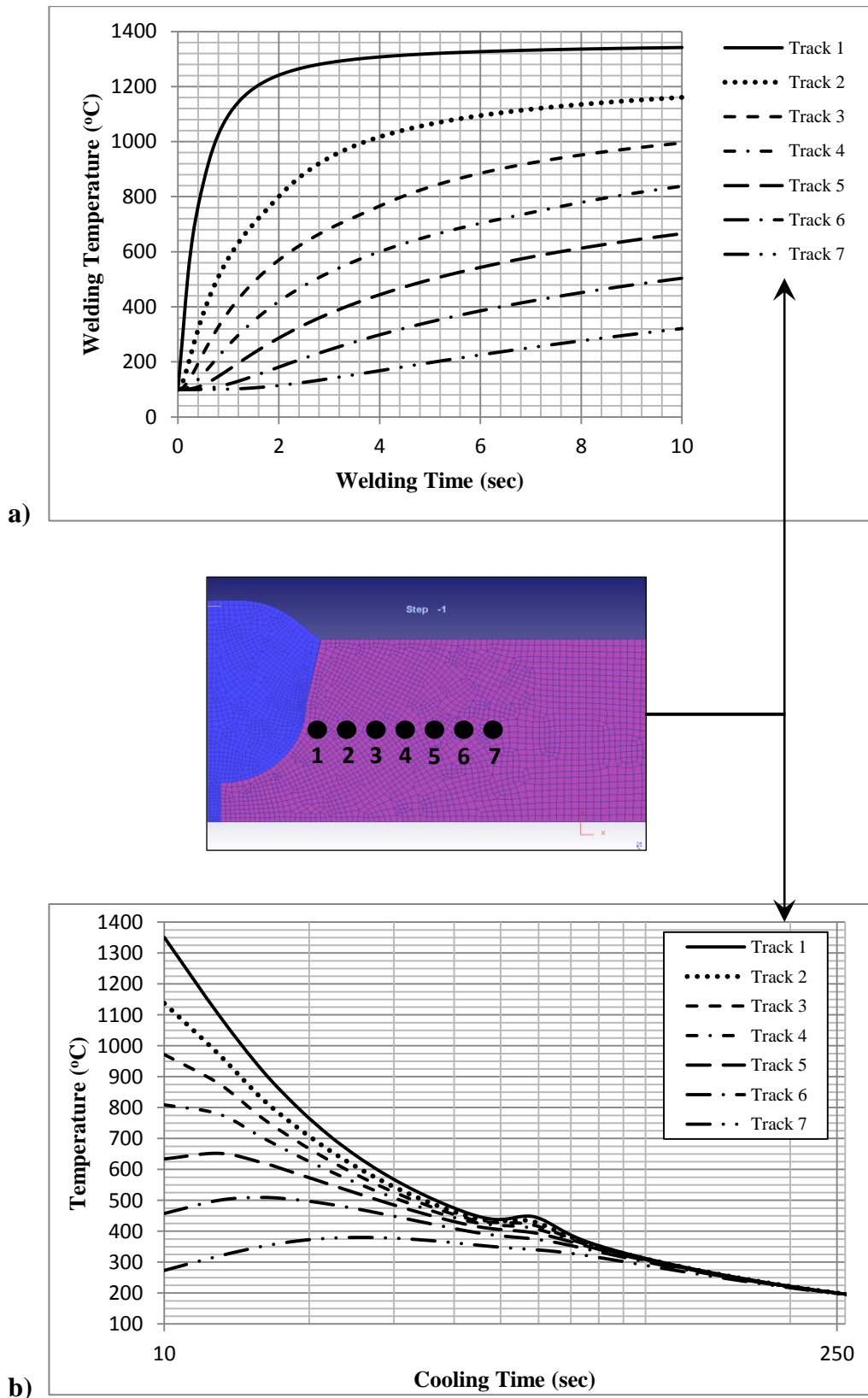


Figure 5.13 U-shape temperature distribution of the HAZ region of the finite element model during **a)** welding time **b)** cooling in still air.

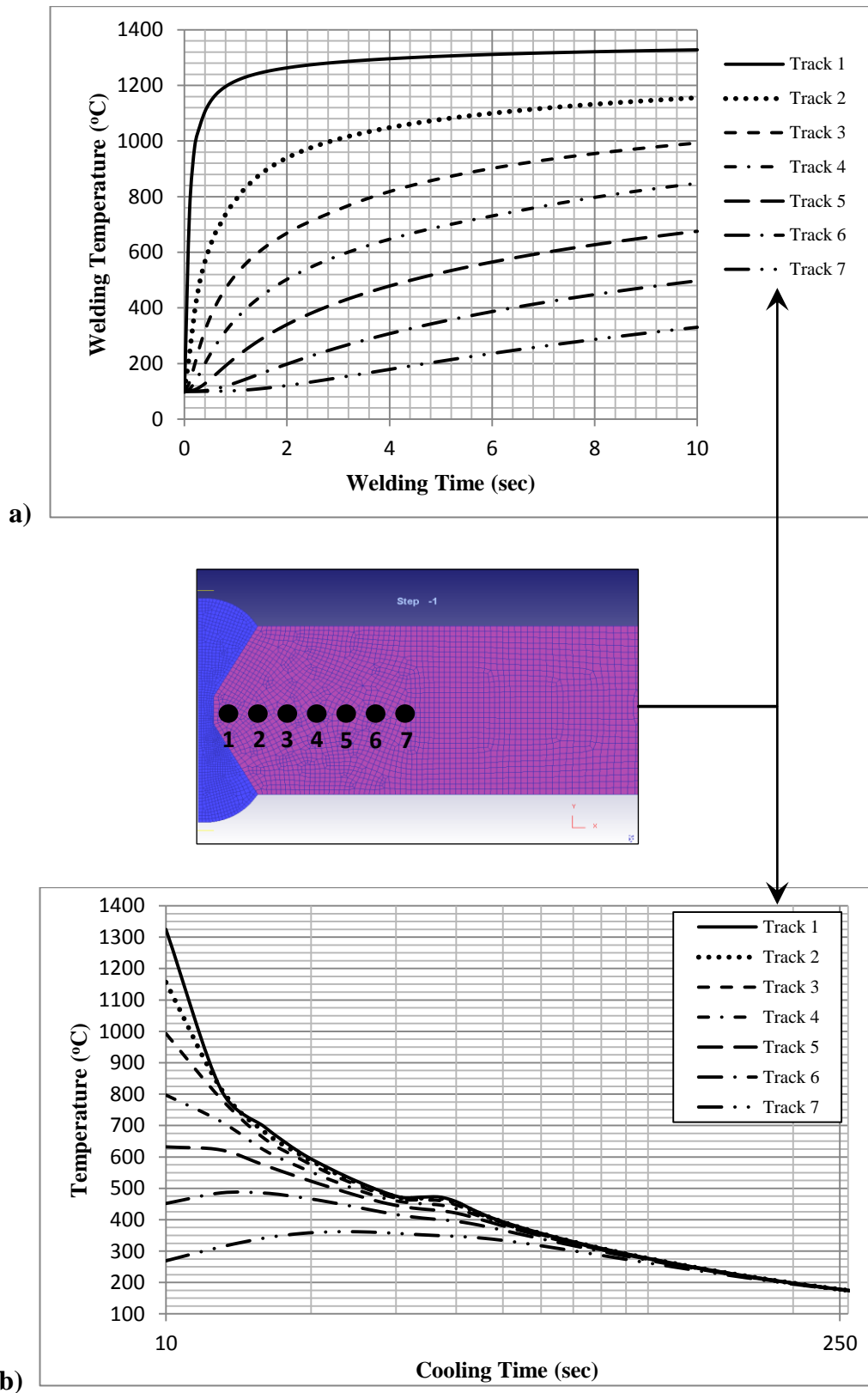


Figure 5.14 Double V-shape temperature distribution of the HAZ region of the finite element model during **a)** welding time **b)** cooling in still air.

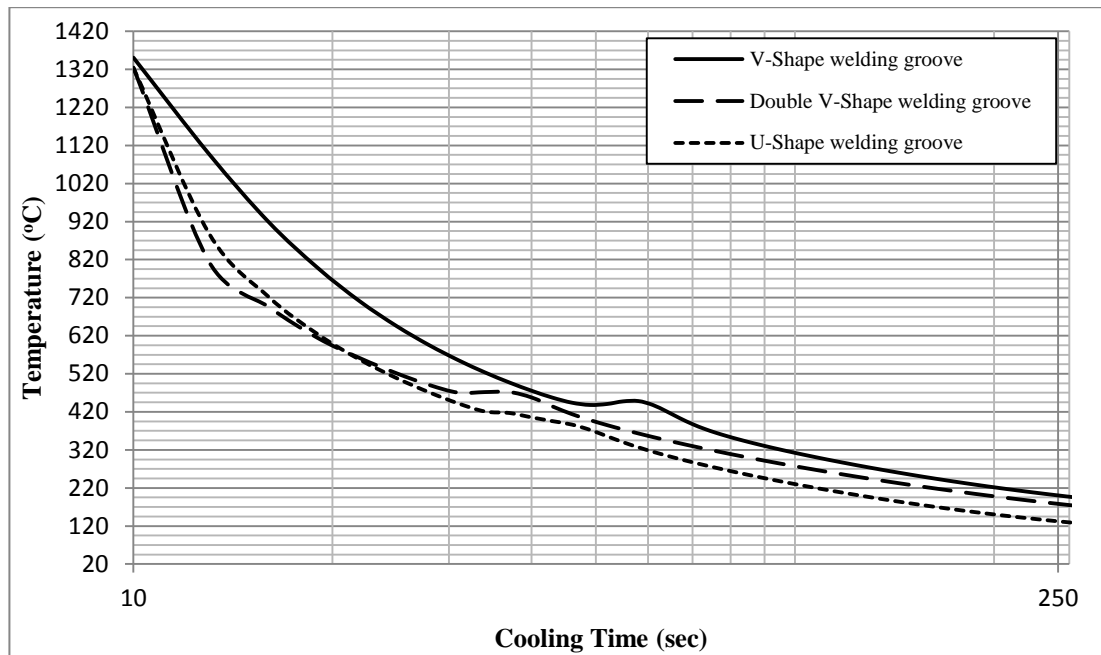


Figure 5.15 Cooling curves of the three types of butt welding groove shapes U, V and double V-shape through the HAZ area in 2D-FEM.

5.4.3 The effect of welding grooves on the grain size and microstructural features in the HAZ

Generally the relative effect of the common alloying elements on the movement of the nose of the Time Temperature Transformation (TTT) diagram to the right whereas, has a significant effect that cause retardation of the critical cooling rate, for this reason increases the opportunity of the formation of the martensite phase. As a result from the cooling curves of the three types of the welding groove shapes and the microstructure features examination of the Heat Affected Zone (HAZ) section area have been seen the formation of the martensite phase during cooling in normal exposed air cooling processes. In the three cases of the welded groove shapes seen that the bainite beginning phase transformation temperature of the AISI 1045 steel was evaluated 612°C, and the martensite beginning phase transformation temperature was evaluated 480°C, but in a different points and martensite volume fraction (MVF). In the Figure 5.16 of the single V - shape weldment, the maximum values of martensite volume fractions were % 18.3 for section (A) and % 29.3 MVF for section (B). In the Figure 5.17 of the U - shape weldment, the maximum values of martensite volume fractions were % 51.3 for section (A) and % 14.7 MVF for

section (B). In the Figure 5.18 of double V-shape weldment, the maximum values of martensite volume fractions were % 43.5 for section (A) and % 38.1 MVF for section (B). Eventually, if we compare the maximum values as a section in the three weldment shapes, the maximum martensite volume fraction was in the U - shape weldment, but if summarize the results of the sections of each shape, the maximum martensite volume fraction was found in double V-shape weldment. This means that, the double V-shape weldment is more hazardous shape for the hydrogen cracking. Since V-shape weldment has a lower value of the martensite volume fraction than two shapes.

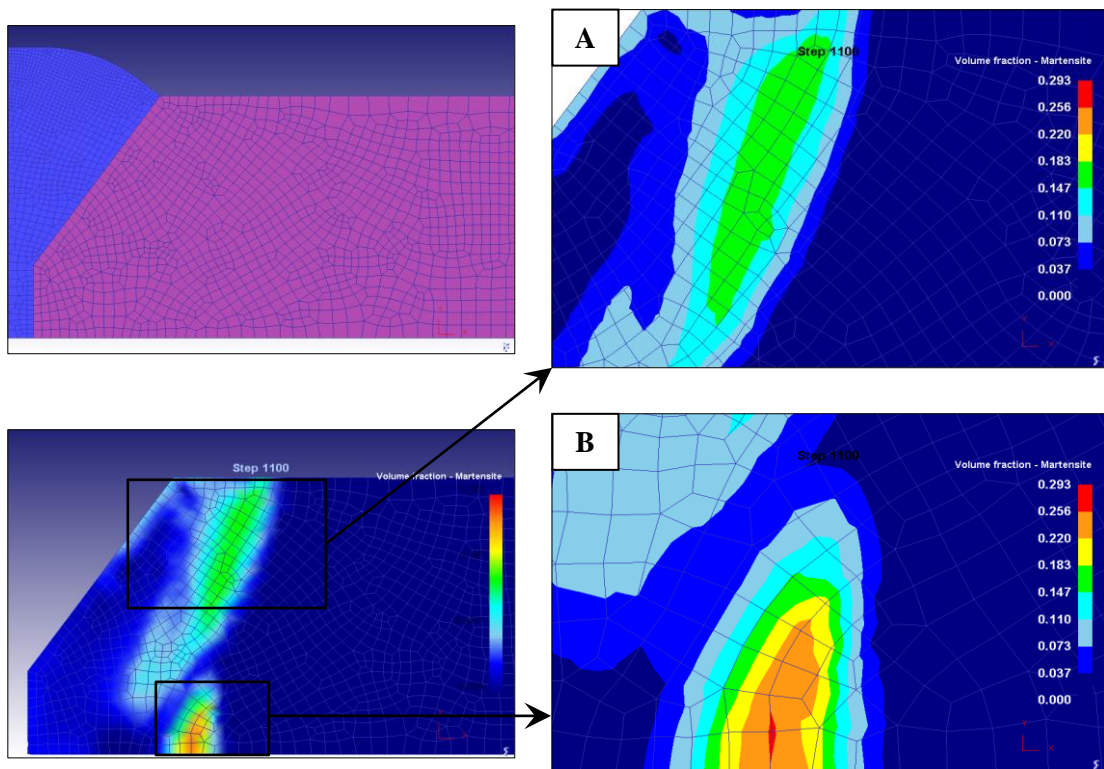


Figure 5.16 Microstructure of martensite phase transformation AISI 1045 steel in the HAZ area of V-Shape weldment in still air cooling process.

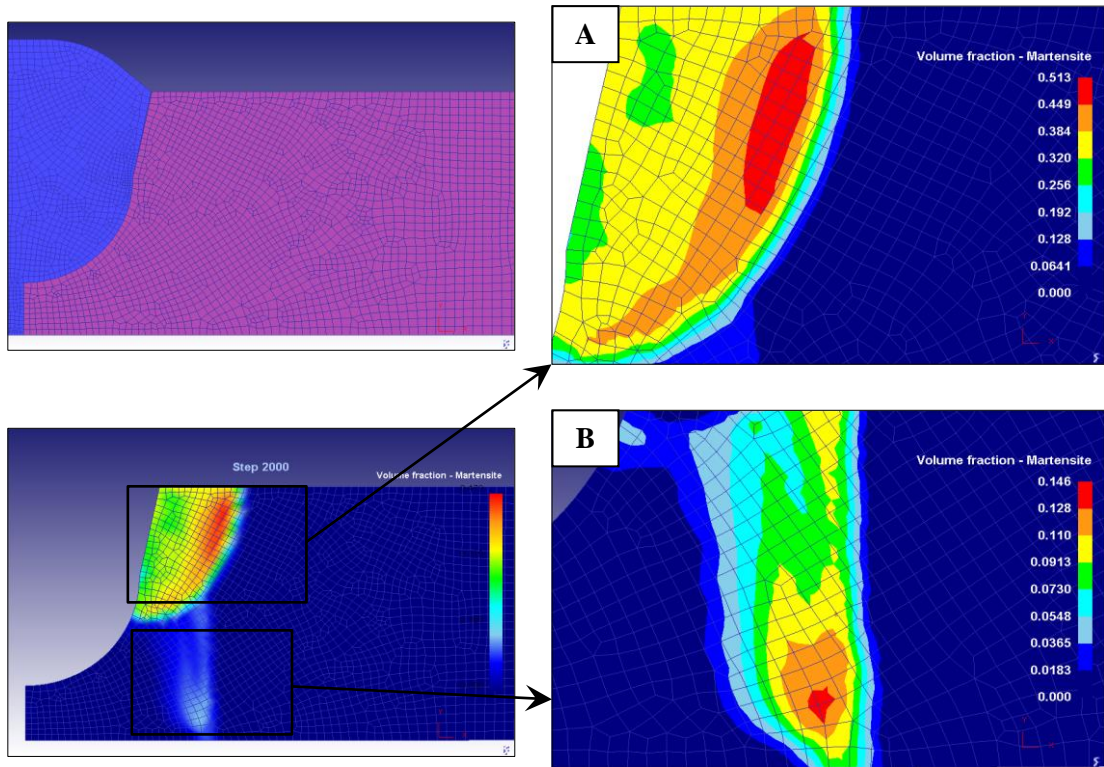


Figure 5.17 Microstructure of martensite phase transformation AISI 1045 steel in the HAZ area of U-Shape weldment in still air cooling process.

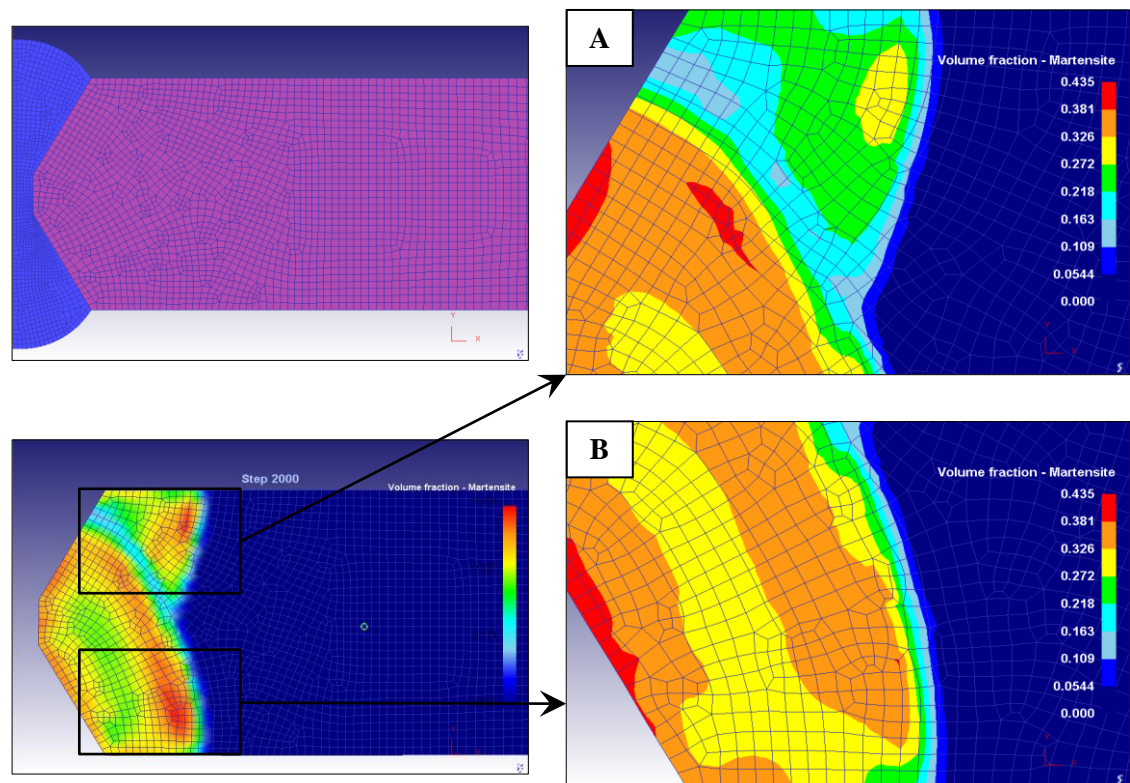
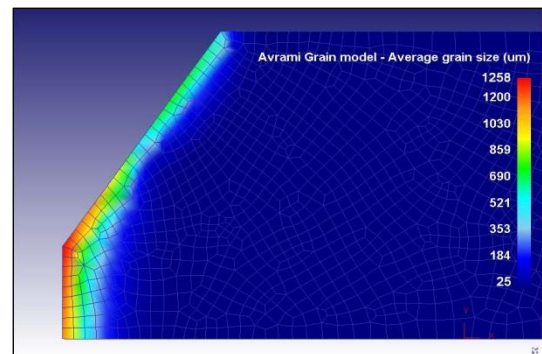


Figure 5.18 Microstructure of martensite phase transformation AISI 1045 steel in the HAZ area of double V-Shape weldment in still air cooling process.

The measured average grain size for the three shapes weldments has been carried out successfully in 2D-FEM. In the Figure 5.19 found that, the maximum average grain size adjacent to the fusion line for the three shapes are; 1258 μm for V-shape, 1377 μm for U-shape and 1100 μm for the double V-shape weldments respectively. In this case, the maximum value of average grain size adjacent to the fusion line found in U-shape weldment while the minimum value found in the double V-shape weldment, as it is shown in the Figure 5.20. As we have mentioned before, the grain size effect on the hardness of the metal, whereas with increasing grain size hardness decreases. This means the effect of the grain growth with the martensite phase are working opposite each other. On the other hand, the effect of grain size on the metal hardness is very small compared with the effect of martensite phase formation.

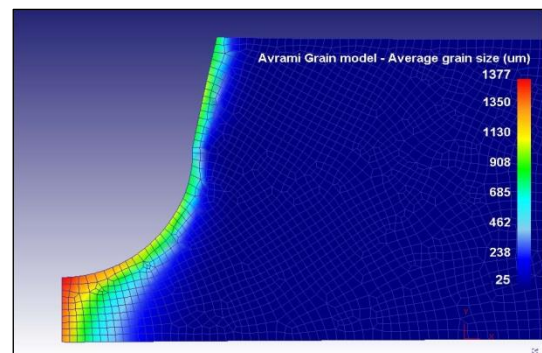
a) V-shape

Average grain size=1258 μm .



b) U-shape

Average grain size=1377 μm .



c) Double V-shape

Average grain size=1100 μm

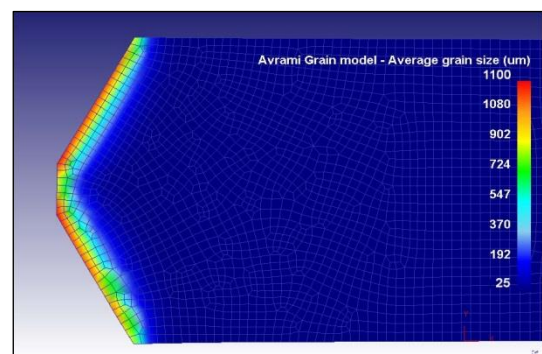


Figure 5.19 Average grain size for the weldment shapes V, U and double V in FEM.

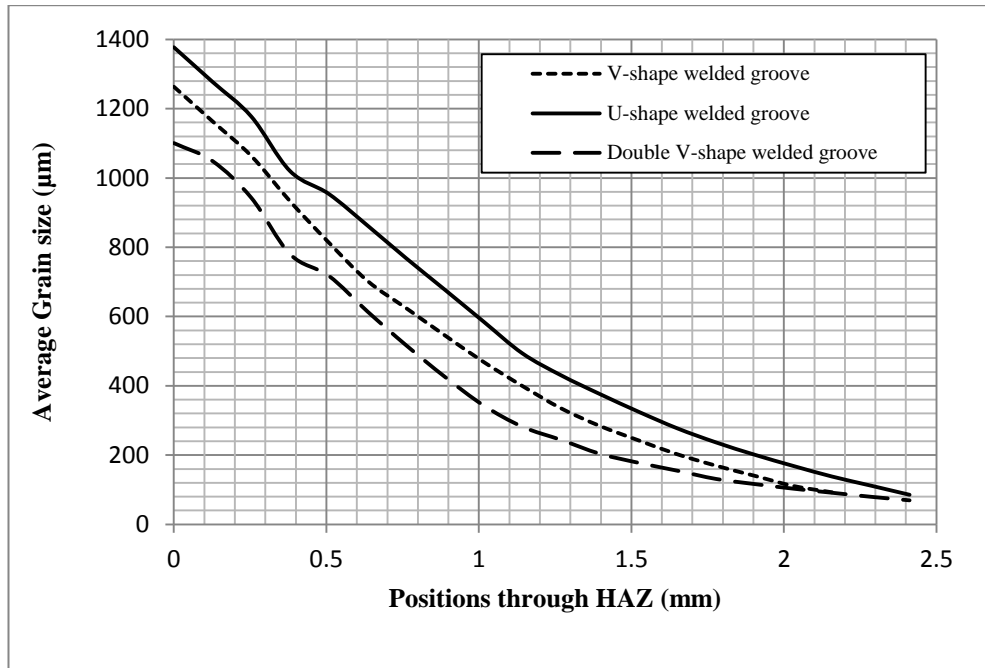


Figure 5.20 Comparison between the average grain sizes of the three weldment groove shapes through the HAZ area of AISI 1045 steel.

5.4.4 Preheating effect on AISI 1045 steel welding

After obtaining practical results and simulated 2D-FEM and compare it with each other to find out the validity of work performance 2D-FEM modeled part. Through the results obtained such as; microscopic examination and measurement of hardness test. The preheating temperature is the temperature of the parent metal immediately before welding commences. The main aim of the preheating process is to avoid martensite phase transformation that is liable for hydrogen cracking. Where preheating are applied locally to the joint preparation the required temperature are existed in the parent metal for a distance of 100 mm in any direction for the joint preparation. In V-shape weldment is pre-heated and the martensite volume fraction MVF has been found in each state for preheating process, where at 100°C was % 18.2 MVF, at 200°C was % 14.7 and at the 225°C, 0% of MVF was found, as it is shown in the Figure 5.21. U-shape weldment is preheated and the martensite volume fraction MVF has been found, at 100°C was % 46.4 MVF, at 200°C was % 18.7 and at 300°C zero percent of MVF, as it is shown in the Figure 5.22. Eventually, for double V-shape weldment is preheated and the martensite volume fraction MVF has been found, at 100°C was % 26.6 MVF, at 200°C was % 10.1 and at 350°C zero percent of MVF, which is shown in the Figure 5.23.

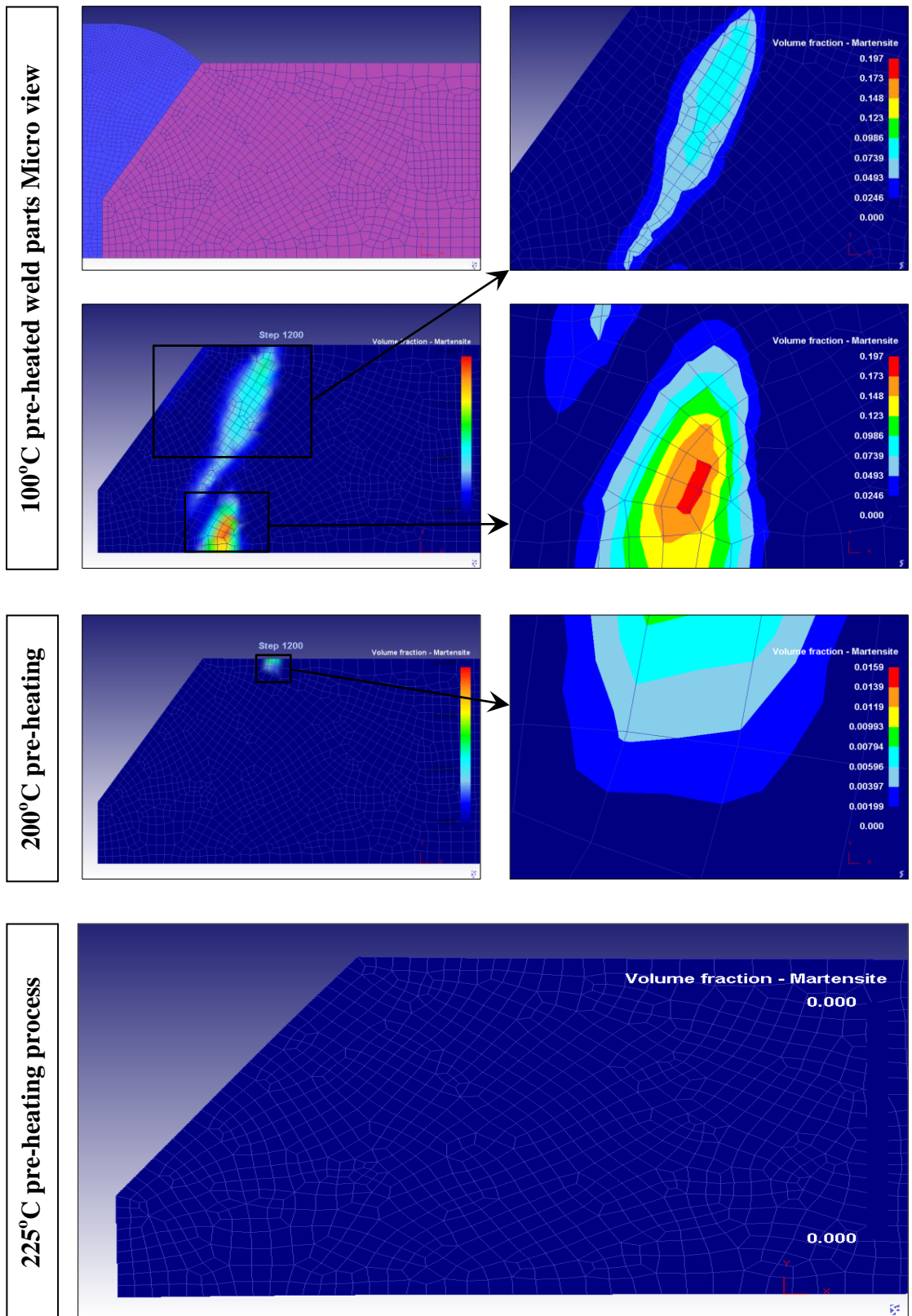


Figure 5.21 Pre-heating process and martensite microstructure view of HAZ area for the butt V-Shape groove weldment of the AISI 1045 steel.

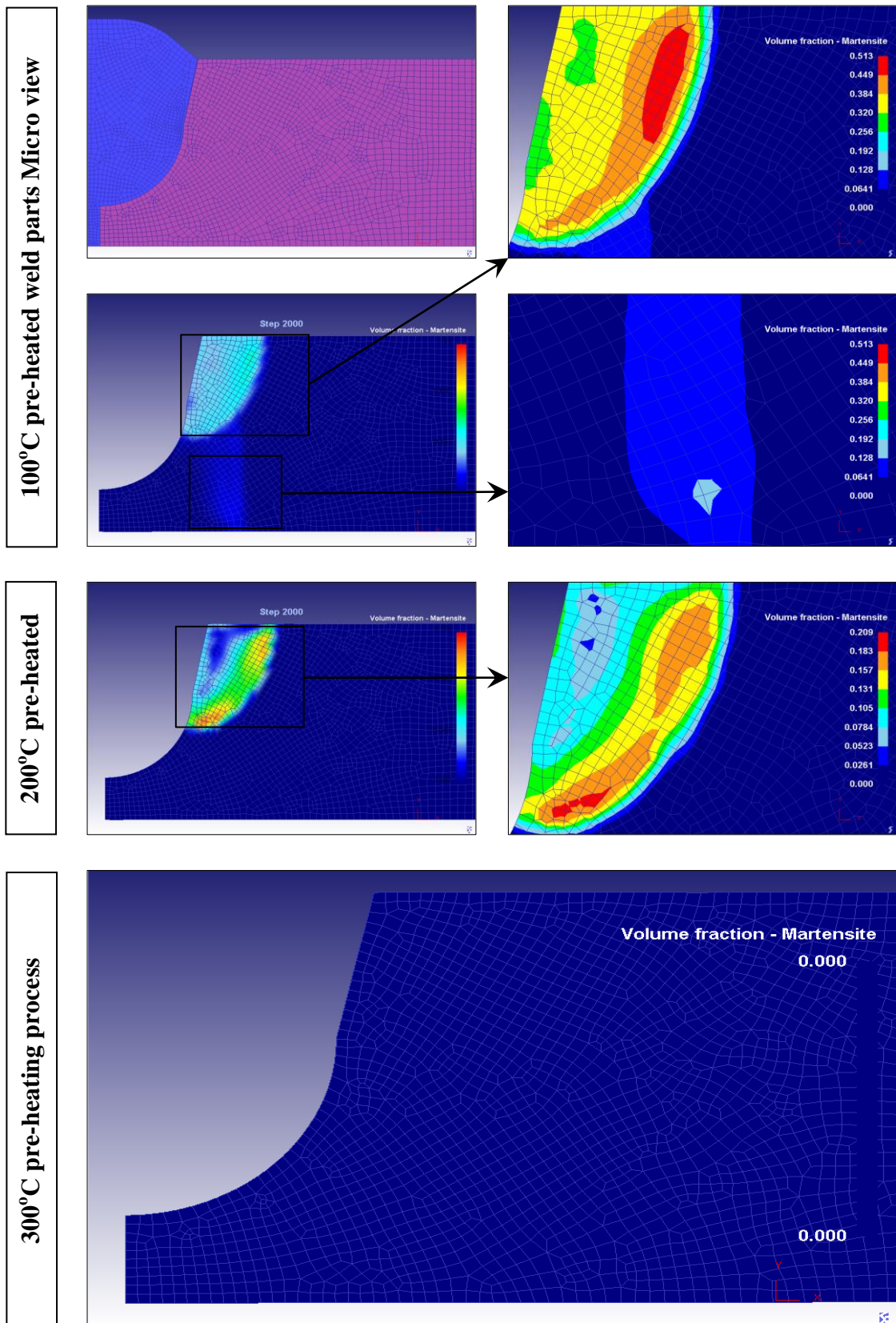


Figure 5.22 Pre-heating process and martensite microstructure view of HAZ area for the butt U-Shape groove weldment of the AISI 1045 steel.

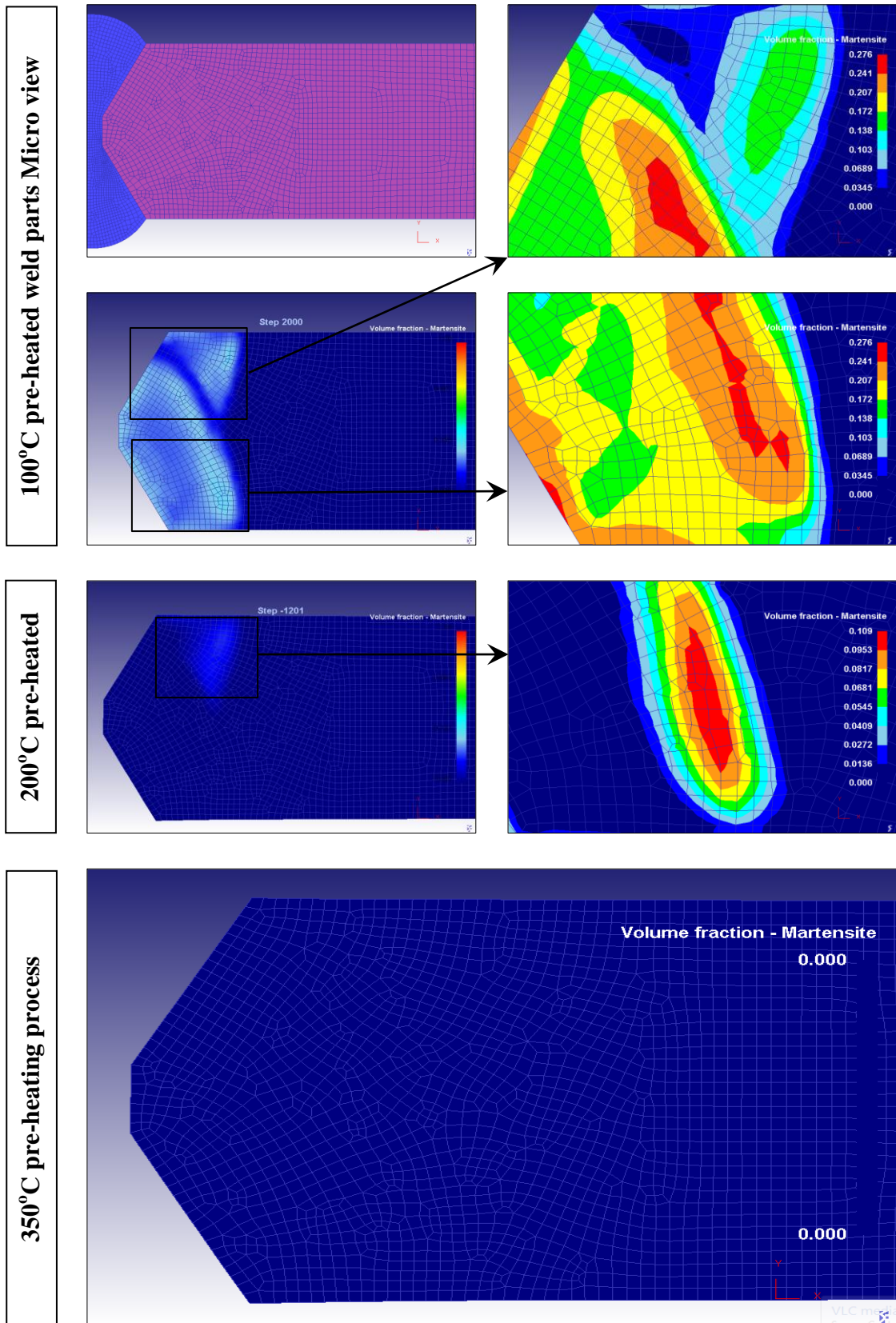


Figure 5.23 Pre-heating process and martensite microstructure view of HAZ area for the butt double V-Shape groove weldment of the AISI 1045 steel.

After the attempted elimination of martensite phase by preheating processes at several successful temperatures, meanwhile through the preheating process the hardness measurements with an average grain size of the AISI 1045 steel have been carried out. From the Figures 5.24, Figure 5.25 and Figure 5.26 for V, U and double V-shape welding grooves respectively seen that, the results of the average grain in comparison with the martensite volume fraction working opposite each other and there is a complex competition between the effect of grain refining and HAZ cooling cycle strengthening. The hardness test for the three welding groove shapes has been carried out also in this investigation. In the Figure 5.27 showed the hardness distribution of the HAZ for V-shape weldment at no pre-heating process with the performed preheating processes, while same modelling test is done on the U-shape weldment which is shown in the Figure 5.28 and for the double V-shape weldment shown in the Figure 5.29. From the results of the martensite volume fraction, the average grain size and hardness distribution of preheating process seen that, the martensite formation has a significant effect on the hardness. While, the elimination of martensite phase formation in the heat affected zone HAZ leads to prognosticate of the mutualized the mechanical properties of the HAZ region with base metal.

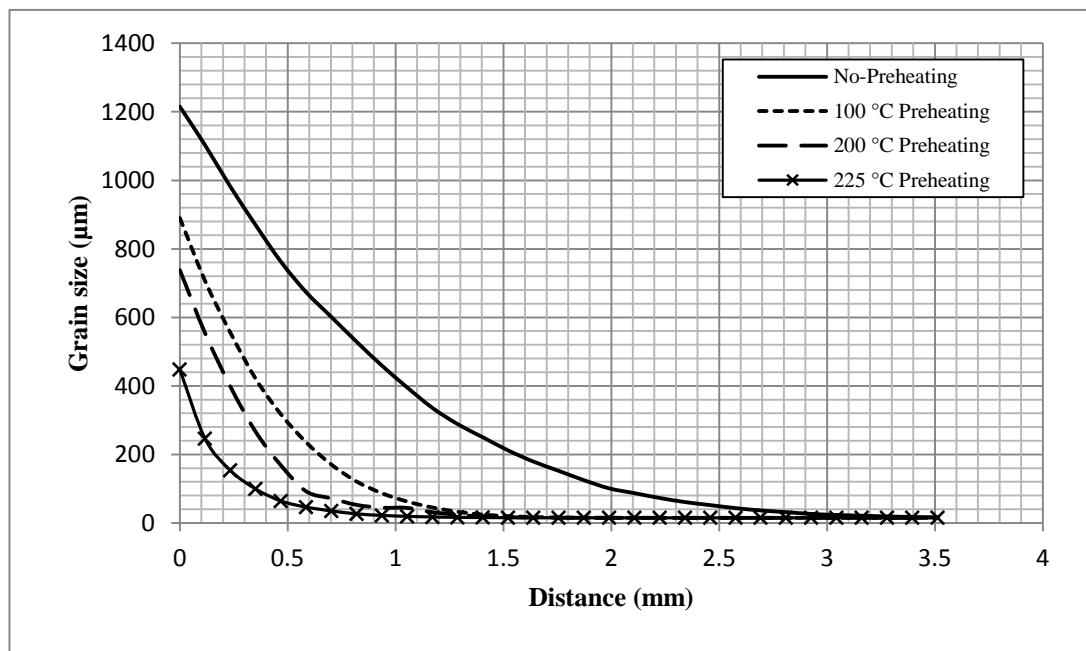


Figure 5.24 Distribution of average grain size of V-shape welding groove at the mid transverse direction of the welding line through the HAZ for different states of preheating.

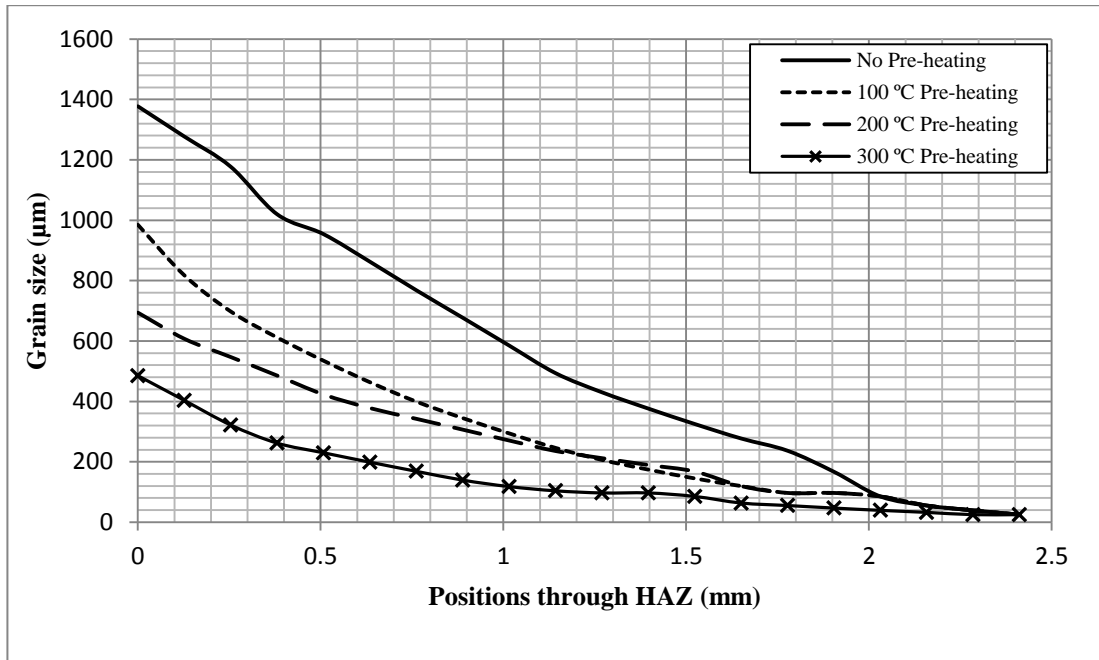


Figure 5.25 Distribution of average grain size of U-shape welding groove at the mid transverse direction of the welding line through the HAZ for different states of preheating.

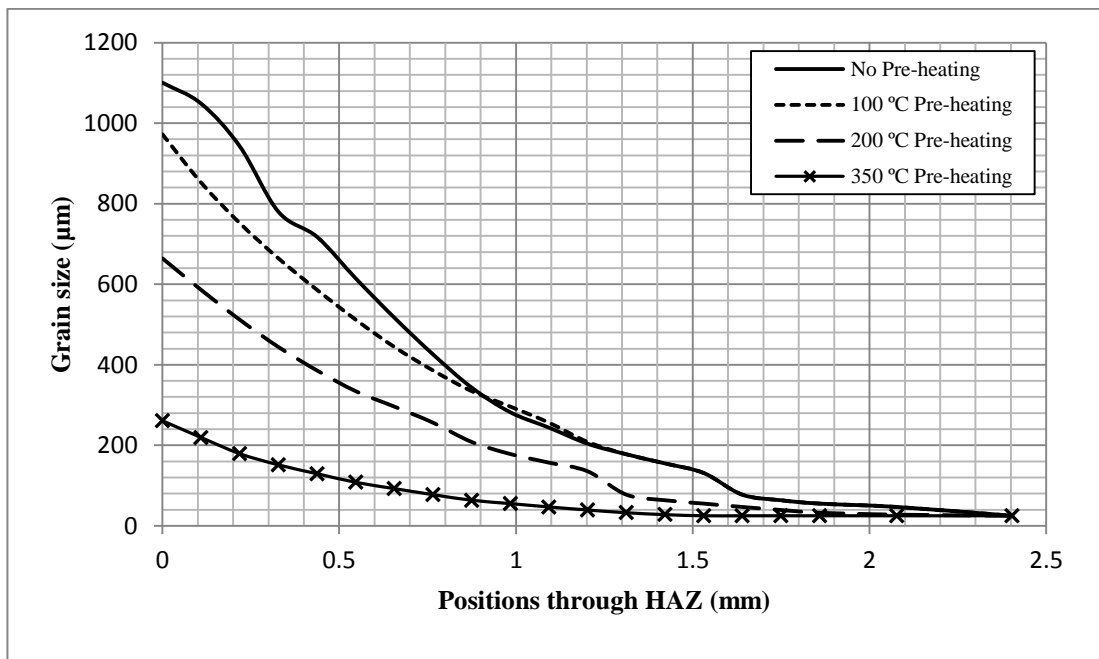


Figure 5.26 Distribution of average grain size of double V-shape welding groove at the mid transverse direction of the welding line through the HAZ for different states of preheating.

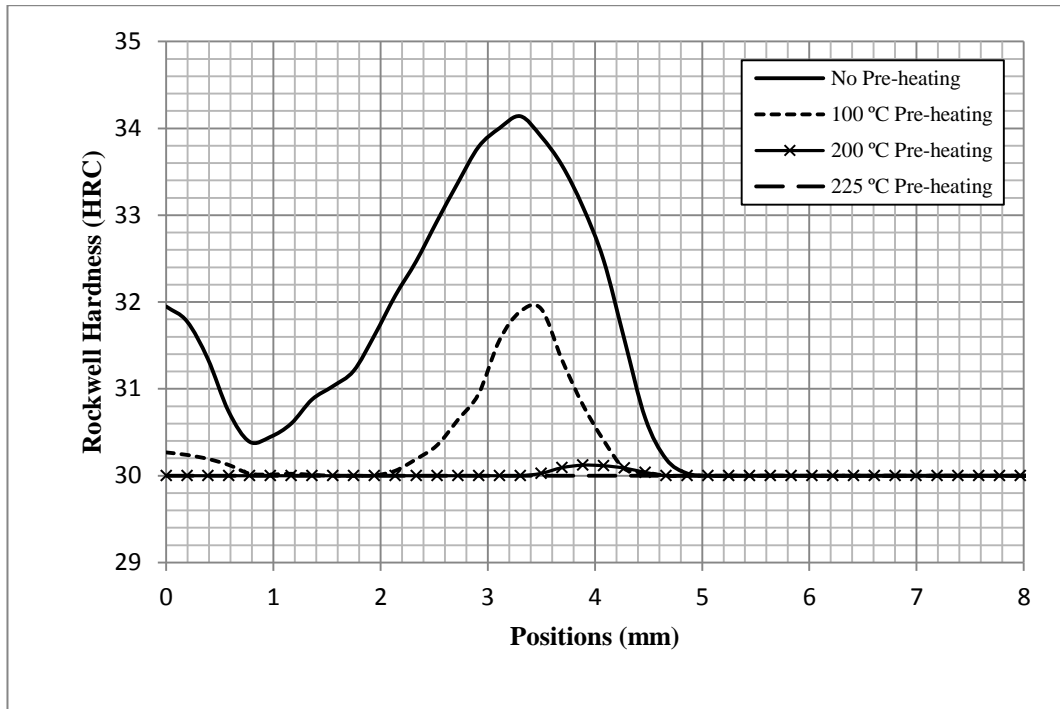


Figure 5.27 Distribution of hardness of the V-shape welding groove at the mid transverse direction of the welding line through the HAZ for different states of preheating.

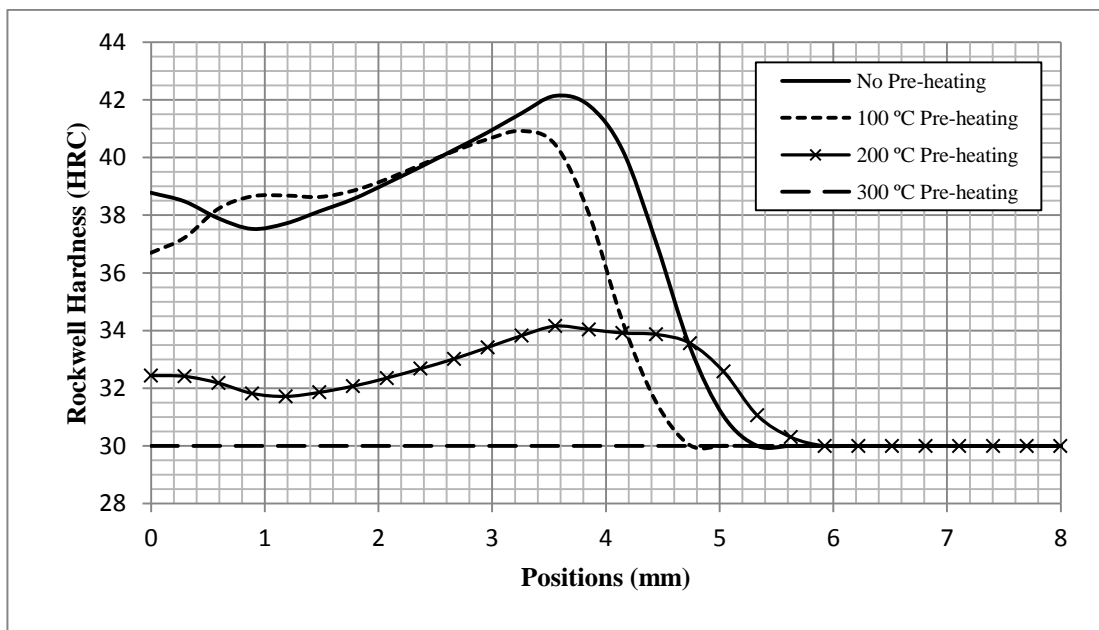


Figure 5.28 Distribution of hardness of the U-shape welding groove at the mid transverse direction of the welding line through the HAZ for different states of preheating.

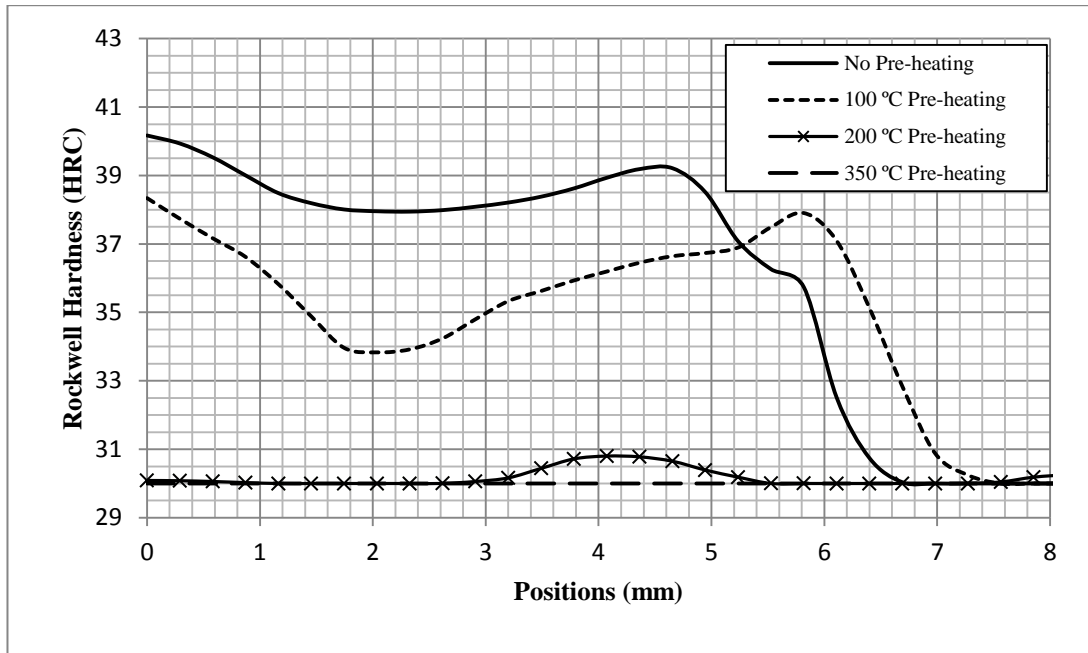


Figure 5.29 Distribution of hardness of the double V-shape welding groove at the mid transverse direction of the welding line through the HAZ for different states of preheating.

CHAPTER 6

CONCLUSIONS AND RECOMMENDATIONS

6.1 Conclusions

In this study, 2D finite element model of three shape butt welding grooves of AISI 1045 steel is presented. The temperature distribution, microstructure, grain growth, and the hardness of the heat affected zone (HAZ) were simulated. The results of the simulation were compared with the experimental ones. The main aim was to eliminate the martensite phase formation in the HAZ region by using pre-heating on the three types of welding groove shapes single V, double V, and U-shape respectively. According to the results obtained in the study, the followings may be concluded:

- The very close agreement between the simulation and experimental results show that the FE model is very effective for predicting the microstructure, the phase transformation, the grain growth and the hardness.
- One of the most practical methods to eliminate martensite formation during cooling of the welding is preheating. So that the proper selection of the preheat temperature is important in terms of time and cost. It was found that preheating the material to 225°C, 300°C and 350°C eliminates martensite formation completely for 12 mm thick, V, U and double V-shaped butt welding of AISI 1045 steel respectively.
- The presented FE model can be used easily for different thicknesses and groove shapes to evaluate the quality of the welding process.

- The martensite phase formation is significantly affected by temperature distribution caused by welding process, where during welding and cooling time become different according to the type of weld pool groove shapes, while the V-shape welding groove low martensite volume fraction has been noticed with the lowest preheating requirement for martensite elimination for 12mm thick.
- Hardness profile across the welded joints can be effectively used to predict the martensite phase formation in the HAZ area of free welds. Where seen that, the results of the average grain in comparison with the martensite volume fraction working opposite each other and there is a complex competition between the effect of grain refining and HAZ cooling cycle strengthening. The martensite phase formation has a significant effect on the hardness.

6.2 Recommendations

Finite Element Method for welding is relatively new technique, and has been ultimately invented for different application in the field of construction and manufacturing processes for analysing and computing in the different difficult conditions where it need long period of time to implement or execute it by experimental work, therefore there is a great opportunity to explore and investigate this topic and there still a lot of work to be done for adequate understanding of the technique and its suitability for use in different welding types. Hence the following topics are recommended for future works;

1. Investigating the effect of multi-passes on microstructural developments, preheating process and mechanical properties of AISI 1045 steel welded joints in the different thickness.
2. Investigating the fatigue behaviour of AISI 1045 steel welded joints, by using the finite element package.
3. Using experimental and finite element modelling for computing residual stresses for different groove shapes welded weldments.
4. Investigating the exact relation between process parameters and microstructural developments after post weld heat treatments.

REFERENCES

1. Uday S. Dixit (1997). “*Finite Element Method*”, Department of Mechanical Engineering, Indian Institute of Technology Guwahati-781 039, India.
2. ASM Handbook (2004). Volume 09: “*Metallography and Microstructures*”, P31-38.
3. Lars-Erik Lindgren (2007). “*Computational Welding Mechanics Thermomechanical and Microstructural Simulations*”, Cambridge England.
4. W. A. Johnson and R. A. Mehl (1996). “*Reaction kinetics in the processes of nucleation and growth*”, Trans. AIME Vol.135.1939. P416.
5. DEFORMTM Manual (2006). Heat treatment laboratory & Modelling of microstructure evaluation.
6. Sindo Kou, Professor and Chair Department of Materials Science and Engineering, University of Wisconsin (2003). “*Welding Metallurgy*”, Second Edition, Published by John Wiley & Sons, Inc., Hoboken, New Jersey. Published simultaneously in Canada.
7. Te-Chang Tsai, Chih-Chung Chou, Deng-Maw Tsai, and Ko-Ta Chiang (2011). Modeling and analyzing the effects of heat treatment on the characteristics of magnesium alloy joint welded by the tungsten-arc inert gas welding, *Materials and Design*, **32**, 4187–4194.
8. Guodong Zhang, Changyu Zhou, Zhaoxi Wang, Fei Xue, Yanfen Zhao, Lu Zhang, and Yan Liu (2012). Numerical simulation of creep damage for low alloy steel welded joint Considering as-welding residual stress, *Nuclear Engineering and Design*, **242**, 26– 33.

9. Masanori Kikuchi, Yoshitaka Wada, Yuto Shimizu, and Yulong Li (2012). Crack growth analysis in a weld-heat-affected zone using S-version FEM, *International Journal of Pressure Vessels and Piping*, **90-91**, 2-8.
10. Z. Barsoum, and A.Lundbäck (2009). Simplified FE welding simulation of fillet welds – 3D effects on the formation residual stresses, *Engineering Failure Analysis*, **16**, 2281–2289.
11. I. Sattari-Far, and M.R. Farahani (2009). Effect of the weld groove shape and pass number on residual stresses in butt-welded pipes, *International Journal of Pressure Vessels and Piping*, **86**, 723–731.
12. D. Akbari, and I. Sattari-Far (2009). Effect of the welding heat input on residual stresses in butt-welds of dissimilar pipe joints, *International Journal of Pressure Vessels and Piping*, **86**, 769–776.
13. V.K. Goyal, P.K. Ghosh, and J.S. Saini (2009). Analytical studies on thermal behaviour and geometry of weld pool in pulsed current gas metal arc welding, *journal of materials processing technology*, **209**, 1318–1336.
14. Dean Deng (2009). FEM prediction of welding residual stress and distortion in carbon steel considering phase transformation effects, *Materials and Design*, **30**, 359–366.
15. Zacharia, T., et al. (1995). Modeling of fundamental phenomena in welds. *Modelling and Simulation in Materials Science and Engineering*. 3: 265-288.
16. Akhlagi, M. and J. Goldak (2005), *Computational Welding Mechanics*. Springer.
17. Radaj, D., *Grundlagen and Anwendungen* (1999). *Schweissprozess-simulation*, Fachbuche Schweisstechnik, German. 141, p. 193.
18. Radaj, D. (2003). *Welding residual stresses and distortion. Calculation and measurement*. DVS-Verlag.

19. Ramirez, M., G. Trapaga, and J. McKelliget (2003). A comparison between two different numerical formulations of welding arc simulation. *Modelling and Simulation in Materials Science and Engineering*.
20. Zhu, P. (1998). Computer simulation of gas metal welding arcs. In *5th International Conference on Trends in Welding Research*. Pine Mountain, Georgia: American Welding Society.
21. DebRoy, T. (1999). Mathematical modelling of fluid flow and heat transfer in fusion welding. In *Mathematical Modelling of Weld Phenomena*. Seggau, Austria: IOM Communications.
22. Winkler, C., et al. (2000). The effect of surfactant redistribution on the weld pool shape during GTA-welding. *Science and Technology of Welding and Joining*.
23. Do-Quang, M. and G. Amberg (2003). Modelling of time-dependent 3D weld pool flow. In *Mathematical Modelling of Weld Phenomena Graz, Austria*.
24. Pavlyk, V. and U. Dilthey (2004). Simulation of weld solidification microstructure and its coupling to the macroscopic heat and fluid flow modelling. Vol. 12. S33.
25. Pavlyk, V. and U. Dilthey (1999). A numerical and experimental study of fluid flow and heat transfer in stationary GTA weld pools. In *Mathematical Modelling of Weld Phenomena*. Seggau, Austria: IOM Communications.
26. Sudnik, W., D. Radaj, and W. Erofeew (1998). Computerized simulation of laser beam weld formation comprising joint gaps. *Journal of Physics D: Applied Physics*.
27. Sudnik, W., et al. (2000). Numerical simulation of weld pool geometry in laser beam welding. *Journal of Physics D: Applied Physics*.

28. Alexander, R., E. Bohnart, and R. Witcraft (2000). *Welding, The Fundamentals of Welding, Cutting, Brazing, Soldering, and Surfacing of Metals*. John Deere Publishing.
29. Althouse, A., K. Bowditch, W. Bowditch, and C. Turnquist (1988). *Modern Welding*. The Goodheart-Wilcox Company, Inc.
30. American Welding Society (2008). *The AWS Certified Welder Program (Brochure)*.
31. Anderson, W., T. Hoerner, and V. J. Morford (1988). *Metals and Welding*. Hobar Publications.
32. American Welding Society (1993). *AWS QC7-93 Standard for AWS Certified Welders*.
33. Matthews, J. & Sellon, W. (2012). *Arc Welding: A Basic Manual of Instruction for Learning How to Use Arc Welding*. The James F. Lincoln Arc Welding Foundation. Cleveland, OH.
34. Corinne Charles and Niklas Järvistråt (2006). *Finite Element Modelling of Microstructure on GTAW Metal Deposition of Ti-6Al-4V*.
35. M. Cronje, December (2005). *Finite Element Modelling of Shielded metal Arc Welding*, Stellenbosch University, 7602 Matieland, South Africa.
36. American Society for Metals, Metals Park, Ohio (1977). *TTT diagram after Atlas of Isothermal Transformation and Cooling Transformation Diagrams*.
37. George E. Totten (2006). *Steel Heat Treatment, Equipment and process design*, Second edition, Portland USA, P166.
38. Robert W. MESSLER, Jr. (2004). *Materials Science and Engineering Department Rensselaer Polytechnic Institute Troy, NY. Principle of Welding; Processes, physics, chemistry, and metallurgy*.

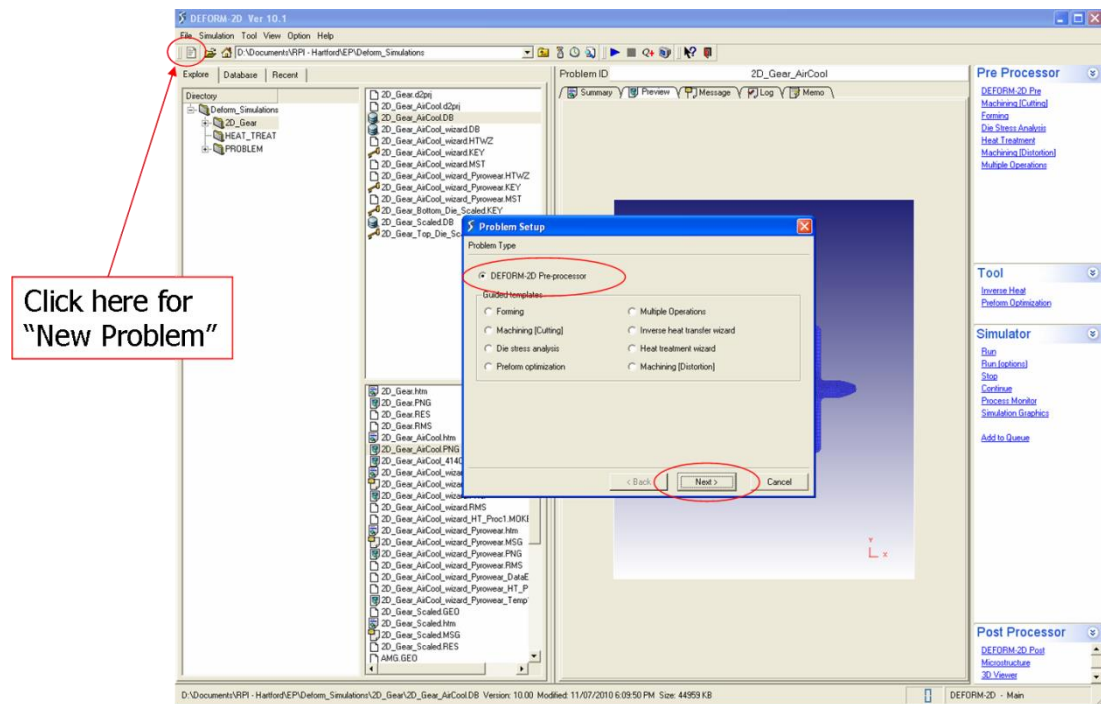
39. F.G. Fontana (1986). Corrosion Engineering; Third ed. McGraw-Hill Book Company, New York.
40. Michaleris, P. and A. DeBiccari (1996). Prediction of Welding Distortion, Welding Journal, 76(4): 172s-180s.
41. G. R. LIU and S. S. QUEK (2003). “*The Finite Element Method*”, Butterworth-Heinemann An imprint of Elsevier Science Linacre House, Jordan Hill, Oxford.
42. A. J. DAVIES Professor of Mathematics, University of Hertfordshire (2011). “*The Finite Element Method*” , Second Edition, , Oxford University press, , P274
43. Goldak, J., Bibby, M., Moore, J., House, R., Patel, B. (1986). Computer Modeling of Heat Flow in Welds, Metallurgical Transactions B, Volume 17B, p 587 – 600.
44. Bonifaz, E.A. (2000). Finite Element Analysis of Heat Flow in Single-Pass Arc Welds, Welding Journal, v 79, p 121s – 125s.
45. Deo, M.V., Michaleris, P., Sun, J. (2002). Prediction of Buckling Distortion of Welded Structures, Science and Technology of Welding and Joining.
46. Weaver, M.A. (1999). Determination of Weld Loads and Throat Requirements Using Finite Element Analysis with Shell Element Models – A Comparison with Classical Analysis, Welding Journal, v78, n4, p 116s – 126s.
47. A to Z materials Network UK Ltd.
<http://www.azom.com/article.aspx?ArticleID=6130>.
48. International Standard Organization ISO 9692 (2008). Common welding groove shapes dimensions.

49. International Standard Organization ISO 2560 (2008). Electrode selection for medium carbon steel.
50. American Society for Testing and Materials ASTM E3 (2012). Standard Guide for Preparation of Metallographic Specimens.
51. American Society for Testing and Materials ASTM E112 (2012). Standard Test Methods for Determining Average Grain Size.
52. American Society for Testing and Materials ASTM E92-03 (2012). Standard Test Method for Vickers Hardness of Metallic Materials.
53. G. F. Vander Voort (1991). Atlas of Time-Temperature Diagrams for Irons and Steels ASM International.
54. DEFORMTM user's manual released (2011). V. 10.0.
55. ASM Handbook (1991). Heat Treating, Volume 04 ASM International.
56. American Society for Testing and Materials ASTM E140-97 (2012). Standard Hardness Conversion Tables for Metals Relationship.
57. J R Davis and associates (1993). ASM international handbook committee, 5th edition, PP 393-398.
58. T Hirata, T Oguri, H Hagino, T Tanaka, S W Cheng, Y Takigawa and K Higashi (2007). "Influence of friction stir welding parameters on grain size and formability in 5083 aluminum alloy", Journal of materials science and engineering A 456, PP. 344-349.

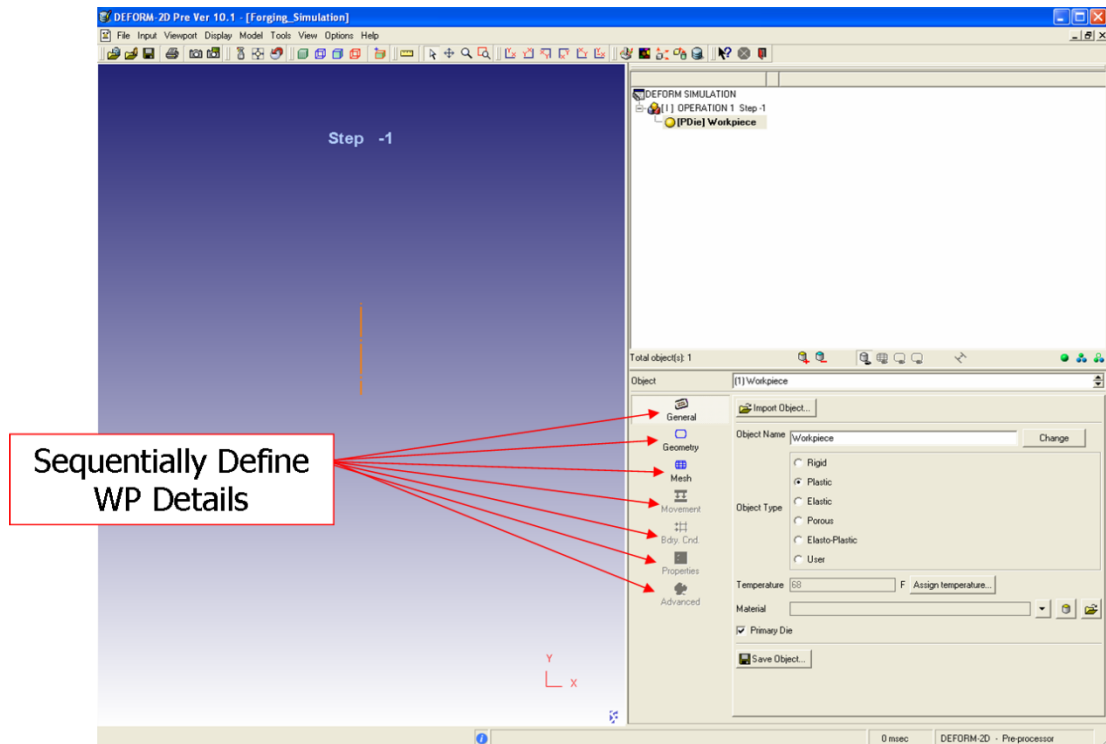
APPENDIX A

2D-DEFORM™ User's Guide

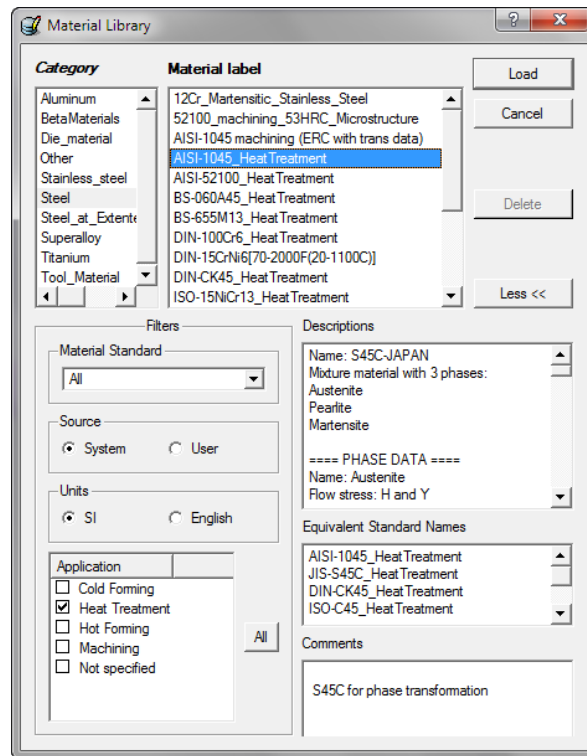
The following gives some instruction about setting up a 2D welding simulation in 2D-DEFORM™. The instructions are intended for the use of version 10.0 on a PC. To get started, find “2D-DEFORM™” in your programs list under the start menu. When the program opens, go to the top left corner of the screen and click to start a new problem. When the “Problem Setup” menu comes up, selects “2D-DEFORM™ Pre-processor” and “next” as shown below:



The next screen will ask about the user directory. All program files will be stored in this directory, so it is wise to store this in a convenient and accessible location. After the directory is selected, the user is prompted to name the project. No spaces or punctuation characters allowed, so name the project something like “Arc_Welding”. Now, the user is directed to the main pre-processor module. The first object that must be defined is the work piece. The details for the work piece including material behaviour, temperature, material, mesh, boundary conditions, et cetera are all done here sequentially in the object “tree” as shown in the followed page.



Fill out the general information by selecting the material behaviour to be “Elastic-Plastic” for the welding operation. Select a temperature of the work piece to be at the beginning of the welding operation, such as 20°C as an environment temperature, by clicking “Assign Temperature”. Next, a material should be assigned by clicking the button that looks like a cylinder to the right of “Material”. This will allow the user to load a material from the 2D-DEFORM™ library. It is important here to select a material that is or accurately represents the flow stress of the material of the work piece. Here, AISI 1045 steel is selected. As seen in the image below, the user can select a general material such as steel or aluminium from the “Category” list on the left and see the assortment of alloys available under “Material Label”. Material Standard such as AISI can be selected as well. For a welding simulation, it is wise to uncheck all but “Heat treatment” in the “Application” list at the bottom left hand side of the Material Library window. This will allow the user to select only from materials that have the proper material properties for the application selected. Once the desired material is selected, click “load”.

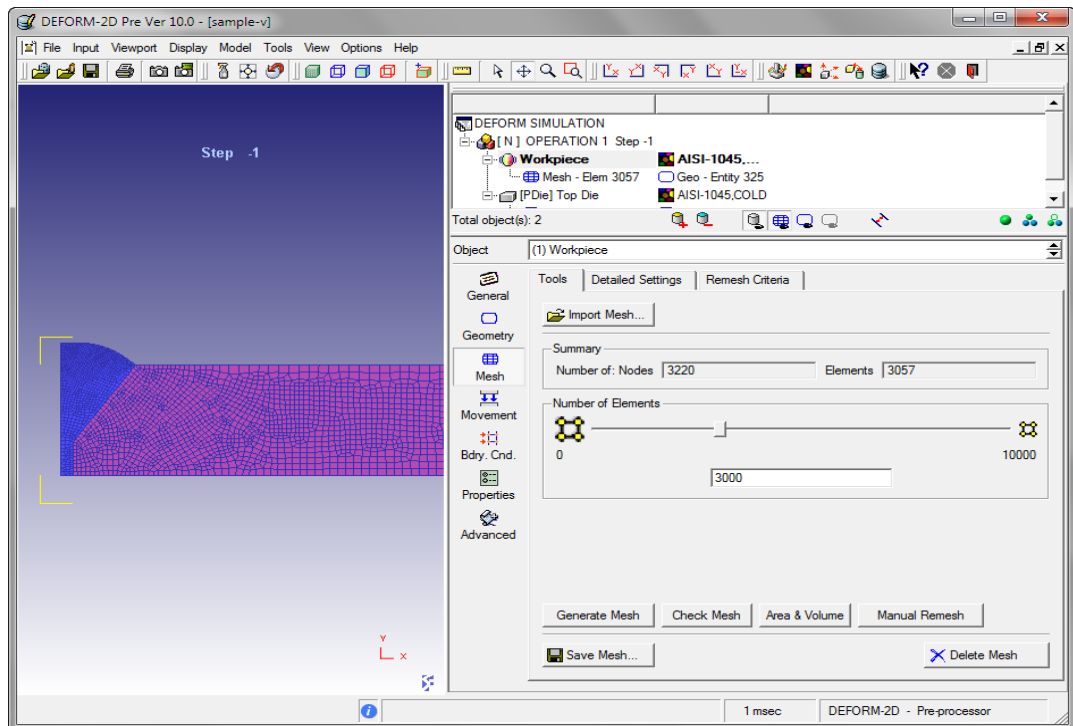


Next, the user can move to “Geometry” in the object tree and import a geometry file in formats such as IGS, KEY, DXF, DB or GEO. The user may also create a simple geometry by defining points in tabular format to be connected by straight lines or arcs. This may be accessed with the “Edit” tab. If the geometry is defined manually by points, the user should select “Check Geometry” under the tools tab to ensure the geometry can be read by 2D-DEFORM™. The user can specify a closed or open loop here. “Check and Correct Geometry” should be clicked to see if the geometry created is sufficient. There is also an option to scale geometry, which may be useful for modifications to work piece and die geometry. For the purpose of this welding operation, the workpiece will be modelled as a rectangular piece with sharper edges.

Next, the user should move to “Mesh” in the object tree. The work piece geometry can be manipulated on the screen now in the following manner:

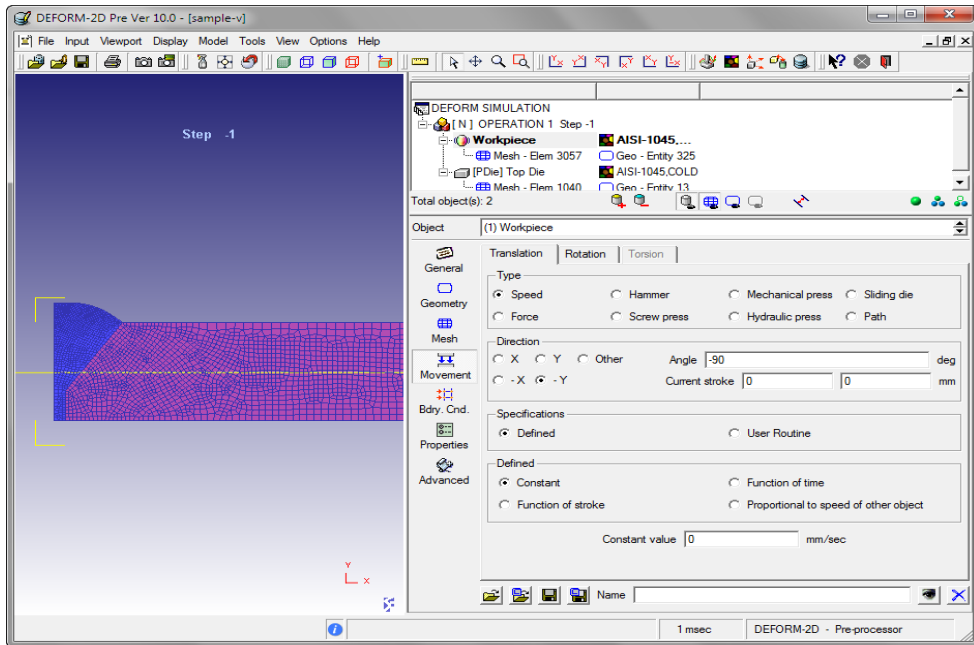
- | | |
|---------------------------------|------|
| Shift + Left Mouse Button | Pan |
| Shift + Alt + Left Mouse Button | Zoom |

The user can select how refined a mesh is necessary for the work piece. Here, the workpiece will be meshed with 3000 elements. This is done by setting “Number of Elements” to 3000 as seen below;

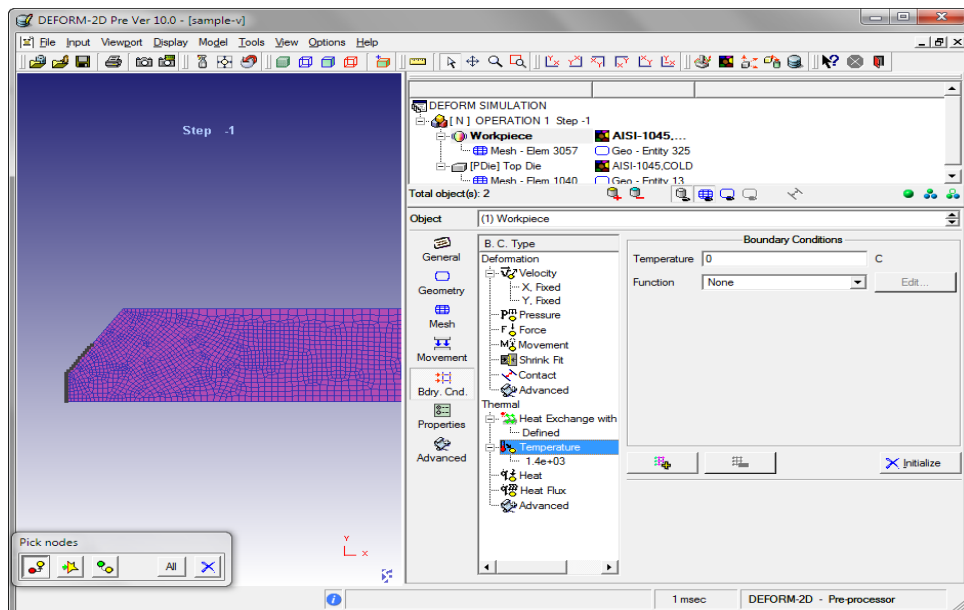


The user should also set the “Re-mesh Criteria” under the tab with this name. The re-mesh criteria specify the amount of interference allowed before the work piece is re-meshed. If the re-mesh criteria are too fine, the workpiece will re-mesh more often and the model will take longer to run. However, this may yield better results as the welding shape is more accurately represented when it is re-meshed during the simulation. The user can read more in detail about this in the 2D-DEFORM™ manual.

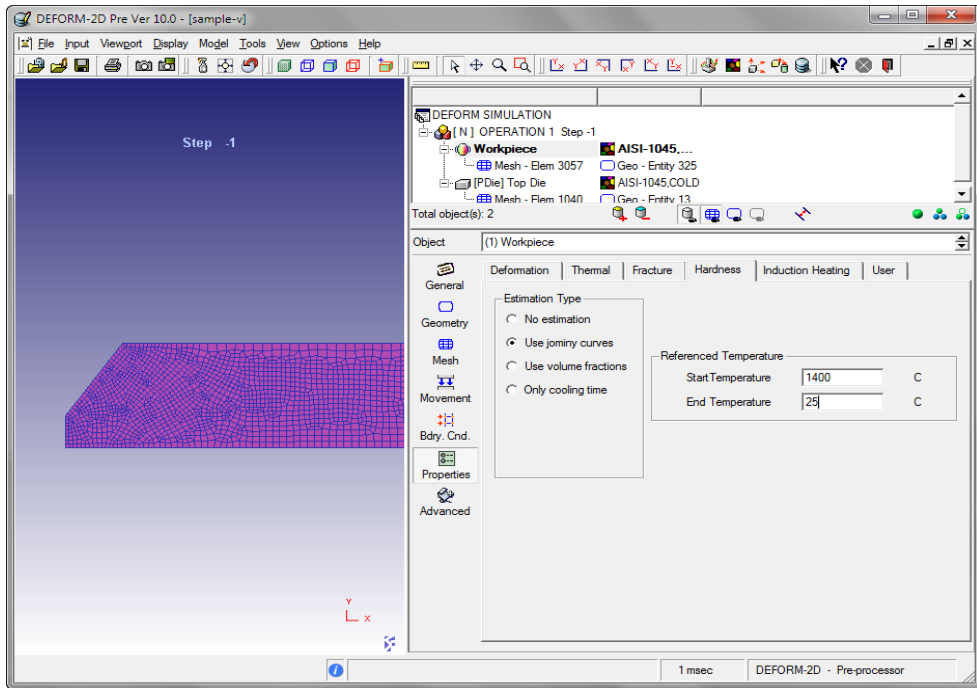
Next, move to “Movement” in the object tree. During this welding operation, the workpiece will be stationary state. Therefore, no movement definition is needed for either the work piece and it should be left as the default “constant value” = 0 in/sec as seen in the followed page.



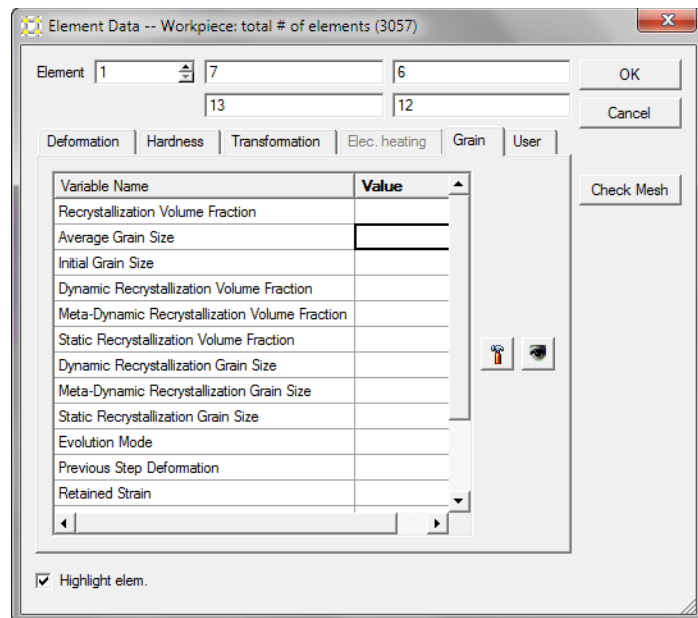
Next, move to Boundary Conditions and Properties in the object tree and fill any specific details about the workpiece. These settings are not required for all simulations, but exist so that the user may add details to the simulation if desired. The most important part of the welding process is the heat source. Three parts of the BC tab has been defined “Velocity, Heat exchange with the environment and temperature of the welding source” as shown below;



The next move going to be on the Properties tab, where the Hardness test has been defined as well, which is shown below;

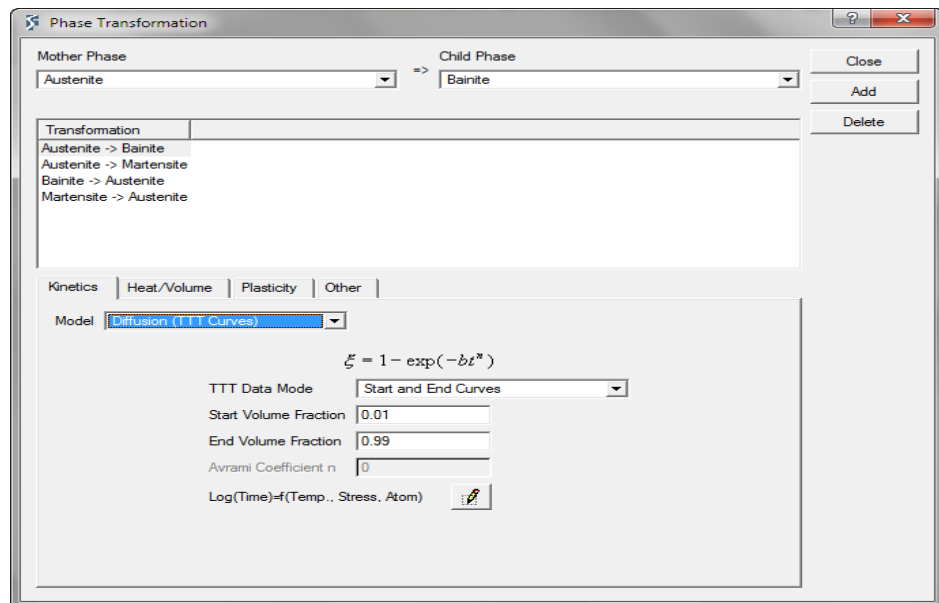
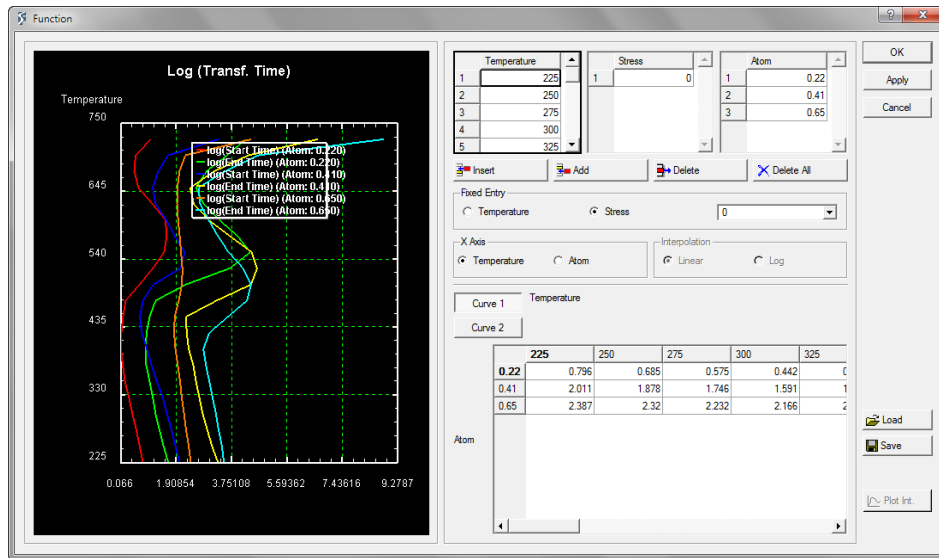


After that moving on the Advanced tab, to define average grain size and all the constants as it is given in the Appendices B where all constant value has been automatically defined after entering the initial grain size for the material. As it is shown below;

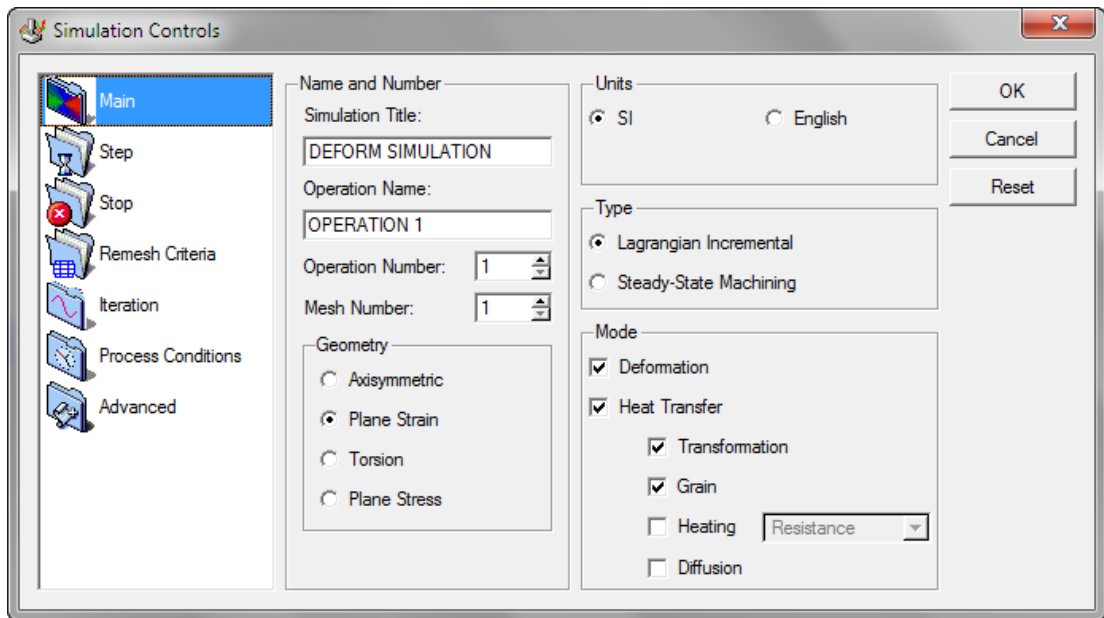


Exit from the material properties window and by loading the keyword AUSTEN.KEY file from the library of the 2D-DEFORM™, the other phase transformation of the material properties determined by the volumetric weighting of the first three material groups. After that on the material properties window the

transformation is edited from one phase to another as a mother to child by selection of the phases then loading the transformation key from the library of the 2D-DEFORM™ MAR_TTT keyword file then the TTT time temperature transformation diagram will be created for the AISI 1045 steel for 0.41 percent carbon content. In 2D-DEFORM™ program Avrami equation solving volume fraction and transformation, as it is shown below;



Next step in the preparation of the modelling is Simulation control, here the number of steps and the duration of the welding time has been defined according to the practical work data as it is shown below;



APPENDIX B

Table B-1 Young Modulus according to temperature and Carbon content:

Young Modulus (MPa.)		Carbon content	
		0.14 %	0.6 %
Temperature	0 °C	204468	198580
	200 °C	192900	187361
	400 °C	175416	170415
	600 °C	152018	147742
	800 °C	122704	119342
	900 °C	114451	111347

Table B-2 Constants of grain size AISI 1045 from the 2D-DEFORM™ manual:

a₁	n₁	m₁	Q₁	c₁	a₂
0 4.659e-3	0	0.1238	49520	0	0.83
a	b₁	b₂	Q₂	h₄	n₄
10000	0	0	0	0	-1.42
m₄	Q₄	β_m	k_m	a₇	h₇
-0.408	196000	0.693	1	4.85e+10	0
n₇	m₇	Q₇	c₇	m	a₉
-0.41	-0.028	-240000	0	2	9.44e+19
Q₉					
467114.7					